FINAL REPORT

Taiwan – USA AFOSR Nanoscience Initiative

(AOARD-04-4074)

Dispersion and Reinforcement of Nanotubes in High Temperature Polymers for Ultrahigh Strength and Thermally Conductive Nanocomposites

Principal Investigator

Arnold C.-M. Yang

acyang@mse.nthu.edu.tw

Department of Materials Science and Engineering

National Tsing Hua University

101, Kuang Fu Road, Section 2, Hsinchu City, Taiwan

Phone: +886-3-572-0792, FAX: +886-3-572-2366

Report Documentation Page

Form Approved
OMB No. 0704-0188

1. REPORT DATE	2. REPORT TYPE	3. DATES COVERED
03 OCT 2007	**FInal**	**23-06-2004 to 22-09-2005**

4. TITLE AND SUBTITLE
Dispersion and Reinforcement of Nanotubes in High Temperature Polymers for Ultrahigh Strength and Thermally

5a. CONTRACT NUMBER
FA520904P0440

5b. GRANT NUMBER

5c. PROGRAM ELEMENT NUMBER

6. AUTHOR(S)
Arnold Chang-Mou Yang

5d. PROJECT NUMBER

5e. TASK NUMBER

5f. WORK UNIT NUMBER

7. PERFORMING ORGANIZATION NAME(S) AND ADDRESS(ES)
National Tsing Hua University,101, Kuang Fu Rd, Sec 2,Hsinchu 30043,Taiwan,TW,30043

8. PERFORMING ORGANIZATION REPORT NUMBER
N/A

9. SPONSORING/MONITORING AGENCY NAME(S) AND ADDRESS(ES)
AOARD, UNIT 45002, APO, AP, 96337-5002

10. SPONSOR/MONITOR'S ACRONYM(S)
AOARD

11. SPONSOR/MONITOR'S REPORT NUMBER(S)
AOARD-044074

12. DISTRIBUTION/AVAILABILITY STATEMENT
Approved for public release; distribution unlimited

13. SUPPLEMENTARY NOTES

14. ABSTRACT
Fundamental approaches for controlled dispersion of multiwalled carbon nanotubes in polymers and the molecular reinforcement in their nanocomposites were studied to design and fabricate well-dispersed percolated carbon nanotube networks in high temperature polymers.

15. SUBJECT TERMS

16. SECURITY CLASSIFICATION OF:			17. LIMITATION OF ABSTRACT	18. NUMBER OF PAGES	19a. NAME OF RESPONSIBLE PERSON
a. REPORT	b. ABSTRACT	c. THIS PAGE			
unclassified	**unclassified**	**unclassified**	**Same as Report (SAR)**	**72**	

Abstract

In this research, the fundamental approaches for controlled dispersion of multiwalled carbon nanotube in polymers and the molecular reinforcement in its nanocomposite were studied. The ultimate goal is to design and fabricate well-dispersed percolated carbon nanotubes network in high temperature polymers to impart ultrahigh strength and conductivity to the soft materials. The research work was segmented into three related focuses whilst phased with model systems and target systems. The three segmented focuses are 1) Dispersion of surface-grafted carbon nanotubes and nano-mechanical interactions with polymer chains in polymeric nanocomposites, 2) Covalent crosslinking of surface-grafted nanotubes in polymer nanocomposites, and 3) Conductivity in polymeric nanocomposites percolated with surface grafted carbon nanotubes. These parallel research endeavors were structured with a model system as the first phase where polystyrene (PS) was used as the model polymer for synthesis and analyses and then followed by the second phase of high temperature polymers, the target systems, where poly(benzoxasoles) (PBO) and polyimide (PI) were synthesized and studied.

The major goal of the first research focus was to explore the ultrahigh strength capability of nanotubes-reinforced polymeric composites. Via the reactions of 4-vinylbenzyl chloride with pre-attached carboxylic acids on the nanotubes, PS chains can grow from the nanotubes surface following free radical polymerization. When blended with PS in a solution, the surface-grafted nanotubes formed a percolated network of multi-walled carbon nanotube (MWNTs) in the polymer thin film cast from the solution. The nanotubes network dramatically reinforced the brittle polymer by suppressing the growth of the micro-deformation zones of crazes. With only 1-2 % of carbon nanotubes, the reinforced PS can withstand strains greater than 20% without undergoing any microcracking. For higher concentrations of nanotubes, solubility difference between the surface-grafted nanotubes and the host polymer gave rise to an intrinsic microstructure that shows roughened surface and non-uniform morphology which, however, seemed to have no negative effect on the toughness imparted by the nanotubes. The chain length of the grafted polymer on the nanotubes has important effect on the reinforcement and the onset of this micro-separation. Nanocomposites of high-temperature polymers of PBO and PI embedded with nanotubes surface-grafted with the respective polymer were also successfully prepared. Particularly, PBO was synthesized in either an one-step approach in poly(phosphoric acid) or a two-step approach where poly(hydroxyamide) (PHA) was first synthesized and then thermally cure to form PBO. The micro-deformation mechanism of the high concentration

nanotubes in PS, PI, and PBO were being investigated.

The main purpose of the second research focus is to crosslink the surface-grafted nanotubes in a polymer host to trigger, when subjected to an external force, the toughest mode of deformation directly stemmed from the unique mechanical properties of carbon nanotubes. The carbon nanotubes are characterized with a ultrahigh modulus (~ 3 TPa) and remarkable elastic deformation limit around 30% whilst an additional plastic deformation mode of un-sheathing was reported operative at high elongations. The covalent linkage between neighboring nanotubes of the network also can provide much improved conductivity properties to the composites since contact resistance at nanotubes junctions was reported to dominate the electrical conductivity of the nanocomposites. This work was challenged by the task of overcoming the unexpectedly strong π–π interactions between growing chain ends and nanotubes surfaces during graft copolymerization. The π–π interactions restricted the extension of the grafted polymer, causing severe nanotubes conglomerates when crosslinking reactions were completed. Another hurdle was to synthesize sufficient long polymer chains to bridge nanotubes in the solution. These problems were finally solved by using atomic transfer radical polymerization (ATRP) to prepare a prepolymer of controlled crosslinking density by directing reactions of the multiple-functioned polymer chains with small molecules before further reactions with surface-functionalized nanotubes. Covalently linked nanotubes uniformly dispersed in a PS host were successful prepared which demonstrate excellent mechanical properties. Crosslinking methods either with delayed or inhibited cure agents or by controlled electron radiation were undergoing. This work will be extended to the high temperature polymer systems for testing the effects on conductivity and ultrahigh strength capability.

The third research focus was designed to understand the conductance in a nanotubes-embedded polymer with a percolation theory that enables us of quantitative analyzing the gelation transition below and above the electric percolation threshold. First, it was found that although surface-grafted nanotubes distributed uniformly in the host polymer, enabling full percolation with much less nanotubes, the intrinsic electric conductivity of the nanotubes decreased dramatically due to the insulation effect of the grafted polymer over the nanotubes, rendering the composite inferior in conductance. The contact resistance between neighboring nanotubes holds key control over the conductance properties of the nanocomposite. This problem can be overcome by grafting the nanotubes with electric conducting polymer. PBO-grafted nanotubes have shown excellent conductance behavior, approaching the theoretical limit

promised by the nanotubes. The surface-grafted approach, however, suffered negative impact due to damages to the native nanotubes from functionalization and improvements are being attempted by gold-particle templating and p-p interaction approach. Theoretical analysis is currently underway to examine the local resistance at nanotubes contacts.

These results outlined in the above have provided a sound foundation for further advancing towards the realization of the novel materials that embodied with ultrahigh mechanical strength, high electrical/thermal conductivity, and low mass density in high-temperature soft materials. The work also provides fundamental understanding on the intrinsic physical behavior of polymer chains through examinations of nanomechanical properties, polymer-nanotube interactions, contact resistance on nanotubes surfaces, and optical properties of the nanocomposites.

Prologue

The discovery of carbon nanotubes (CNTs) by Iijima [1] in 1991 had brought a widespread research enthusiasm for unveiling the fundamental properties, fabrication techniques, and novel applications of the nanotubes. It is now well documented that CNTs possess quite unique and remarkable properties with respect to mechanical [2], electrical [3,4], thermal [5,6] and chemical behavior. For example, due to the high aspect ratio of their external shapes, nanotubes can form percolated networks even at very low filler fractions (<5 wt. %) to impart tremendous filler reinforcement effects. Intensive research is being focused on their potential applications such as field emission sources [7], AFM tips [8] and storage devices, hydrogen storage [9], nano-electronic or nano-photonic devices, and nanocomposite materials [10].

Owing to the fact that carbon nanotubes possess extremely high Young's modulus, stiffness, elastic flexibility, conductivity and field emission properties [11], carbon nanotubes are being used to disperse in polymer matrices using melt processing, solution processing or in-situ polymerization in the hope to enhance properties. Extensive efforts had been devoted to exploit nanotubes as fillers in thermoplastics or epoxy matrixes which demonstrated greatly enhanced mechanical, [12,13] electrical, [14,15]and thermal [16,17] properties. It also had been shown that with only 1 wt % multiwalled carbon nanotubes (MWNTs) added as the filler, huge increases, 36-42%, in the elastic modulus of the composites could be resulted [18]. Small-diameter MWNTs were reported as the best candidates for polymer reinforcement [19]. However, the dispersion of the fine nanoscale nanotubes in polymers had been proven to be a formidable challenge. The composites would demonstrate inferior performances if the nanotubes were poorly dispersed. Furthermore, the adhesion between the nanotubes and the polymer matrix also plays a vital role in the reinforcement and electron conduct mechanisms.

In this research, three related topics were explored and divided into three chapters: **Chapter 1:** Dispersion of surface-grafted carbon nanotubes and mechanical interactions with polymer chains in polymer nanocomposite thin films, **Chapter 2:** Covalent crosslinking of surface-grafted nanotubes in polymer nanocomposites, and **Chapter 3:** Electrical conductance in polymeric nanocomposites percolated with surface-grafted carbon nanotubes.

Chapter 1

Dispersion of carbon nanotubes and mechanical interactions with polymer chains in polymer nanocomposite thin films

The chain behavior of macromolecules in the glassy state dictates the physical properties in a wide spectrum of polymer applications. A glassy polymer chain is first deformed uniformly and elastically upon stretching until it yielded, commencing the plastic deformation afterward [20]. Yielding, when appeared in the forms of crazes or shear deformation zones, was found to follow the micronecking mechanics [21]. Crazes, commonly observed in the deformed brittle polymers, are cracklike defects that are load bearing [22-31] and possess a fibrillar microstructure. Here, we attempted to use carbon nanotubes finely dispersed into the polymer chain network to investigate the interactions between the glassy chains and the entanglement network of the nanotubes. The results can provide valuable insights toward the chain behavior of glassy polymers. In this part, polystyrene (PS), polyimide (PI) and poly(phenylene benzobisoxazole) (PBO) were used as the polymeric matrix in the nanocomposites reinforced with the polymer grafted MWNTs. It was expected that adding a stiff polymer-grafted MWNT would dramatically alter the stress transfer network of polymer chains. The performance of the mechanical properties of the composite films that resulted from the interactions between the MWNT network and polymer entanglement networks were reported. In addition, the nanomechanical properties of the MWNT/Polymer composite film were probed by using AFM analysis.

1.1 Carbon Nanotube Functionalization & CNT Graft Polymerizaiton

Due to the large van der Waal forces stemming from large surface areas, inter-particle fusing by impurity amorphous carbon, and tube entanglements, CNTs tend to aggregate when introduced into a polymeric binder without proper pre-treatments. Once aggregation occurred, the intended percolated network would fail to form, and the resulted heterogeneities frequently hurt the very properties that were meant to be enhanced. Good dispersion generally requires proper surface treatments as well as purification and disentanglement pre-treatment [32] of the highly intertwined nanotubes. There were extensive efforts in this regard [33–36]. Physical dispersing [37,38] (e.g., via van der Waals attraction, π - π interaction, etc.) to yield good dispersion of the as-produced nanotubes in aqueous solutions have been reported by Bandyopadhyaya et al. [39] and Fukushima et al. [40] although the effects intrinsically are of temporary nature. Star and Stoddart [41], and Hill et al. [42] Park et al. [38] and Mitchell et al. [43] had demonstrated significant progresses by

chemical modifications of the single-walled nanotubes (SWNT) (via PMMA-grafted SWNT [35,36], polypropylene/nano-carbon fiber, polystyrene (PS)/MWNT [34,43] and in-situ polymerization of PI/SWNT [38]) in polymer matrices to exhibit good mechanical strength. None of them, however, dealt with highly diluted polymer solutions with pre-treated CNTs from which thin polymer films of well-dispersed percolated nanotubes could be produced by solution-cast. In this section, we focused on the development of the methods for stabilizing nanotube dispersion in dilute solutions, from which thin films of the nanocomposites could be obtained by spin-coating.

1.1.1 Experimental Section

Monodisperse polystyrene (Mw/Mn =1.3) of molecular weight Mw = 2,000,000 (Pressure Chemical Co., U.S.A.) was used as the polymeric matrix for this study. The MWNTs (DESUN Nano Co., Taiwan) used in this study were found to have an average outer diameter around 30 nm (Figure 1) and a length of 10-30 μm. Aggregates were commonly observed in the asreceived MWNTs samples. The surface-grafting of the MWNTs was carried out in three consecutive steps. First, the nanotubes were surface-treated by anchoring carboxylic acid groups onto the tube external surfaces (MWNTs–COOH). Then, the carboxylic acid groups in MWNTs–COOH were esterified by further reactions with 4-vinylbenzyl chloride to produce –COOR groups grafting on the tube surfaces (MWNTs–COOR).

Finally, the grafted groups on the tube surfaces were put into the polymerization reaction, initiated with 2,2'-azobisisobutyronitrile (AIBN), with styrene monomers (Scheme 1)[44].

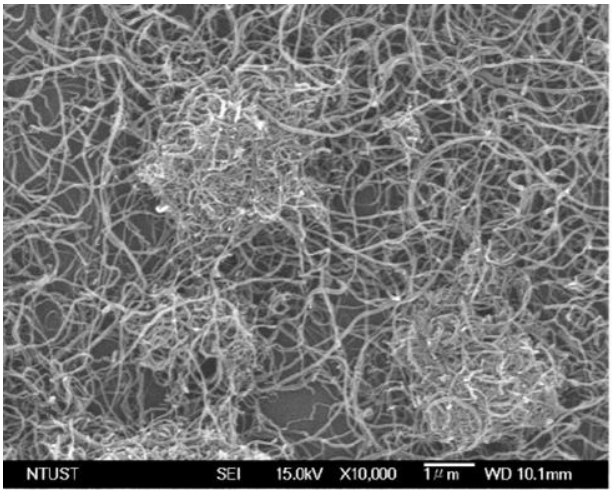

Fig. 1. SEM micrographs of the MWNTs as received

(1) Preparation of MWNTs–COOH:

MWNTs synthesized via a chemical vapor deposition method (purchased from DESUN Nano Inc., Taiwan) had tube diameter of 10–30 nm and 5–15μm in length. The as-received MWNTs were first purified by reflux for 48 h in 2.6M nitric acid, followed by filtration with a PTFE membrane (0.2μm pore size) and finished by repeatedly washing with deionized water. The purified MWNTs were then immersed in H_2SO_4/HNO_3 (mixture of 3:1 in volume) at
90 ◦C for 2 h and then vacuum-filtered through a 0.2μm PTFE membrane. The solid was washed with deionized water again repeatedly until the pH of the filtrate reached 7. In this step, the nanotubes were oxidized by attachment of carboxylic acid groups on the MWNTs external walls. The tube lengths of the nanotubes were also reduced in this step; therefore, the length of the treatment time was carefully controlled to retain optimal tube lengths.

(2) *Esterification of MWNTs–COOH with 4-vinylbenzyl chloride (CMS)*:

The carboxylic acidified nanotubes (MWNTs–COOH) were then dispersed in toluene (10 mg of MWNTs–COOH in 10 ml toluene) with 68 mg of sodium ethoxylate at 40 ◦C by sonication continuously for 1 h to generate MWNT–COONa. Then, 1ml of CMS was added into the solution and the mixture was again sonicated for another 2 h to produce the esterification product (MWNTs–COOR, $R=CH_2C_6H_4CHCH_2$).

(3) *Synthesis of polystyrene grafted-MWNT (p-MWNTs)*:

To grow PS chains from the grafted functional groups on the CNTs, the esterification solution from the above procedure was added with 0.1 mg of AIBN and 1ml of styrene monomer at 95 ◦C to initiate the polymerization reaction. The reaction batch was stirred continuously for 3 h. At the end, the majority of toluene in the solution was removed by low pressure distillation. Then, the polystyrene–MWNTs (p-MWNTs) were precipitated by adding methanol into the solution, and collected after filtration. The non-reacted or non-polymerized monomers (or oligomers) were herein washed and filtered out from the batch. The solid was then washed again in toluene by sonication and then vacuum-filtered through a 0.2μm PTFE membrane. The chain lengths of the grafted PS on nanotubes were estimated from the SEC data of a batch without nanotubes but under the same polymerization conditions, to be around Mn = 6300 and Mw = 7900 (polydispersity = 1.26) (Scheme 1) .

1.1.2 Results and Discussions:

Fourier-Transform Infrared spectroscopy (FTIR) was used to identify the

existence of carboxylic acid groups and the grafted polystyrene chains in the samples. The differences between the FTIR spectra, shown in Figure 2a, of the as-received MWNTs, acid-treated MWNTs and p-MWNTs were noted. Two new peaks emerging at 1720 and 3400 cm^{-1} after the acid treatment corresponded respectively to C=O and -OH stretching, confirming the attachment of the carboxylic acid groups onto the MWNTs. The substitution of carboxylic acid group by ester group during reaction with CMS caused a decrease of height of the -OH peak at 3400 cm^{-1} and a shift of C=O peak from 1720 to 1680 cm^{-1}. Finally, after the graft polymerization, new peaks were observed to emerge in the frequency range from 2800 to 3200 cm^{-1} corresponding to sp^2 (=C-H) stretching (3000–3200 cm^{-1}) and sp^3 (-C- H) stretching (2800–3000 cm^{-1}), a clear evidence for PS grafting on MWNTs.

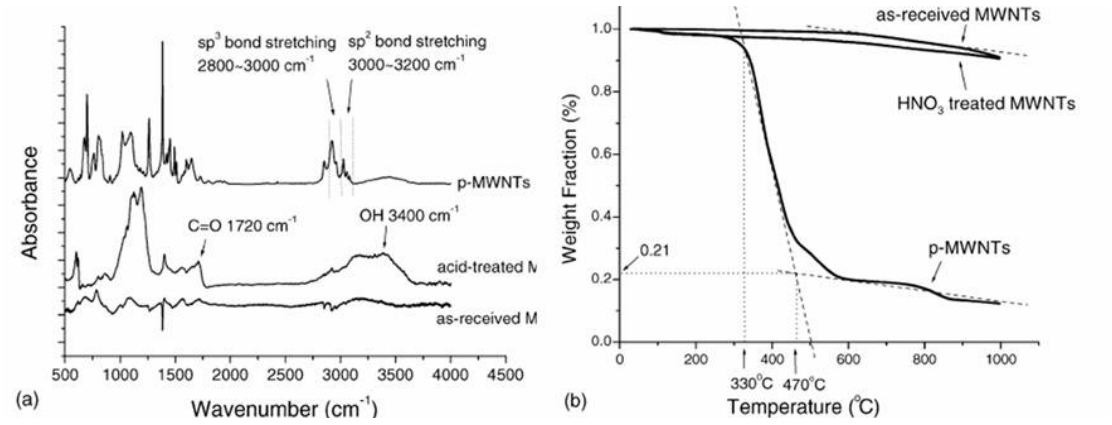

Figure 2. (a) The FTIR spectra of the as-received MWNTs, acid-treated MWNTsand graft polymerizedMWNTs(p-MWNTs); (b) Thermogravimetric curves of the as-receivedMWNTs(purity >−96%), acid-treatedMWNTs with nitric acid and p-MWNTs.

We then used TGA analysis (Figure 2b) to determine the PS weight fraction in the grafted MWNTs (p-MWNTs). Indicative of the purity, the as-received MWNTs retained more than 96% weight fraction up to 1000 ◦C. The carboxylic MWNTs showed a similar but slightly greater weight loss, attributable to the pyrolysis of carboxylic acid groups on CNT surfaces. For p-MWNTs, the TGA weight fractions underwent a sharp decrease at around 350 ◦C, signifying the onset of pyrolysis of the PS chains grafted on p-MWNTs. The weight loss subsequently slowed considerably beyond 550 ◦C, a temperature at which the PS had essentially burnt out, after which a constant decreasing rate comparable to that of the as-received MWNTs in the same temperature range was observed. The weight fraction of grafted PS on the p-MWNTs was determined from the asymptotic cross-sections drawn from the thermogravimetric

curve, to be approximately 80%. On the other hand, the surface grafted MWNTs (p-MWNTs) were then blended with high molecular weight PS (*M*w = 2M) in toluene for casting thin polymer films. The film thickness was around 0.35 μ m. The concentration of p-MWNTs in the solutionwas adjusted so that the nanotube weight fraction, excluding the grafted polymer, was 1.5 wt.% in the solid films. As shown in Figure 3, the solution of p-MWNTs was transparent, indicating that the global dispersion of the CNTs in the toluene was excellent. Minor sedimentation took place after 1 day of sitting, but the solution returned to complete transparency immediately after stirring. In contrast, a control solution of the as-received MWNTs was black and opaque, apparently due to the immense light scattering of the CNTs aggregates.

Figure 3. The toluene solutions of PS (*M*w = 2M) blended with 1%, respectively, of (a) as-received MWNTs (labeled as "pristine MWNTs") and (b) p-MWNTs.

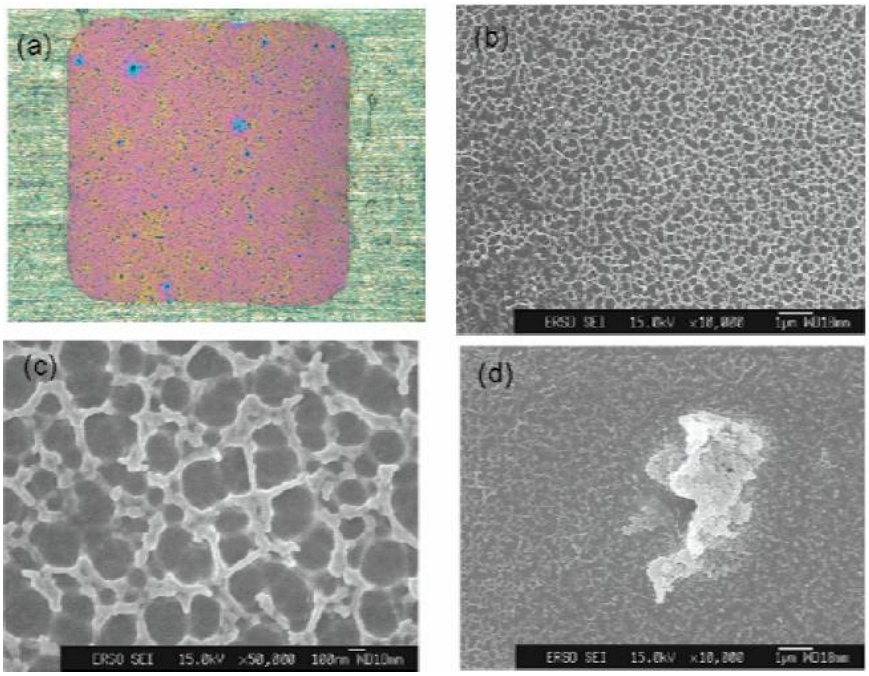

Figure 4. (a) Optical micrograph MWNT/PS films coated on copper grids, without

stretching; and (b,c,d) SEM micrograph of the plasma-etched MWNT/PS film showing the nanotube network (in b and c) and aggregates (in d).

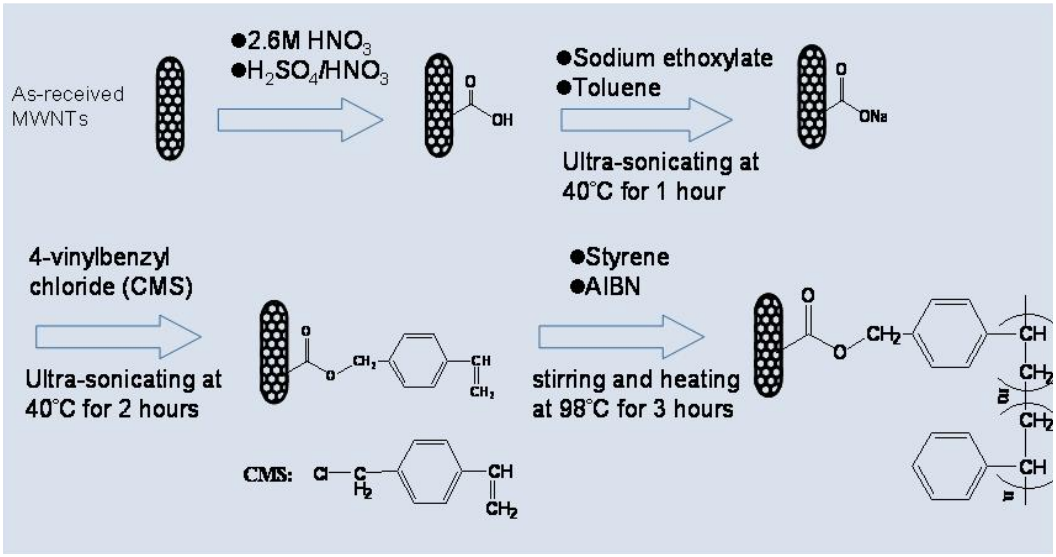

Scheme 1. Synthesis of polystyrene grafted-MWNT

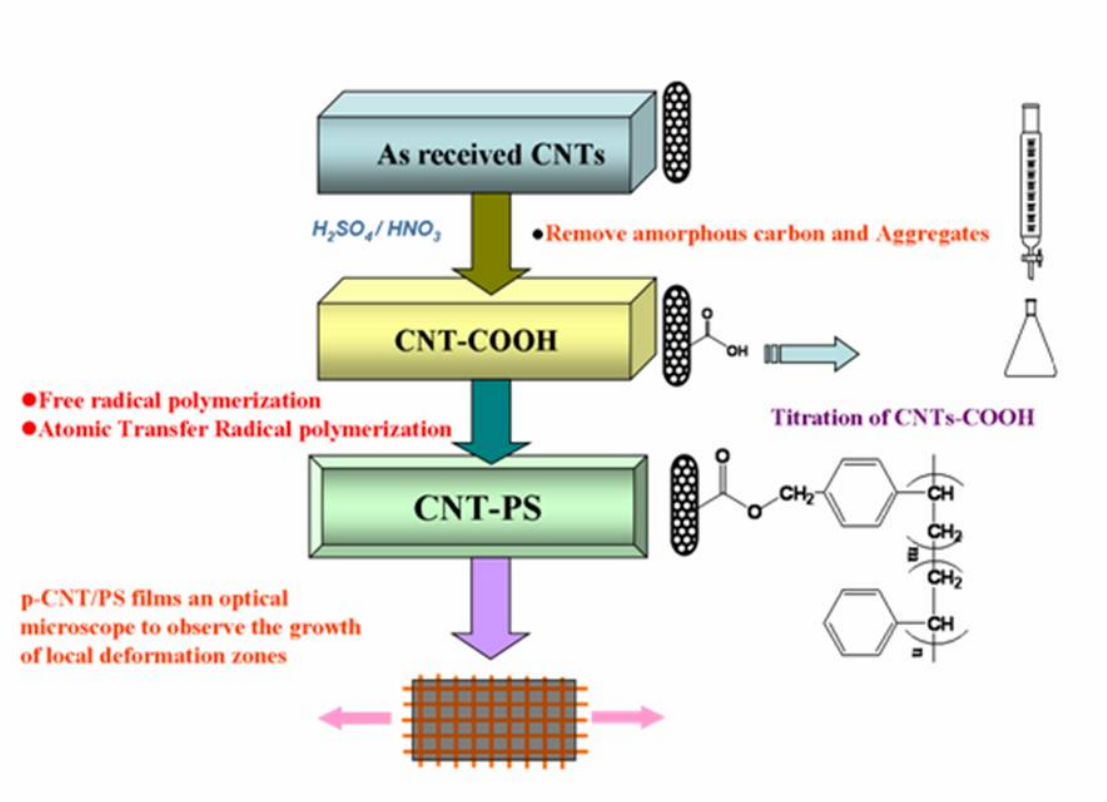

Scheme 2. preparation of PS / PS grafted-MWNT nanocomposite films

1.2 The Nanomechanical Properties of Polystyrene Thin Films Embedded with Surface-grafted Multiwalled Carbon Nanotubes

Thin films of novel properties are ubiquitous at the forefronts of scientific research and industrial applications. Furthermore, the molecular interactions between polymer chains and nanotubes usually can be most conveniently studied in thin films. Therefore, in this section, we focused on the used polystyrene as the polymeric matrix in the nanocomposites reinforced with the polymer grafted MWNTs to understand the nanomechanical interaction between MWNT and polymer chains.

1.2.1 Experimental Section

The PS-grafted MWNTs were mixed, by approximately 1.5 wt % in weight, with the PS in toluene solution. The MWNT/PS films were spun cast from the solution, and the film thickness was controlled to be around 0.35 μm. The MWNT/PS films were floated off the substrate on distilled water and bonded onto supporting copper grids (scheme 2). After following the proper bonding procedure, the specimen was mounted in a strain jig and stretched under an optical microscope to observe the growth of local deformation zones (crazes or shear deformation zones, SDZ). The stretched MWNT/PS films were then examined under an AFM (Digital Instrumental, Nanoscope IIIa) to investigate the nanotopographic information. The AFM topographic data were used to calculate the local nanomechanical information in the local deformation zones. A field emission scanning electron microscopy (FE-SEM) system (JEOL JSM-6500) was then used to observe the surfaces of MWNT/PS films. Scanning transmission electron microscopy (TEM, JEOL JEM-2010) was used to observe the microstructures of the MWNT/PS films. Pristine polystyrene (PS, *M*w =2,000,000) films (0.5 μm thick) were prepared as a control for the experiment [45] (Scheme 2).

.

1.1.2 Results and Discussions

Nanotube Dispersion in Solid Films

The nanocomposite thin films of MWNT/PS showed excellent mechanical properties, indicative of a generally well dispersed, percolated network of MWNTs embedded in the polymer matrix. Nevertheless, sporadic MWNTs aggregates were spotted under an optical microscope, and the surface of the MWNT/PS films was significantly rougher than the pristine PS (Figures 4a and 5a). The dispersion of the MWNTs in the polymer thin film was further explored by conducting a separate experiment using oxygen plasma to mildly etch the nanocomposite films. A uniform

network of MWNT covered by molten polymer emerged after etching (Figures 4b and 4c), attributable to a large difference in etching rate between polymer and carbon nanotubes. The average external diameter of the emerged nanotubes was consistent with the original specification of around 30 nm. Furthermore, the "mesh size" of the nanotube network was around 200-300 nm. Sporadic aggregates were found on the etched surface (Figure 4d), which appeared to be fused nanotubes. As a comparison, the etched surface of the pristine PS film was clean and smooth.

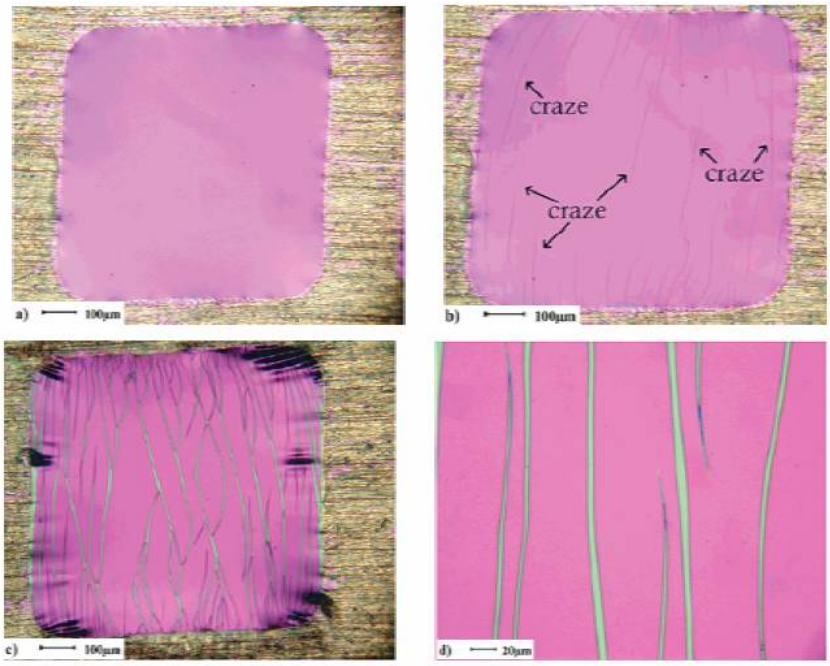

Figure 5. Optical micrograph of pristine PS films coated on copper grids: (a) without stretching, (b) with crazes (some marked with arrows) just initiated, (c) local craze breakdown, and (d) crazes at a higher magnification.

Effects on Microscopic Deformation Behavior

It is well-known that local deformation zones grow in neat polymer glasses upon stretching by tensile stresses. The deformation zones were categorized into crazes (the brittle mode) or shear deformation zones (the ductile mode). Crazes were characterized with an interconnected fibrillar structure, while shear deformation zones were local regions monotonically thinned. In the control experiment of pristine PS films, crazes were usually initiated near the edges of the film squares or local defects such as dust particles or aggregates (Figure 5b). After the initiation of crazes at approximately 1% strain (the crazing strain ε_c), most further deformation was concentrated toward the preexisting crazed areas, and the regions outside the crazes were subjected to virtually no strain beyond ε_c. The crazes were generally straight, widening steadily as the strain increased, and effectively absorbing the externally applied deformation into the tiny zones (Figures 5c and 5d). Very few new crazes

were nucleated after 1.5% strain (Figure 7a). As strain increased further, local fibril breakdowns within the crazes began at approximately 8% strain, and the maximum width of crazes could reach approximately 18 μm as determined from AFM surveys. In contrast, the MWNT/PS films showed a very different behavior. In the MWNT/PS films, the emergence of tiny local deformation zones occurred at a critical strain at around 1.2% (Figure 6a). As the strain increased, the development of the tiny local deformation zones was effectively suppressed with the zone width increased only slightly (Figures 6b). At the same time, however, a large number of new local deformation zones were initiated as the strain increased. Up to the point of maximum strain where the supporting copper grids broke at 23.5% strain, virtually all the local deformation zones in the film remained short and narrow (less than 2 microns wide). Very few local breakdowns were observed. In places where there were breakdowns, primarily caused by the aggregates, the microvoids were readily arrested. These results strongly indicated that the MWNT networks embedded in the PS film effectively retarded the growth and broadening of the local deformation zones and thus increased dramatically the toughness of the glassy polymer. To further examine the effect of MWNTs network on the nanoscopic mechanical properties, the number of the tiny local deformation zones in the stretched sample was counted as a function of the applied strain (Figure 7a). In the pristine PS film, the number of crazes increased only in the range of low strains; it quickly leveled off as the strain increased, reflecting the fact that crazes act as strain sinks in these films. However, in the MWNT/ PS films, the number of local deformation zones increased steadily with strain and started to level off only when the strain exceeded ~15%. The number of local deformation zones in MWNT/PS films was approximately 7 times of that of crazes in pristine PS films at ε_c = 20%. To quantify the role of strain sink played by the local deformation zones, an empirical parameter ζ for gauging the degree of strain localization [46] was defined as the ratio of the total cumulative width of local deformation zones projected along the strained direction to the total sample width. If ζ = 0, strain was entirely endured by the matrix outside the deformation zones with no strain localization, while ζ = 100%, on the other hand, indicated that entire deformation was absorbed in the deformation zones. It was found that, for the MWNT/ PS films, ζ reached to a level greater than 90% at 2% strain, indicating that nearly all the applied deformation concentrated in the local deformation zone as soon as the deformation zones were initiated (Figure 7b). As the strain increased to greater than 10% strain, ζ decreased somehow to approximately 85%. Although coming with a large experimental error bar, it seemed to suggest that the region outside the deformation zones started to participate in strain sharing for about 10-15% of the total deformation.

Microstructure and Micromechanics of the Local Deformation Zones

The microstructure of the local deformation zones were examined under AFM (Figure 8a) and TEM (Figures 9 and 10), and a fibrillar structure was observed, indicating that the tiny local deformation zones are crazes (Figure 8b). A midrib was observed in the central line of the local deformation zones, which was the locus traced behind the craze tip during craze propagation. The highly strained fine features were found to have a width of approximately 70-100 nm in the nanocomposite crazes. The microstructure and the midrib width observed in MWNT/PS films were similar to that found in pristine PS crazes.

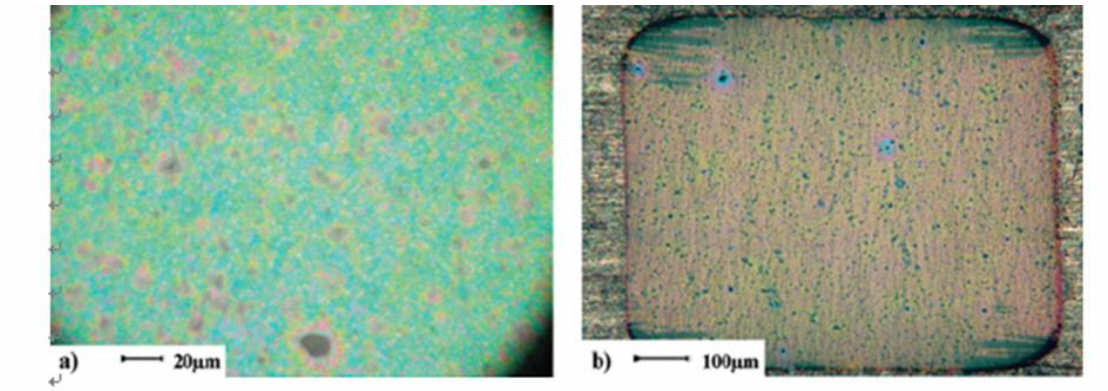

Figure 6. Optical micrograph of MWNT/PS films coated on copper grids: (a) local deformation zones initiated at 1.2% strain (the black spot at the bottom is a nanotube aggregate) and (b) many tiny local deformation zones at 23.5% strain.

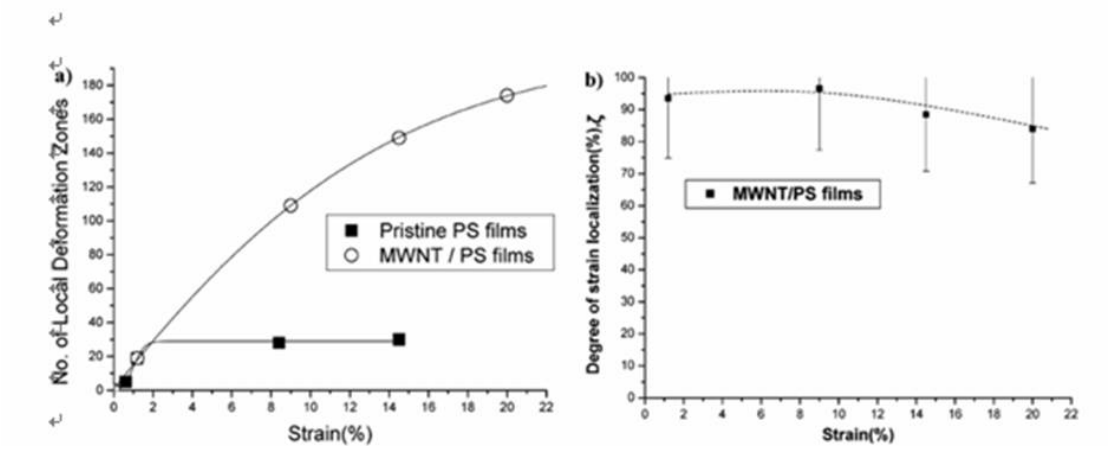

Figure 7. (a) Number of local deformation zones vs strain in the pristine PS and MWNT/PS films, (b) the degree of strain localization ξ vs the strain in the MWNT/PS films.

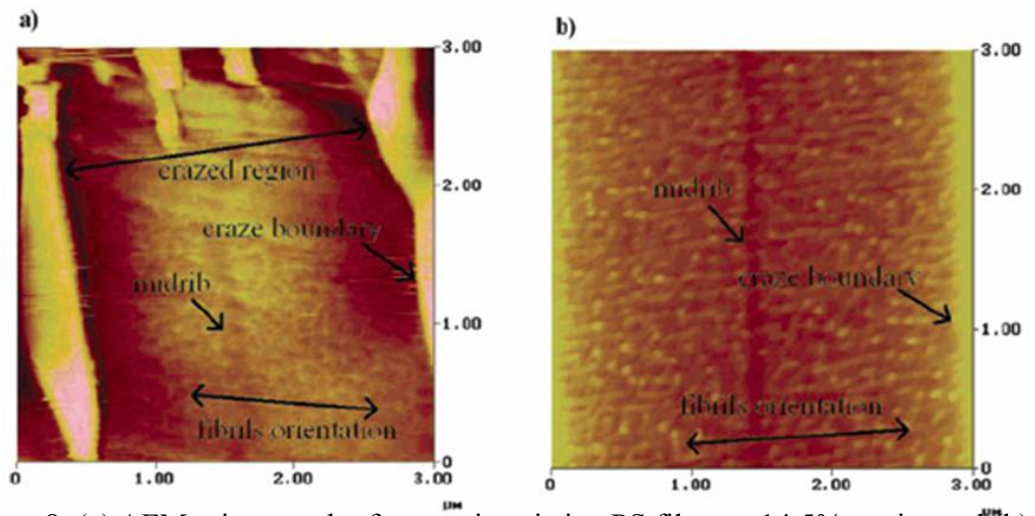

Figure 8. (a) AFM micrograph of crazes in pristine PS films at 14.5% strain; and (b) AFM micrograph of crazes in MWNT/PS films at 23.5% strain,

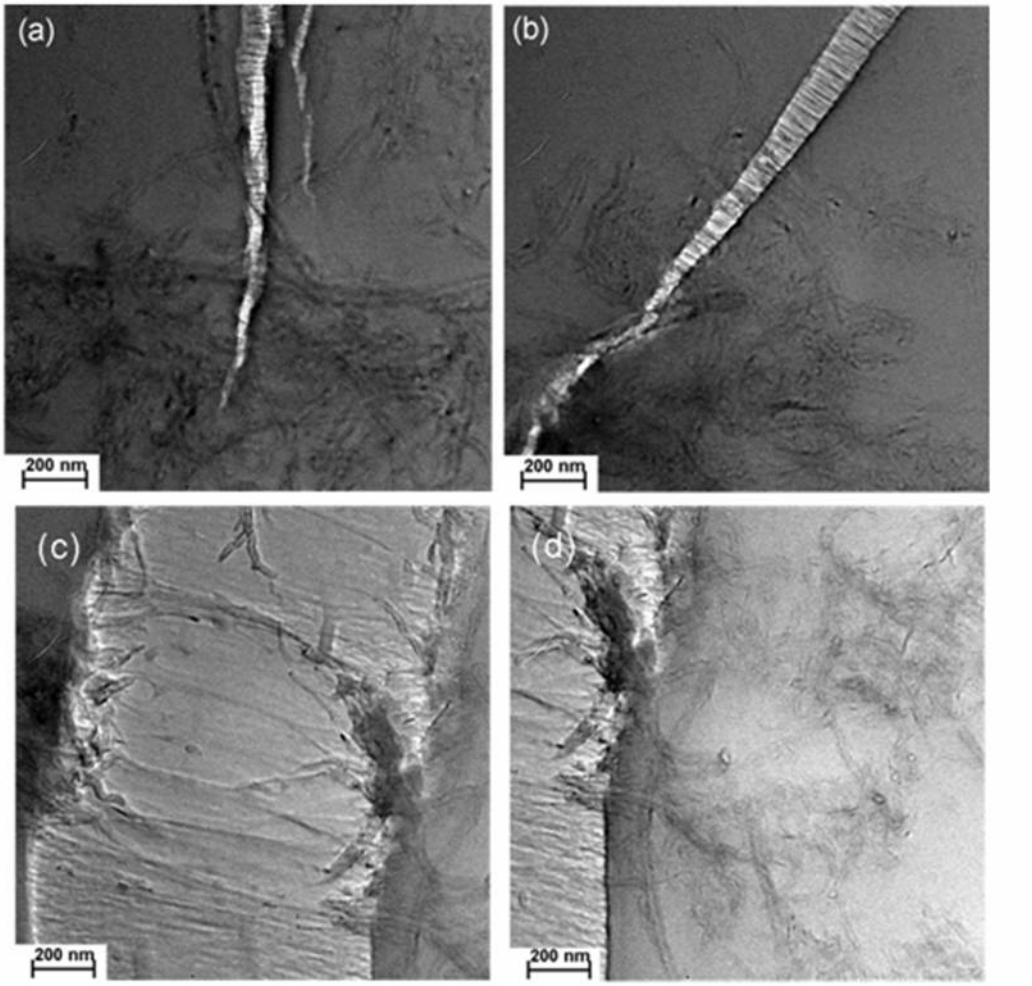

Figure 9. TEM micrograph of stretched MWNT/PS films (23.5% strain)

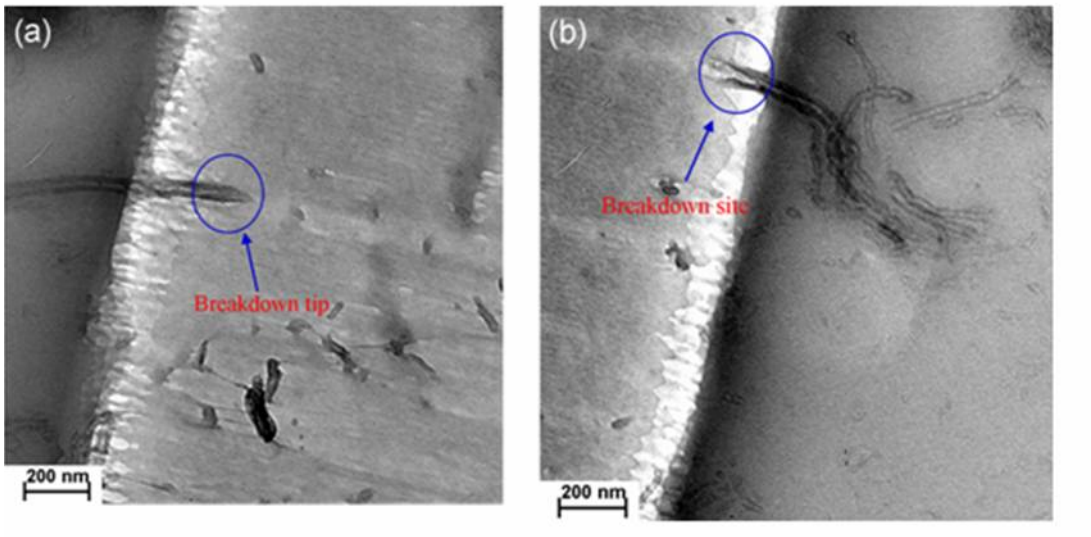

Figure 10. TEM micrographs of fracture nanotubes, (a) breakdown tip, (b) breakdown site.

Figure 11 shows curves of local true strain versus width within a section of craze in pristine PS film and the nanocomposite. In the pristine PS films the strain within the craze can reach 165% at the central neck region. However, it is only 90% in the MWNT/PS films at the craze centers. This hardened behavior apparently was due to the influences of the MWNT embedded in the polymer film. When the width of the crazes in the MWNT/PS film was smaller than 0.3 μm, crazes only strained below 30%. As will be discussed later, this has important implications as the strain of 30% is the elastic limit of MWNT. The microstructure and the growth behavior of craze tips are important for understanding craze nucleation and growth in the composites. In Figures 9a and 9b, the TEM micrograph of MWNT/PS films shows a craze tip interacting with the MWNT. Quite frequently, craze tips were found to terminate at aggregates of MWNTs, indicating that MWNT aggregates behave as stress concentrators capable of attracting crazes. These aggregates also are strong enough such that the attracted crazes can be effectively trapped and contained.

After craze tip has propagated through, the local stresses associated with the craze continue to interact with the polymer chains and the embedded nanotubes via a micro-necking process [31, 45]. For narrow crazes (< 0.3 μm), it can be seen that the MWNTs frequently bridge across the deformation zones, presumably due to lower necking strains at narrow crazes where the MWNT can be stretched elastically and hence remain in the crazes. Note that the elastic limit of MWNTs is around 30%, a

level greater than the strain concentrations in most of the narrow crazes (Figure 11). In contrast, for wide crazes (> 0.3 μm), MWNTs were never observed to bridge the deformation zones (Figure 9c). Instead, the nanotubes were observed to fracture with broken ends separated at both sides of the crazes (Figures 10a and b). This indicates that craze widening can cause breakage of nanotube because of large necking stress and strain. Therefore, it can be envisaged that when craze width exceeds a critical width that gives rise to a local strain greater than the elastic limit of the nanotubes, competition between the mechanisms of nanotube breakdown or suppression of craze widening should occur. If the nanotubes prevail, crazes remain narrow. However, if the local necking dominates, the nanotube broke down and the fracture nanotubes pile up at the edges of the growing crazes. Figure 9d is a magnified picture showing accumulation of MWNT at crazes boundaries. This phenomenon was also consistent with the observed AFM topography and the SEM micrograph of the crazes. The competition in essence is stemmed from the fact that the MWNTs are too rigid to be drawn into the micronecked crazes. In our observation, no pullout of the nanotube [47] was observed in the crazing, indicating good wetting and adhesion between the surface-grafted MWNTs and the PS matrix.

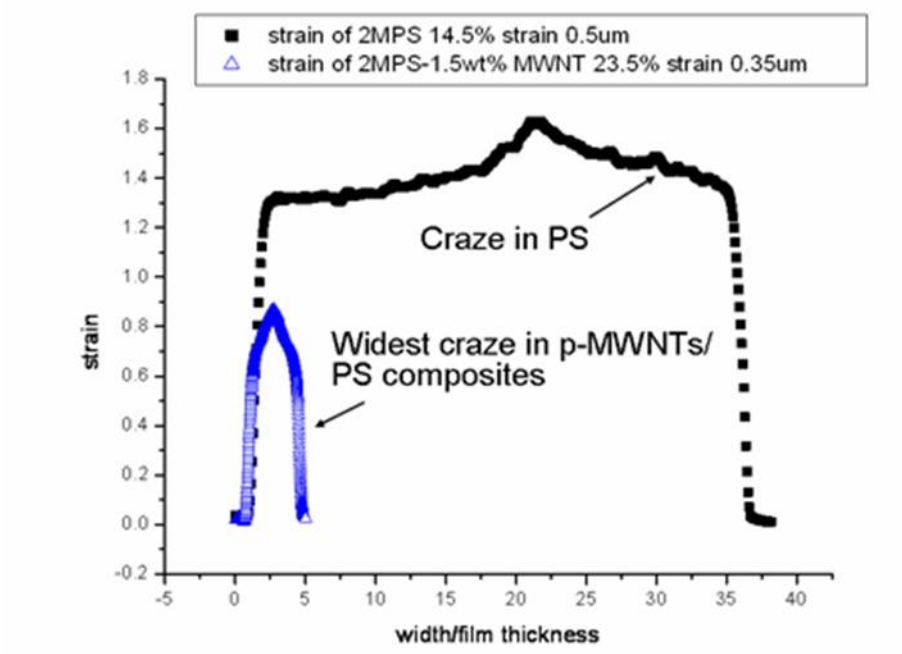

Figure 11. Local strain distribution across the craze width.

Close examinations by using SEM had led to no observation of individual nanotubes on the surfaces of the nanocomposite films (Figure 12). On the surfaces of the films, however, small, round depressions were found by SEM. These features were thought to be either regions of low mass density or bubbles, the origins of the latter were still unclear. The topography of the crazed MWNTs/PS films (Figure 13a) was compared further with that of the neat PS (Figure 13b) by using AFM. The surface of the pristine PS film was quite flat and smooth except for the crazed regions where depressions due to local thinning were found. In contrast, the MWNT/PS film surface was generally rough, and the crazes, usually quite narrow and winding, traveled up and down laboriously on the uneven surface (Figure 13a and c). Craze growth in the neat polymer was shown previously to follow a micronecking process, in which the craze depth d increased linearly with craze width w until the width reached a critical value w_c beyond which the depth remained constant. The critical craze width w_c is around 2.5 μm for 0.5 μm thick PS films. Figure 13b shows a section of the mature craze in pristine PS film with a width around 5 μm and a depth approximately one-third of the film thickness. The craze depth of MWNTs/PS crazes was found to follow the same d versus w curve when normalized to the film thickness, apparently following the same micronecking process (Figure 14). The width of the crazes in MWNTs/PS films, however, never reached w_c, and the craze depth was capped at about 19% of the film thickness. This hardened behavior apparently was due to the influences of the embedded MWNTs in the polymer film.

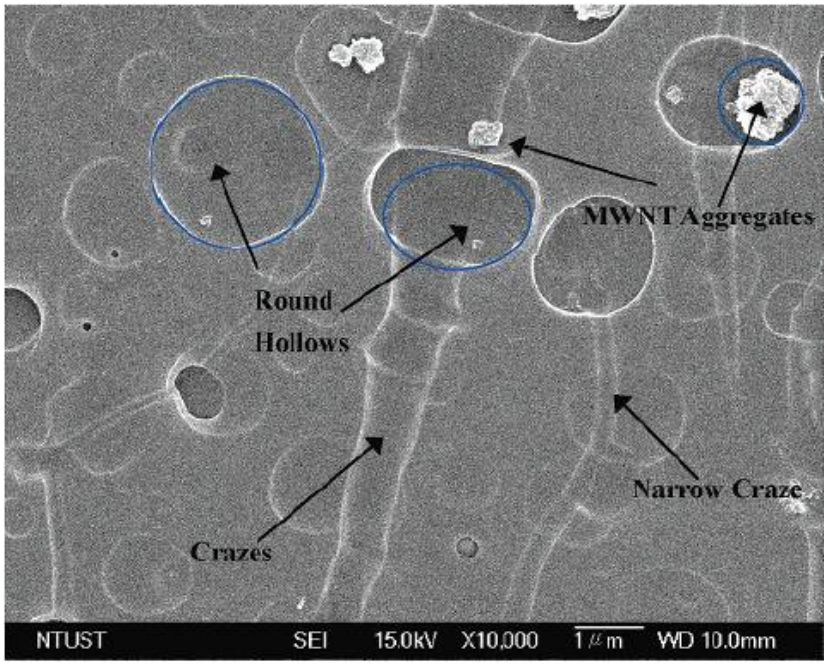

Figure 12. SEM micrograph of stretched MWNT/PS films at 23.5%.

In an attempt to reveal the effect of MWNTs on the development of crazes, some of the crazed samples were mildly etched by oxygen plasma to expose the underlying arrangement of the MWNTs in the stretched films. The AFM topography and the SEM micrograph of the etched crazed MWNT/PS films were illustrated in Figures 13d and 15a in comparison to that of the etched crazed pristine PS shown in Figure 15b. In the MWNTs/PS films, protrusions were seen bulging along the banks on both sides of the crazes after plasma etching. These protrusions, however, were not observed in the etched crazed films of neat PS. The height and width of the protruding ridges were 40-70 nm and 350-1000 nm, respectively, as measured by AFM sectional analysis (Figure 13d-f). The ratio of the height to the width of the protrusions was approximately 1:10, indicating that they were mild surface bulges with surface angle ~10° ($\tan^{-1}(1/5)$). On the basis of above analyses on the experimental observations, it could be concluded that crazes were largely confined in the regions where the nanotube network were loose or sparse. Once the crazes entered the regions of a well-structured nanotube network, the nanotube restricted the propagation and the widening of the crazes. Since these regions of loose MWNTs in effect were regions of defects, the nanomechanical behavior may become quite different when the dispersion of MWNTs is further improved to eliminate these defects entirely. It is also interesting to investigate the existence of the threshold mesh size of the nanotubes network below which craze nucleation and growth would be completely depressed.

1.3 The Microdeformation Behavior and Reinforcement Effects of Surface-Grafted Polystyrene: Effects of Mw and CNT Content

The microdeformation behavior and reinforcement effects of surface-grafted polystyrene as influenced by the molecular weight of grafted chains and the volume fraction of nanotubes in nanocomposite films are being investigated. Preliminary results are described in the following.

1.3.1 Effects of the Molecular Weight of Grafted Chains

In section 1.1, we have described the procedures for carbon nanotube functionalization and the surface graft polymerization. The same methods were used here to synthesize MWNT-grafted-PS of different chain length. The molecular weight of the grafted chains was controlled by adjusting the content of the initiator (AIBN). Figure 16 shows the optical micrograph of PS/ PS-g-MWNT nanocomposite films with same MWNT loaded but different Mw (30k, 60K and 80K, respectively) of surface-grafted PS without stretching. The preliminary results indicate that sufficient

length of the grafted chains, approximately 10k, is required for stable dispersion of the MWNTs in the nanocomposites. However, for the longer chains of the grafted

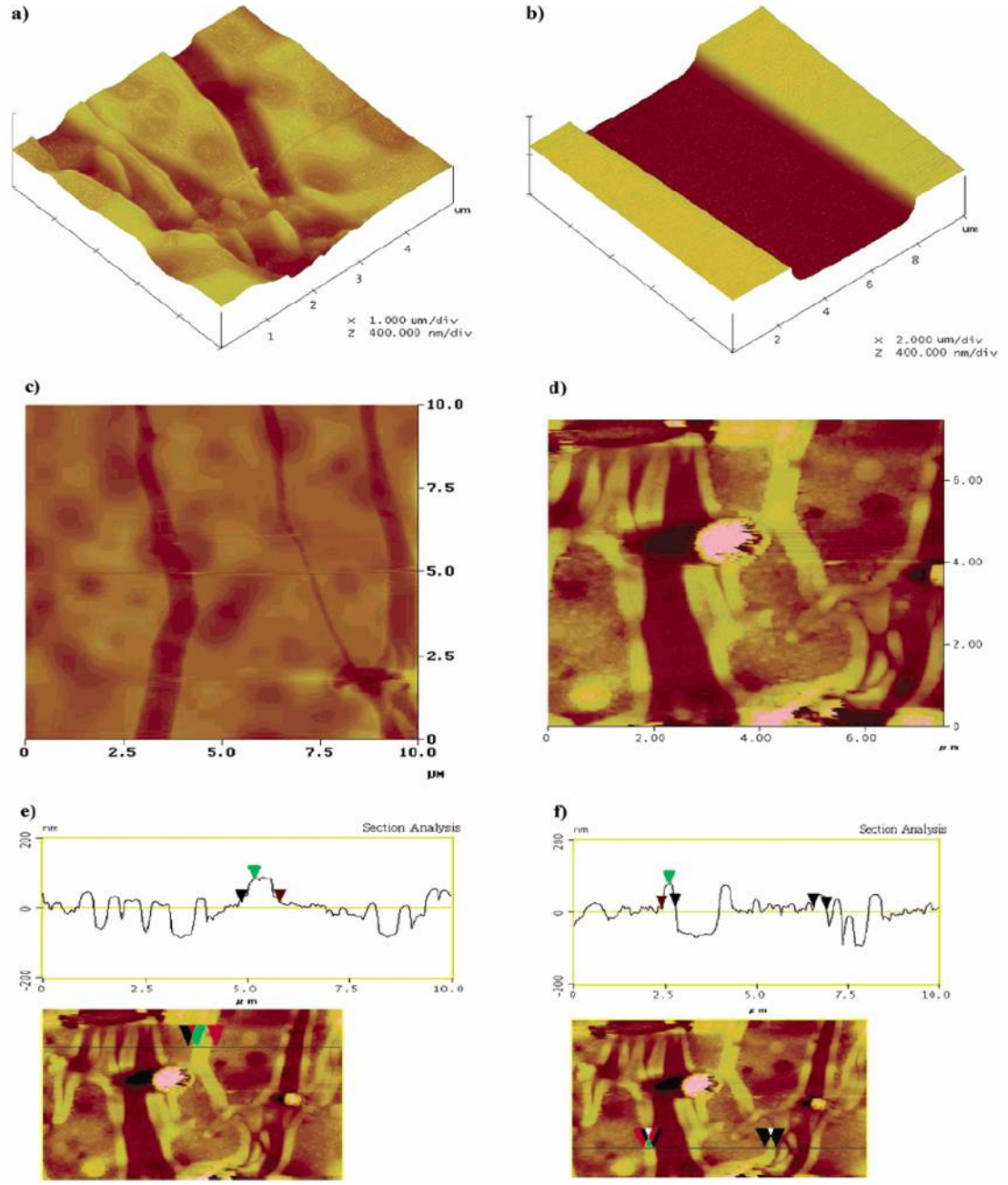

Figure 13. (a) Craze surface topography in MWNT/PS films, (b) craze surface topography in pristine PS films, (c) AFM micrograph of stretched MWNT/PS films without plasma etching, (d) AFM micrograph of stretched and etched MWNT/PS film, and (e, f) sectional topographical analyses at different locations of the MWNT/PS films.

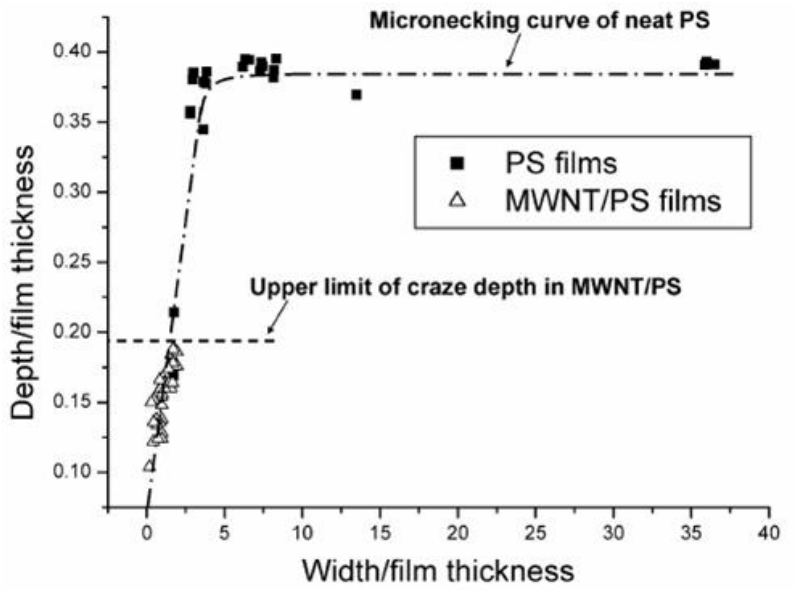

Figure 14. Craze depth *d* vs craze width *w* in the pristine PS and MWNT/PS films.

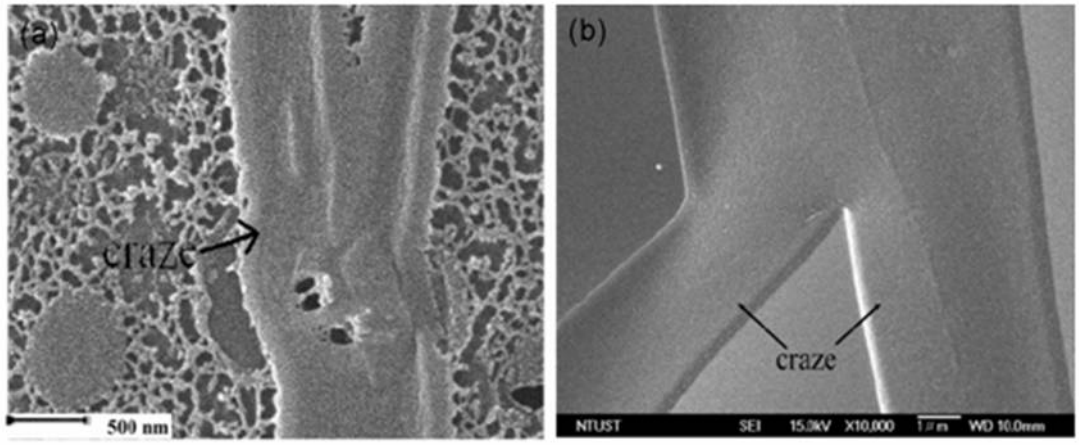

Figure 15. SEM micrographs of etched crazes in: (a) MWNT/PS films, and (b) pristine PS films.

polymers, phase separation is more likely to occur in that surface roughness increases and voided micro-morphology emerges as the volume fraction of the MWNTs grafted with longer chains increases. These features were thought to be induced by chain entanglement effect between MWNTs and PS matrix, which retarded the relaxation of the MWNTs during solidification of spin-coating of the thin nanocomposites films.

The crazes in nanocomposite films reinforced with shorter grafted chains were wider than that in the films with longer grafted PS (Figure 17). The surface roughness of the later films, however, has no detrimental effect on the mechanical reinforcement of the nanotubes in that almost no crazes were observed in the films even stretched to

large strains.

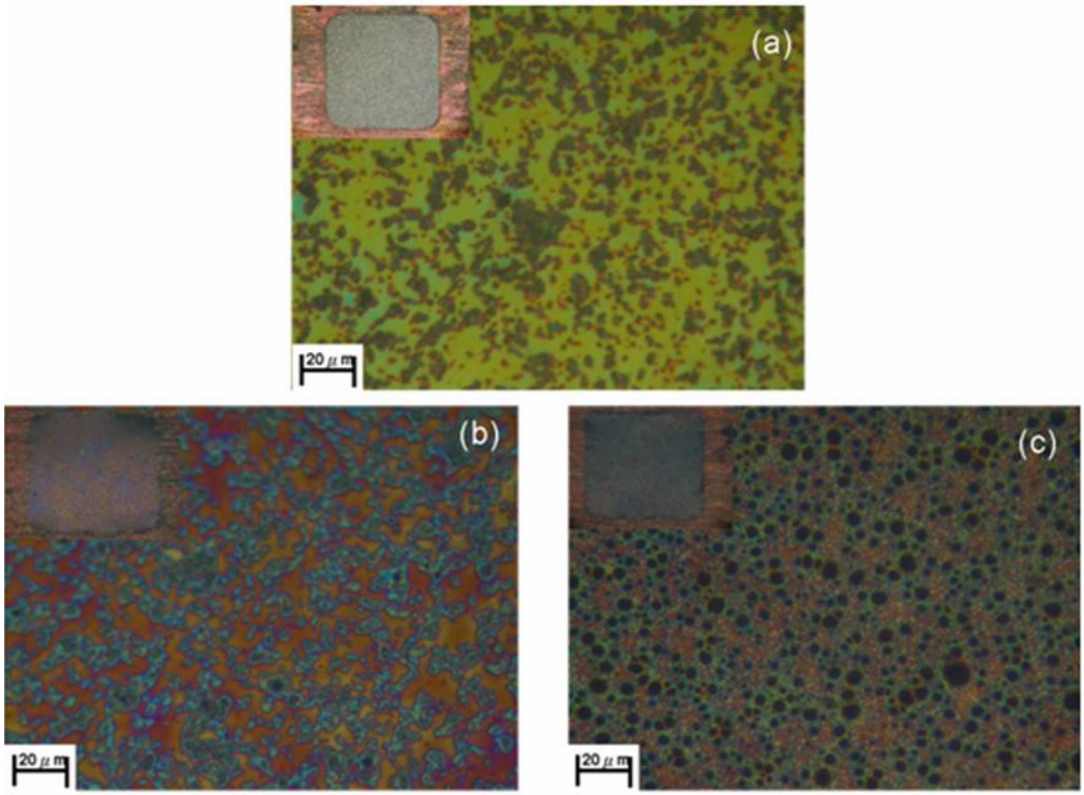

Figure 16. Optical micrograph of PS/ PS-g-MWNT nanocomposite films with same MWNT loaded but different Mw of Surface grafted PS (a) 10K, (b) 60K, (c) 80K without stretching.

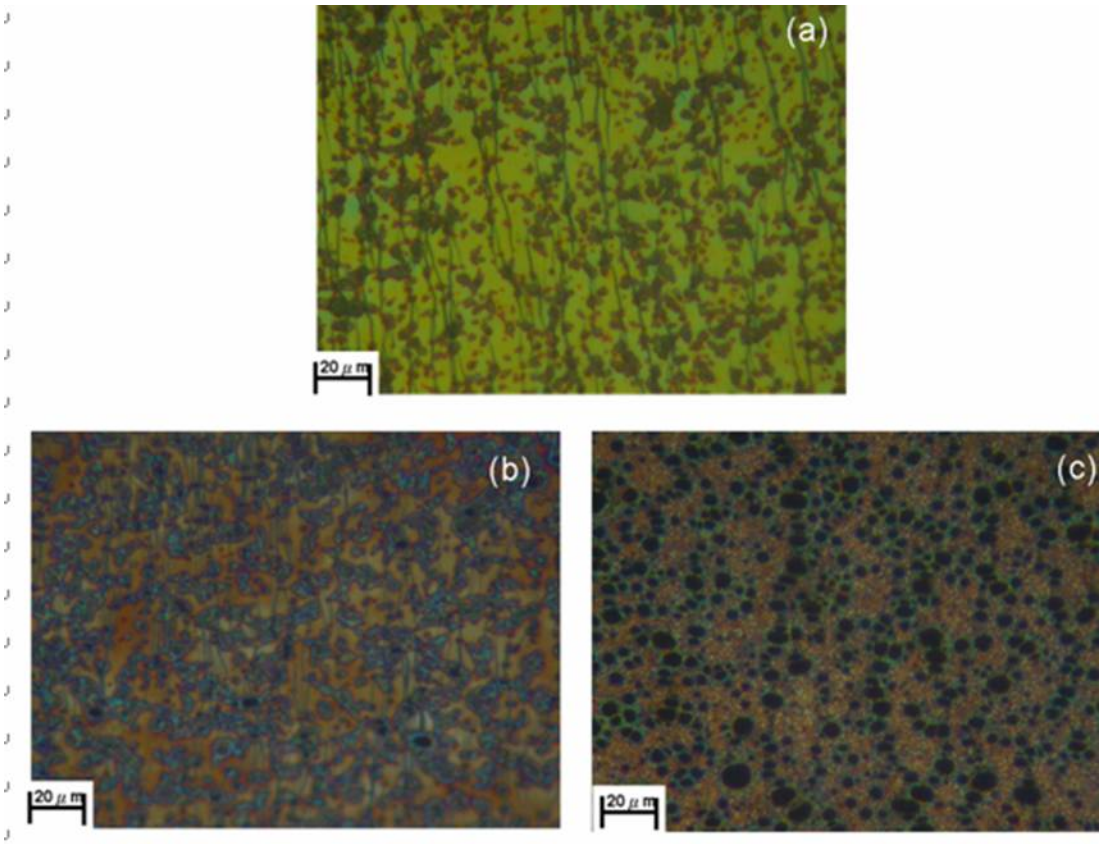

Figure 17. Optical micrograph of PS/ PS-g-MWNT nanocomposite films at 19 % strain with same MWNT loaded but different Mw of Surface grafted PS (a) 10K, (b) 60K, (c) 80K .

1.3.2 Effects of Volume Fraction of MWNTs in the Composite Films

Figure 18a showed the optical micrograph of PS/ PS-g-MWNT nanocomposite films without stretching. The film is loaded with 9 wt% MWNT that grafted with the PS of 60K molecular weight. As the fraction of the MWNTs increases, the surface roughness of the film increases. Upon stretching, crazes as well as shear deformation zones both emerged. Figure 17b shows the coexistence of the crazes and shear deformation zones in the nanocomposite films at 19 % strain. The emergence of the ductile mode of shear deformation indicates a reduction of chain mobility of the entangled network [24] which is generally resulted from increasing of entanglement density [21, 22, 26, 52, 53]. By adding more and more surface-grafted MWNTs, the host polymer chains resist higher stress before undergoing strain softening [24], a clear indication of strong nanotubes-polymer interactions. More detailed study on this type of interactions and its effect of strength of the reinforced polymers is currently underway.

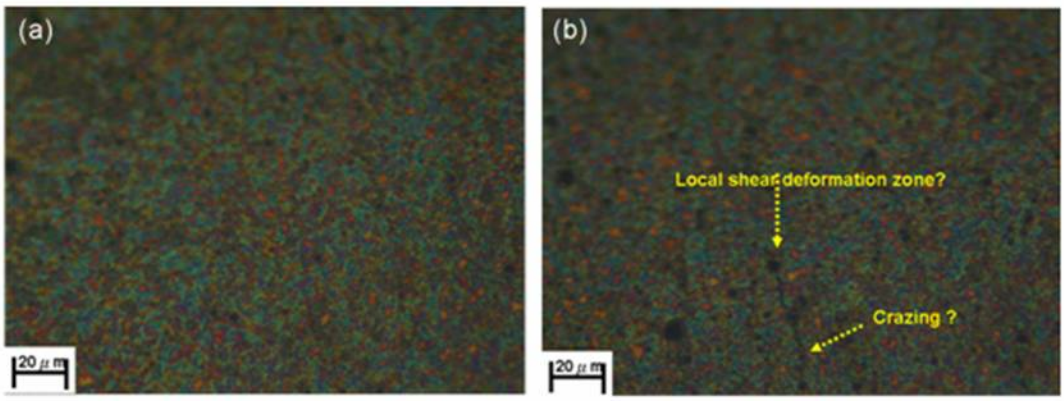

Figure 18. Optical micrograph of PS/ PS-g-MWNT nanocomposite films loaded with 9 wt% MWNTs grafted with chains of Mw 60K: (a) without stretching, and (b) stretched at 19 % strain.

1.4 Dispersion and Reinforcement in Nanocomposites of High Temperature Polymers: PI and PBO

In this section, the host polymer was changed from the model system of polystyrene (PS) into a high temperature rigid-rod polymer which was either

polyimide (PI) or poly(benzoxazoles) (PBO). The rigid-rod polymer was synthesized as a surface grafting polymer from the functionalized nanotubes. Host polymers of the rigid-rod macromolecules were also synthesized for studying the dispersion and molecular reinforcement effects. The electric conductance study of this material was also carried out and the results are presented later in Chapter 3. The work presented here serves as a basis for the quests of novel materials of both ultrahigh strength and thermal/electric conductivity based on soft macromolecules of controlled glass transition temperature.

1.4.1 The Polybenzoxazoles (PBO) System

PBO are a class of heterocyclic polymers of excellent thermal stability with the decompose temperature T_d around 650C. The Young's modulus is around 270 GPa, greater than that of steel fibers. PBO had been developed by US Air Force researchers as a super heat resistant polymer that surpasses Kevlar through the stream of the research of ladder polymers [48]. However, the polymer is brittle, undergoing catastrophic fracture at a low elongation of 2-3%. The chemical structure of PBO is shown in scheme 3. Since the molecular reinforcement by surface-grafted nanotubes is spectacular in the model system of PS, on of the main drive here is to improve the mechanical toughness of PBO by the incorporation of nanotubes.

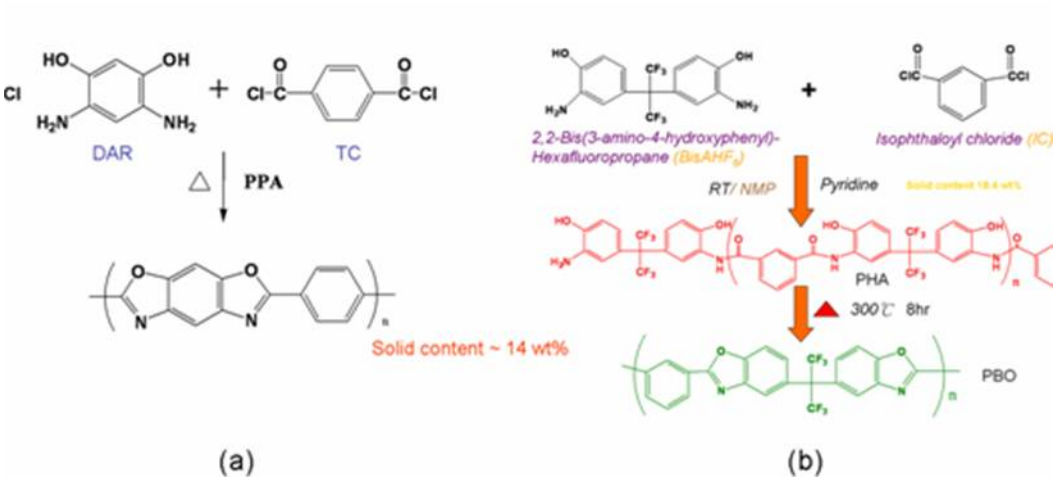

Scheme 3. Synthesis of PBO by (a) one step polymerization , (b) two steps polymerization

PBO can be synthesized in two fashions: (1) one-step polymerization of bis(o-aminophenol)s with aromatic diacid in poly(phospheric acid) (PPA) (scheme 3a) and (2) two-step polymerization of bis(o-aminophenol)s with aromatic diacid chlorides in polar aprotic solvents (scheme 3b). The one-step method is more suitable

for making polymer of high molecular weights. However, since PBO dissolves only in strong acids such as sulfonic acid, this approach is handicapped with the necessity of working with these acids as the processing solvent. The subsequent material processing of blending, grafting, and molding are therefore generally difficult. On the other hand, the two-step polymerization process is a great improvement for this deficiency in that flexible polymer of poly(hydroxyamide) (PHA) was first synthesized and then thermally converted into PBO at 350C when the material processing is completed. In this section, attempts of synthesizing the MWNTs grafted with PBO chains via the one-step or the two-step methods were presented. In the final composite, the percolated network of well-distributed nanotubes was used to strengthen the stress transfer mechanism of this remarkable rigid-rod polymer.

1.4.1a Synthesis of PBO /MWNT Nanocomposite by One-Step Polymerization

Into a 25 mL glass flask, equipped with a mechanical stirrer and a nitrogen inlet/outlet, were placed 426.12 mg (0.002 mol) of 1,4-diaminoresorcinol dihydrochloride, 406.05 mg (0.002 mol) of terephthaloyl chloride, and 1.247 g of phosphoric acid (85%). The resulting mixture was dehydrochlorinated under a nitrogen atmosphere at 65 °C for 16 h and subsequently at 80 °C for 4 h. At this stage, 16.64 mg of MWNT-COOH nanotubes was added to the reaction flask. The mixture was heated to 100 °C for 16 h while stirring and then cooled to room temperature. P_2O_5 (804m g) was added to the mixture to generate poly(phosphoric acid). The mixture was stirred for 2 h at 80 °C and then cooled to room temperature. Further, P_2O_5 (715m g) was then added to the mixture to bring the P_2O_5 concentration to 83% and the polymer concentration to 23wt %. The mixture was heated at 160 °C for 16 h with constant stirring. Stirring opalescence was observed during this step. The mixture was finally heated to 190 °C for an additional 4 h while stirring. An aliquot of the polymer solution (generally referred to as dope) was precipitated, washed in water, and dried under vacuum at 100 °C for 24 h (Scheme 4) [49]. An intrinsic viscosity of 10 dL/g was determined in methanesulfonic acid at 30 °C. A control polymerization of pure PBO was also carried out under the same conditions without adding MWNT-COOH. Intrinsic viscosity values of PBO is 25 dL/g (Mv ≈ 26K, determinate by Mark-Houwink eq) [50]. The MWNT/PBO composite was dissolved in PAA solution. The MWNT/PBO films were spun cast from the solution, and the film thickness was controlled to be around 0.5 μm. The MWNT/PBO films were floated off the substrate on distilled water and the film was washed with de-ionized water again repeatedly until the pH of the filtrate reached 7 to removed PPA. Finally the neutral film bonded onto supporting copper grids.

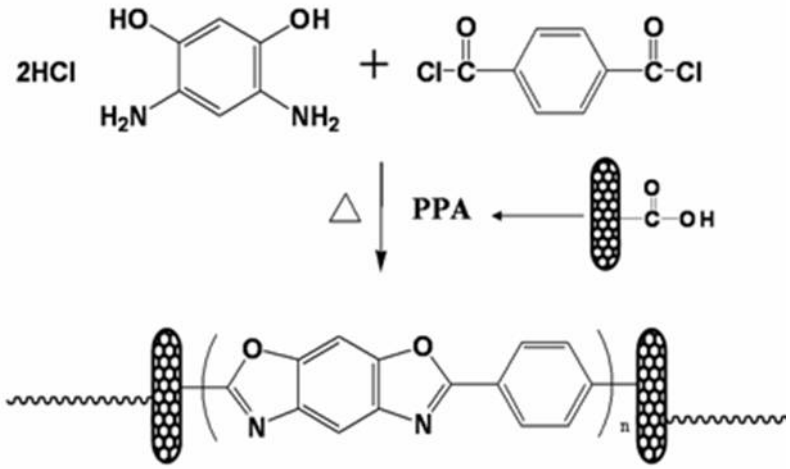

Scheme 4. Synthesis of MWNT/PBO nanocomposite by one step polymerization

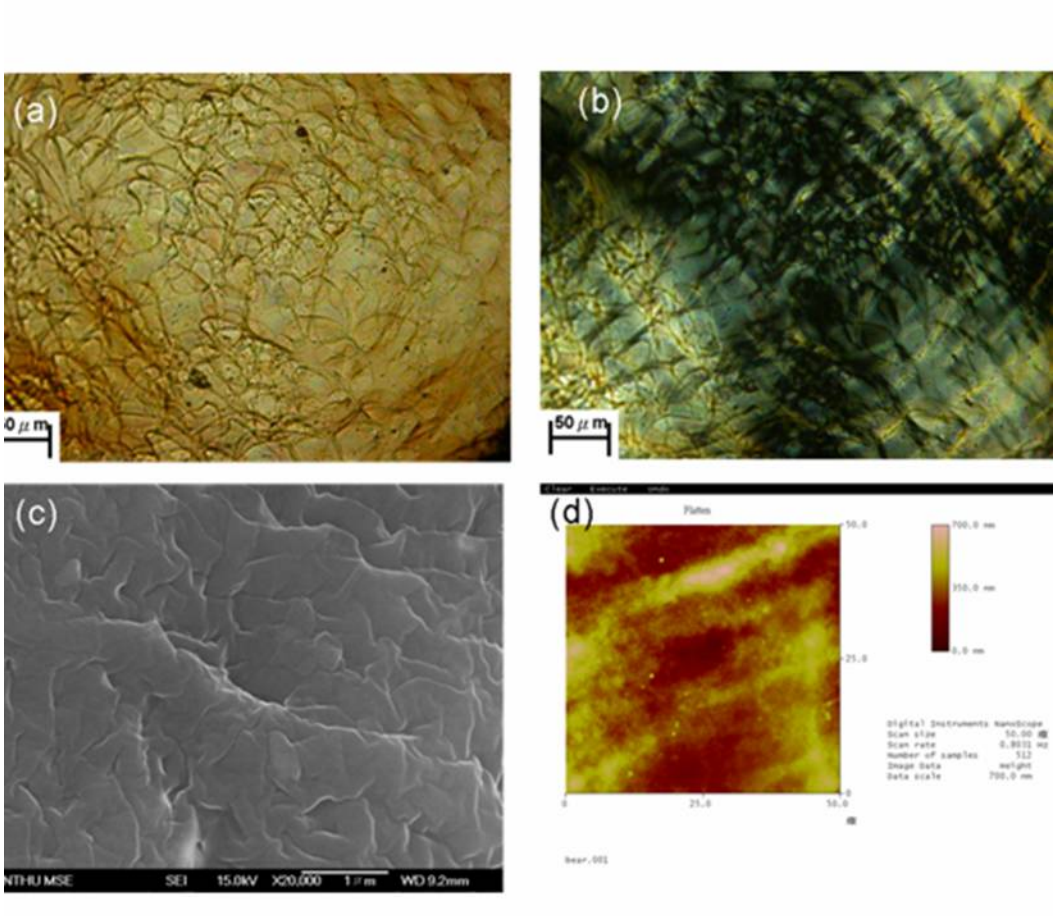

Figure 19. a) Optical micrograph, b) polarized light micrograph, c) SEM, and d) AFM surface topography of the PBO films under no strain.

Figure 19 showed the surface structure of the neat PBO film. Interestingly, there are no prior studies on neat PBO films that can be found in the literatures. The optical

micrograph shown in Figure 19a revealed some surface roughness of the PBO films which when viewed under a pair of cross polarizers show distinctive optical textures, presumably due to the embedded crystallinity. The tendency of chain ordering of the rigid-rod polymer is immense in that mere spin-casting is capable of generating strong crystalline structure. Under SEM and AFM (Figures 19c and 19d), the film, however, demonstrates a sheet-like stacking fine structure. When the films were stretched, local deformation zones emerged in the films. The deformation zones were nucleated after 0.5% strain. As strain increased further, local fibril breakdowns was noted within the deformation zones, indicating that within the crazes began at approximately 5% strain (Figure 20a), and the maximum width of crazes could reach approximately 20 μm. This result revealed the PBO film was very brittle. The TEM micrograph (Figure 20b) of PBO films shows the craze structure was different with typical PS, no fibrils observed inside PBO crazes It maybe that a stiff molecular chain of PBO in the film. Thus when PBO film under crazing, the PBO fibrils are not easily drawn inside the craze from the outside. Furthermore, the PBO fibrils were scission and existed at craze boundary.

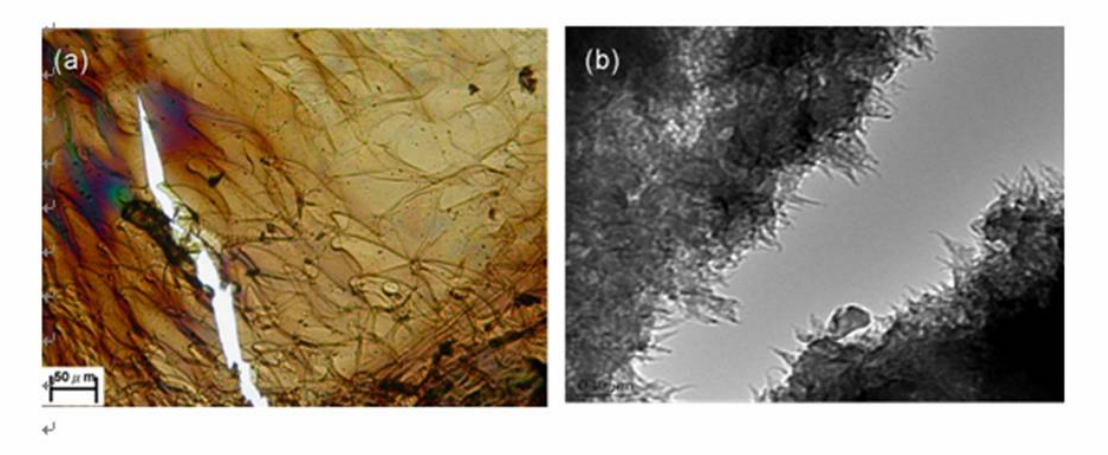

Figure 20. (a) OM and (b)TEM micrograph of stretched PBO films (5% strain)

Figure 21 shows optical micrograph (Figure 21a) and crossed polarizer optical micrograph (Figure 21b) of PBO/MWNT (2 wt%). No aggregates are observed in the PBO/MWNT composite film, suggesting good MWNT dispersion at the optical scale during PBO polymerization conditions. The micro-mechanical testing of PBO/MWNT composite films were shows that no enhanced mechanical property of PBO films. The crazes were nucleated after 0.5% strain. As strain increased further, local fibril breakdowns within the crazes began at approximately 3% strain (not shown in here). Because of the molecular weight of PBO/MWNT composite is lower than neat PBO under same polymerization condition (Mv≈16K vs. 26K, respectively).

Due to the viscosity and solid content of PBO/MWNT system was higher than neat PBO system under polymerization, thus the monomers of PBO were difficult diffusion to reaction sited. Until now we keep going to find out the best condition of synthesis of high Mw PBO/MWNT nanocomposite by one step method.

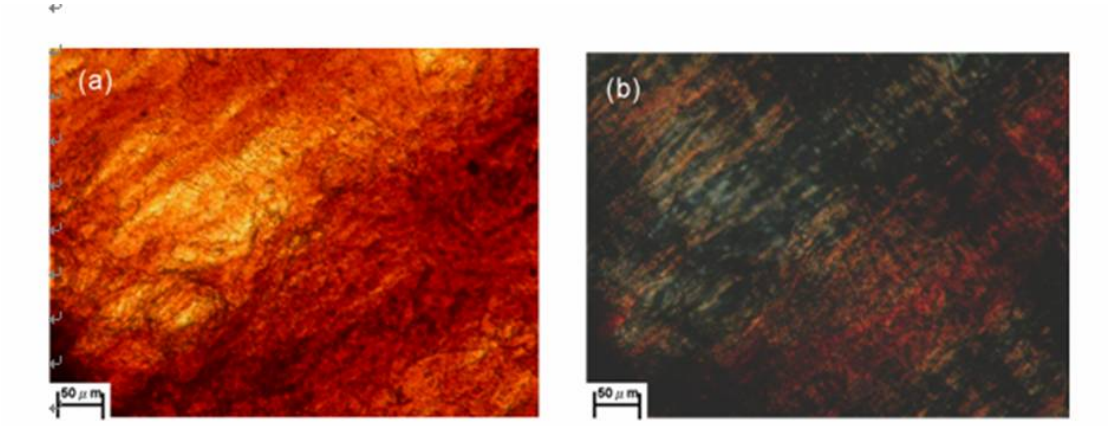

Figure 21. The (a) Optical micrograph (b) polarization Optical micrograph of MWNT/PBO films without stretching.

1.4.1b Synthesis of PBO/ MWNT Nanocomposite by Two-steps Polymerization:

Preparation of poly(hydroxyamide) (PHA) precursor for the two-step process proceeds as follows. To a dry 25ml glass flask equipped with a nitrogen inlet and mechanical stirrer were added 377.58 mg (1mmole) of 2,2-bis(3amino-4-aminophenol) hexafluoropropane (BisPF6), 162.89 mg (2mmole) of anhydrous pyridine and 4 ml of anhydrous NMP. After the BisPF6 was completely dissolved, the solution was cooled to 5℃with ice water bath and isophthaloyl chloride (IC) (207.16 mg, 1mmole) was added slowly to the solution. The reaction mixture was stirred at room temperature for 16 h. The viscous solution was added water to precipitated polymer and wash with methanol, and then dried at 80℃for 24 h. Intrinsic viscosity values of PHA is 0.97 dL/g measured at 30℃ in NMP. The PHA can be converted into PBO upon subsequent heating at 350 ℃ 8hr (scheme 3b).

Synthesis of the grafting PHA follows the main flow chart of that described in the preceding section with only the difference being fine tuning the BisPF6 and IC mole ratio to 1:0.98, to form BisPF6 terminated PHA prepolymer. The MWNT-COCl was then added into the reactor. The reaction mixture was stirred at room temperature for 16 h (scheme 5). The resulting viscous solution was washed in NMP by sonication and then vacuum-filtered through a 0.2μm PTFE membrane to remove the free polymer.

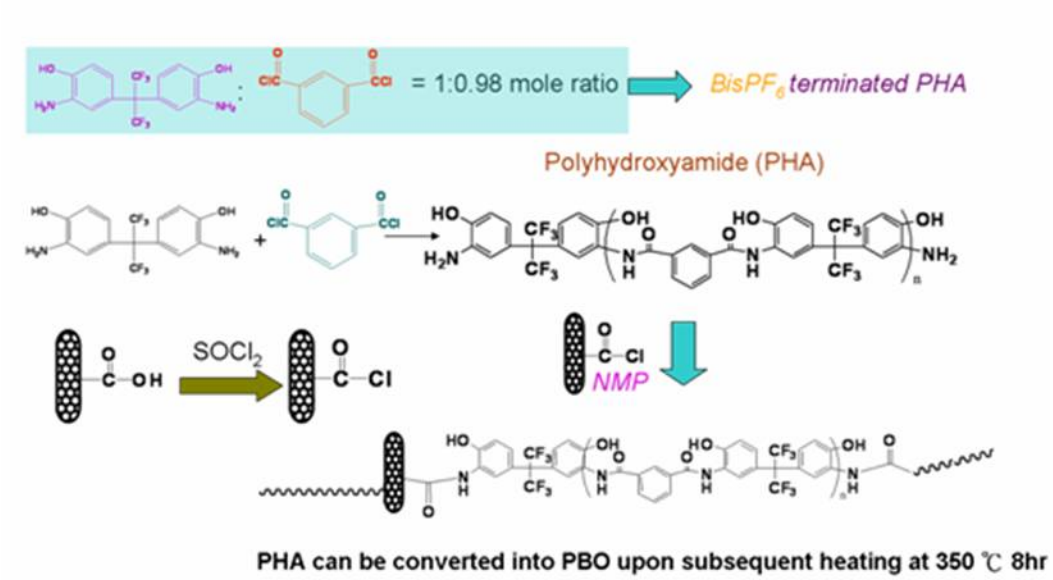

Scheme 5. Synthesis of PHA or PBO grafted-MWNT via two steps polymerization

Fourier-Transform Infrared spectroscopy (FTIR) was used to identify the existence of PHA and PBO grafted on the MWNT (Figure 22). After graft polymerization, new peaks were observed emerging in the frequency range from 2800 cm^{-1} to 3200 cm^{-1} that contained absorptions due to sp2 (=C-H) bond stretching (3000 ~ 3200 cm^{-1}) and sp3 (-C-H) bond stretching (2800 ~ 3000 cm^{-1}), both being clear evidence for PHA grafting on the MWNTs (Figure 22a). After heating at 350 ℃ 8hr the PHA grafted MWNT can be converted into PBO grafted MWNT (Figure 22a).

The fine nanostructure of PHA grafted MWNT was measured by transmission electron microscopy. As shown in figure 23a, the MWNTs are wrapped by PHA chains can be observed. This suggesting that the PHA was effective grafted on MWNT. Thus the MWNT-g-PHA can well-dispersed in common solvent such as NMP (figure 23b). On the other hand from the TGA data (at heating rate of 10 ℃ /min from RT to 800 ℃ under a N_2 atmosphere, figure 24), the difference in the weight loss at 800 ℃ between MWNT-g-PHA and MWNT-COOH shows that the PHA graft amount to ~89% of total weight of the synthesized MWNT-g-PHA.

Problems still being worked on:

We also try prepared to PHA/MWNT nanocomposite via MWNT-g-PHA and neat PHA. But it is very difficult to preparation of composite films. Because of molecular weight of PHA is to low, the inherent viscosity of PBO is abut 1 dl/g (Mv ≈ 4300, determinate by Mark-Houwink eq), already the highest ever reported in the

literatures. The humidity is very sensitive in polymerization reaction by two step method.

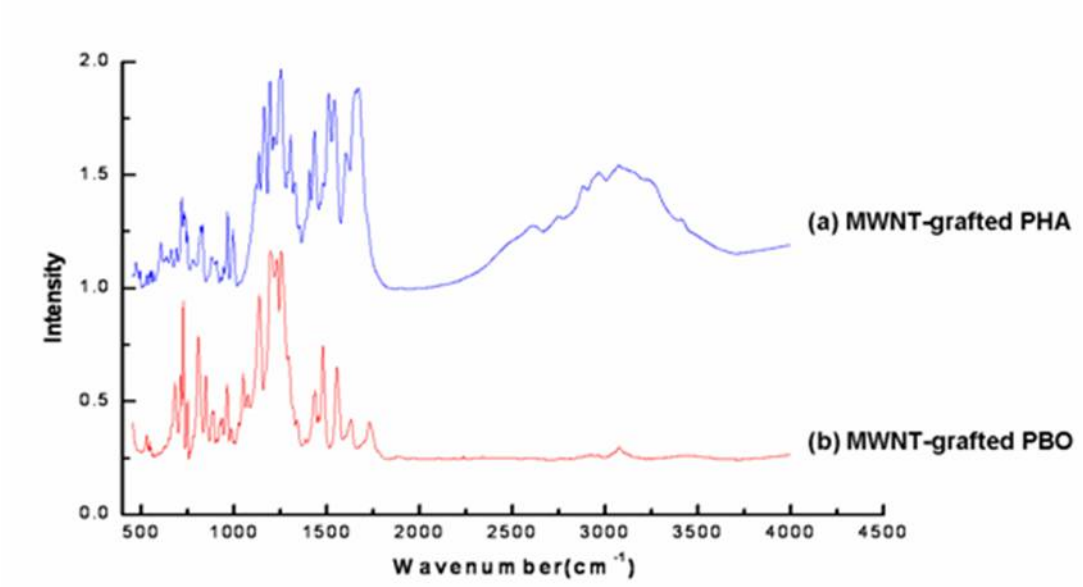

Figure 22. FTIR spectrum of (a) MWNT-grafted PHA, (b) MWNT-grafted PBO

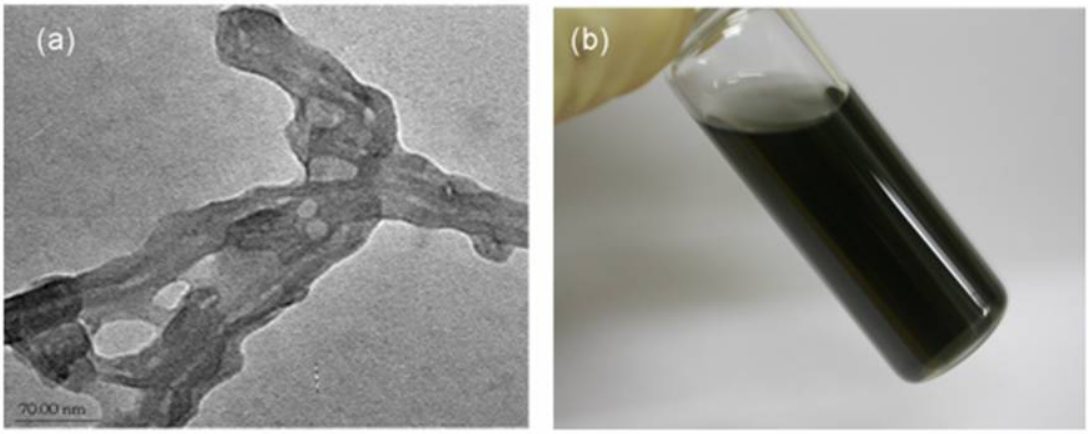

Figure 23. (a) The TEM micrograph shows that MWNTs are wrapped by PHA chains. (b)The MWNT-g-PHA can well disperse in common solvent such as NMP.

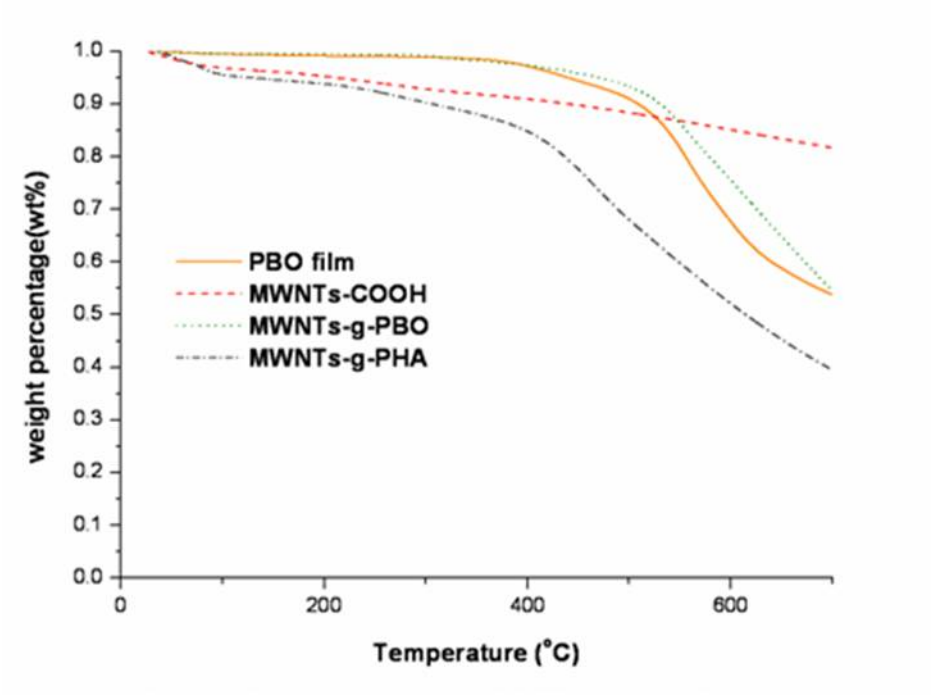

Figure 24. TGA analysis of MWNT-grafted PHA

1.4.2 The Polyimide System

Because aromatic polyimides have outstanding thermal, mechanical, and electrical properties as well as solvent resistance, they have been used for interlayer dielectric for semiconductor devices, wire coating materials, or as substrates for flexible printed circuits. Here we report an approach by synthesizing MWNT-bound amino functional group for reactions with anhydride in polyimide polymerization. The resulting polyimide functionalized carbon nanotubes were found to be soluble in the common solvent such as NMP. A significant advantage with this approach is that the functionalized nanotube samples can be used directly for polyimide-carbon nanocomposites of relatively higher nanotube contents.

Synthesis of MWNT-grafted PAA and MWNT-grafted PI

Chemical functionalization of MWNT–NH_2 was carried out using the acid chloride and amide. MWNT-COOH sample (20 mg) was stirred with 3 ml of $SOCl_2$ at 45 ℃ for 16 h. The mixture was cooled, diluted with 3 ml THF, filtered through a PTFE membrane filter and washed with THF. The resulting solid of MWNT-COCl was suspended in 6 ml DMAc, phenylendiamine (PDA) to suspension together. After shaking for 2 h the mixture was centrifuged at 8000 rpm for 3 min, decanted, four times washed with DMAc and finally with iso-propanol and filtered through a membrane filter (pore size 0.2μm).

Synthesis of MWNT grafted PAA was prepared as follows. 4,4-diaminodiphenylether (ODA) (2.0024g, 0.01mol) and MWNT–NH_2 were dissolved in dry DMAc (10 mL) in a round-bottom flask. After the solution was cooled in an ice bath for 15 min, pyromellitic dianhydride (PMDA) anhydride (2.18g, 0.01mol) was added with vigorous stirring. The ice bath was removed after 1 h, and the reaction mixture was maintained at room temperature for 36 h. finally, the viscosity solution was diluted with DMAc and filtered through a membrane filter (pore size 0.2μm) to remove the free polymer. PAA can be converted into PI upon subsequent heating at 300 ℃ 8hr (scheme 6).

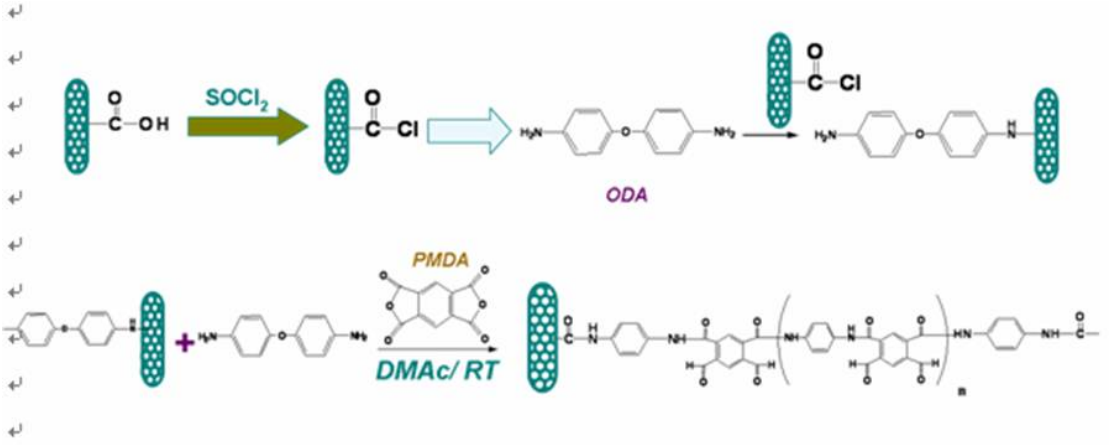

Scheme 6. Synthesis of PAA(PI)-grafted-MWNT

Preparation of PI/MWNT-grafted PI nanocomposite:

Preparation of PI/MWNT-grafted PI nanocomposite was used direct mixed. The MWNT-grafted PAA and neat PAA were dissolved in DMAc with a mechanical stirrer. The MWNT/PAA films were spun cast from the solution, and dried in room temperature for 24 h. finally steps heating from RT to 300 ℃ and hold for 8 h.

The bulk nanostructure and morphology of MWNT-grafted PAA was observed with scanning electron microscopy (SEM), as shown in Figure 25a. The PAA functionalized MWNTs look thick compared to the pristine MWNTs. On the other hand the MWNT-g-PAA was also well-dispersed in common solvent such as NMP (figure 25b). In PI/MWNT-grafted PI nanocomposite, a uniform network of MWNT covered by molten polymer emerged after etching (Figures 26), attributable to a large difference in etching rate between polymer and carbon nanotubes. The average external diameter of the emerged nanotubes was consistent with the original specification of around 30 nm. About the mechanical properties of PI/MWNT and

PBO/MWNT nanocomposite we are still being worked on.

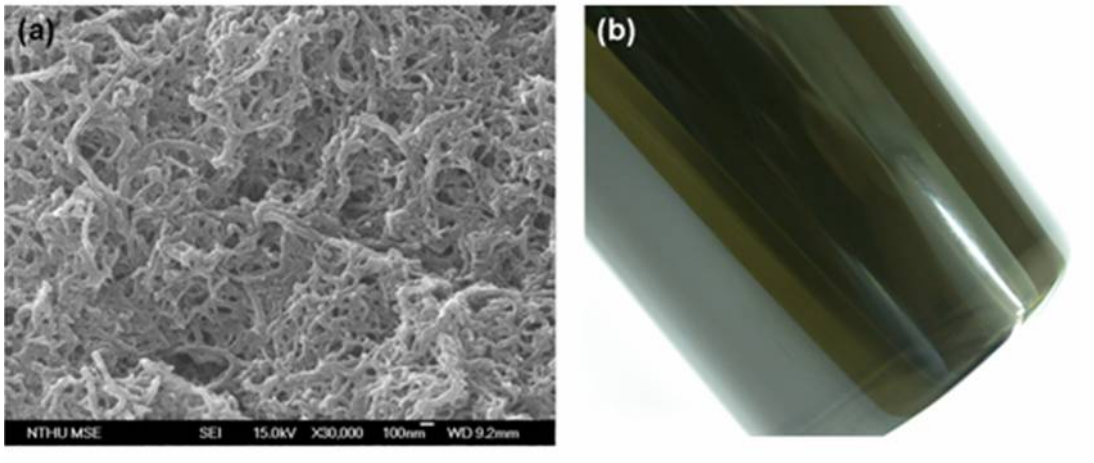

Figure 25. (a) SEM micrograph of the surface-grafted nanotube, PAA-g-MWNT, and (b) the PAA-g-MWNTs disperse well in common solvent such as NMP.

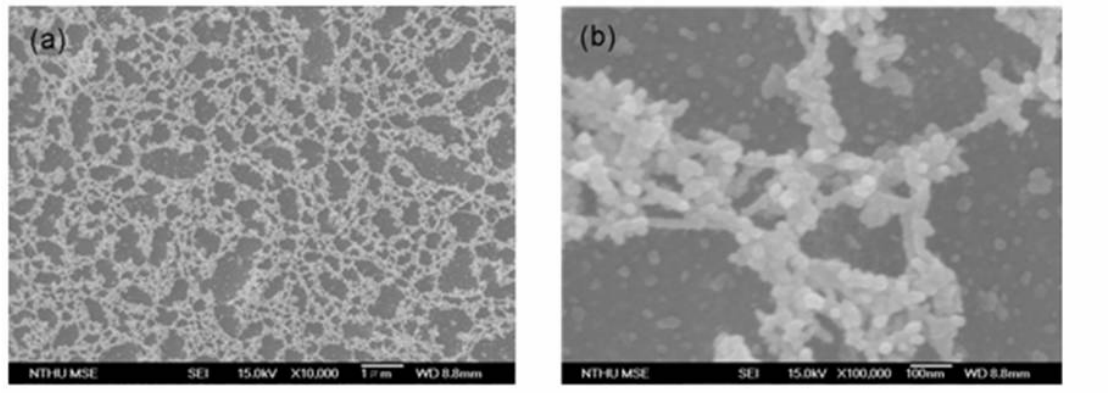

Figure 26. SEM micrograph of plasma-etched MWNT/PI film showing the nanotube network.

Chapter 2

Covalent crosslinking of surface-grafted nanotubes in polymer nanocomposites

We employed the ATRP (atomic transfer radical polymerization) method to grow polymers from the carbon nanotube surface. ATRP is a living polymerization method for producing well-controlled chain length of macromolecules. We expect the covalent bonds of the well-dispersed nanotubes to trigger excellent mechanical behavior of the nanotubes for the composites. (Grafting only exerted passive effects through constraining of the polymer chains.) The polystyrene is supposed to wrap on the surface of MWNTs because of π-π interaction, enabling the chain end of the polystyrene to remain on the surface of MWNTs. In order to solve the problem, synthesis of prepolymers by employing ATRP was used, where the polymer chain end reacts with functionalized MWNTs.

First, initiators with only one bromide was used, where divinyl benzene (DVB) was very important to crosslink MWNTs. The results of the experiment indicate that concentrations of Crosslinked-MWNTs are 4.1% and 11%. Craze always grows passing around the aggregates, and measured approximately 2um in width. It seems to indicate the existence of something different in the aggregates that are capable to provide additional local strength there. While there can be no doubt that the morphology of craze is very different, the results point to the gap between our knowledge of strength mechanisms and the behavior of Crosslinked-MWNTs observed here.

Next, initiators with two bromides were used. Switching the initiator from one bromide to two is advantageous since syntheses become controllable and the use of DVB unnecessary. The Crosslinked-MWNTs/PS films at 21.5% strain obviously decreased to less than 1 micron in width. MWNTs-network of Crosslinked-MWNT/PS film was presented under SEM micrograph. However, the issues which has been often mentioned but not extensively explored include the percentage of MWNT crosslinking and the differences between the films of MWNTs/PS and Crosslinked-MWNTs/PS.

2.1 ATRP Methods for Synthesizing Linear Bridges between Nanotubes

2.1.1 Experimental Section

Our experimental research involved four key steps. First, acid treatment of

MWNTs was used and dried MWNT-COOH was subsequently suspended in $SOCl_2$. This reaction caused MWNT-COOH transfer to MWNT-COCl. The MWNT-COCl was mixed with glycol to produce MWNT-OH. Next, anhydrous $CHCl_3$, DMAP, and triethylamine was evacuated and thrice filled with N_2. Afterwards, 2-bromo-2-methylpropionyl bromide was added. The product which acts as ATRP's initiator was produced. Furthermore, MWNT-Br, CuBr, PMDETA, diphenyl ether and styrene monomer reacted together to produce MWNT-PS. Finally, MWNT-PS reacted with MWNT-CMS. MWNT was linked by polystyrene and formed chain-linked MWNT between polystyrene. This was named Crosslinked-MWNT. The procedures are described in detail below, with a flow chart was shown in Scheme 7.

(1) Synthesis of MWNT-OH：

Dried MWNT-COOH was suspended in $SOCl_2$ and stirred at 65 °C for 24h. The solid was then separated by filtration and washed with anhydrous THF. Subsequently, it was dried under vacuum at room temperature for 2 h to give carbonyl chloride group-functionalized MWNT (MWNT-COCl). The MWNT-COCl was mixed with glycol and stirred at 120 °C for 48 h. The solid was then separated by vacuum filtration using a 0.22 *i*m polycarbonate membrane as mentioned above and washed with anhydrous THF. After repeated washing and filtration, the resulting solid was dried overnight in a vacuum to give hydroxyl group-functionalized MWNT (MWNT-OH).

(2) Synthesis of MWNT-Supported Initiator (MWNT-Br)：

A flask containing MWNT-OH , anhydrous $CHCl_3$, DMAP , and triethylamine was evacuated and thrice filled with Ar. Then 2-bromo-2-methylpropionyl bromide dissolved in 5 anhydrous $CHCl_3$ was added drop-wise at 0 °C for 60 min. The resulting mixture was stirred for 3 h at 0 °C and then at room temperature for 48 h. The solid was then separated from the mixture by filtration and washed five times with $CHCl_3$. The raw product was dispersed in $CHCl_3$, filtered, and washed three times to remove any adsorbed 2-bromo-2-methylpropionyl bromide. The black solid was collected and dried overnight under vacuum at 40 °C, affording MWNT-supported ATRP initiator (MWNT-Br). The reaction process is described in Scheme 7.

(3)Synthesis of MWNT-PS：

Typically MWNT-Br, CuBr, PMDETA, and diphenyl ether were placed in a dry flask, which was then sealed with a rubber plug. The flask was evacuated and filled thrice with N_2, then styrene was injected into the flask using

a syringe. The flask was immersed in an oil bath at 100 °C, and its contents were stirred for 50 h. By the end of the reaction the viscosity had increased dramatically. The mixture was subsequently diluted with $CHCl_3$ and thrice vacuum-filtered using a 0.22 *ím* polycarbonate membrane. To ensure that no free polymer or free reagents were mixed in the product, the filtered mass was dispersed in $CHCl_3$, then filtered, and washed with $CHCl_3$. The resulting solid was re-dispersed in 5 mL of $CHCl_3$ and precipitated by the addition of methanol. The PS-coated MWNT sample was obtained by filtration and drying overnight under vacuum.

(4) Synthesis of MWNT-PS-MWNT (Crosslinked-Nanotube):

MWNT-PS, CuBr, PMDETA, and diphenyl ether were placed in a dry flask, which was then sealed with a rubber plug. The flask was evacuated and filled thrice with N_2. Afterwards, MWNT-CMS dispersed in $CHCl_3$ was injected into the flask using a syringe. The flask was immersed in an oil bath at 100 °C, and its contents were stirred for 50 h. After 50h, the result solid was precipitated in methanol. The Crosslinked-Nanotube sample was obtained by filtration and drying overnight under vacuum.

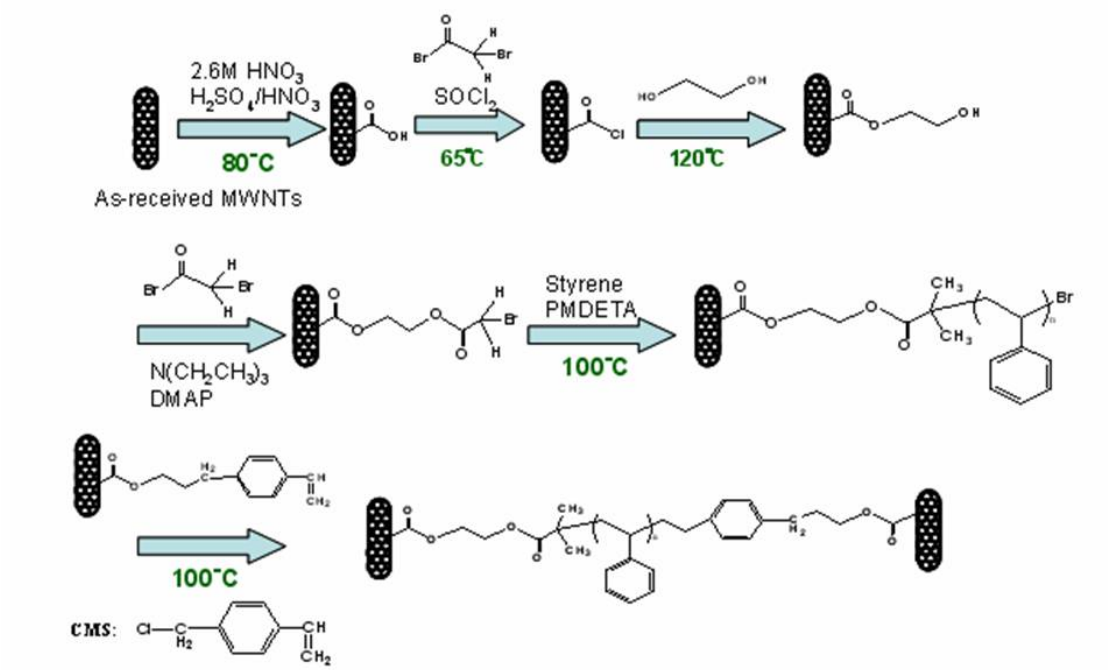

Scheme 7. The procedure of Crosslinked-MWNT.

2.1.2 Results and Discussions

Fourier-Transform Infrared spectroscopy (FTIR) was used to identify the existence of carboxylic acid groups、OH、-Br、grafted polystyrene chains in the samples. The differences between the FTIR spectra, shown in Figure 27, of the

as-received MWNTs, acid-treated MWNTs 、MWNT-Br 、MWNT-PS and Crosslinked-MWNT were noted. The differences between the FTIR spectra, shown in Figure 27, of the as-received MWNTs, acid-treated MWNTs, MWNT-OH, MWNT-Br, MWNT-PS and Crosslinked-MWNT were noted. Two new peaks emerged at 1720 and 3400 cm^{-1} after the acid treatment corresponded respectively to C=O and -OH stretching, confirmed the attachment of the carboxylic acid groups onto the MWNTs. The substitution of carboxylic acid group by ester group during reaction with CMS caused a decrease -OH at 3400 cm^{-1} and a shift of C=O peak from 1720 to 1680 cm^{-1}. For MWNT-OH, the stronger OH absorption peaks were observed at 3400 cm^{-1} .When MWNT-OH transferred to MWNT-Br, the strong OH absorption peaks and C-O-H peaks at 1040 cm^{-1} disappeared. After the graft polymerization, new peaks were observed to emerge in the frequency range from 2800 to 3200 cm^{-1} corresponding to sp^2 (=C-H) stretching (3000–3200 cm^{-1}) and sp^3 (-C- H) stretching (2800–3000 cm^{-1}), a clear evidence for PS grafting on MWNTs. Finally, after adding MWNT-CMS, there were the same peaks with MWNT-PS.

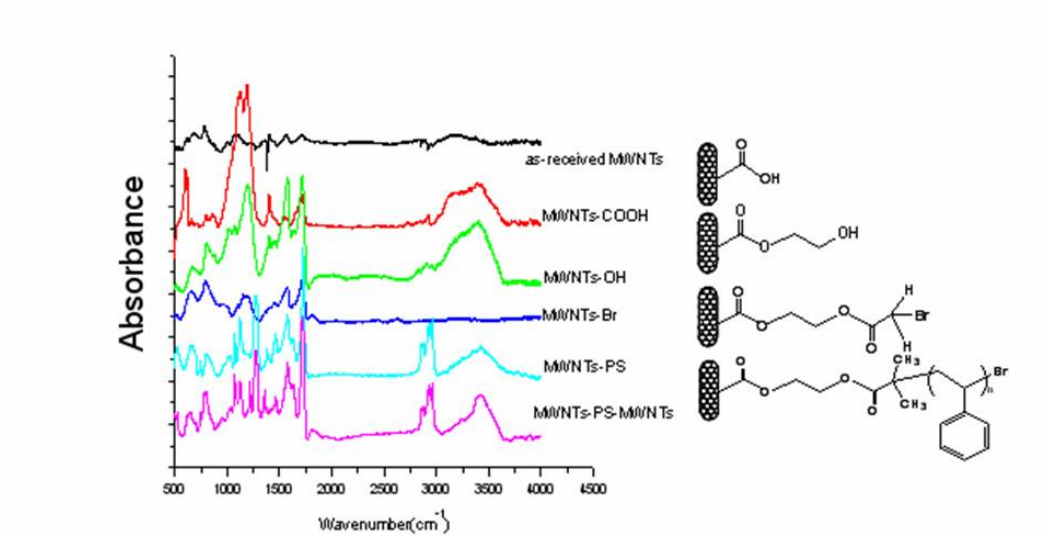

Figure 27. The FTIR spectra of the as-received MWNTs, acid-treated MWNTs , MWNTs-OH, MWNT-Br, MWNTs-PS and MWNTs-PS-MWNTs (attrevitive Crosslinked-MWNTs)

TGA analysis (Figure 28) was used to determine the PS weight fraction in the Crosslinked- MWNTs. Indicative of the purity, the as-received MWNTs retained more than 96% weight fraction up to 1000 ◦C. The carboxylic MWNTs showed a similar but slightly greater weight loss, attributable to the pyrolysis of carboxylic acid groups on CNT surfaces. For Crosslinked-MWNTs, the TGA weight fractions underwent a sharp decrease at around 350 ◦C, signifying the onset of pyrolysis of the PS chains grafted on Crosslinked-MWNTs. The weight loss subsequently slowed

considerably beyond 450 ◦C, a temperature at which the PS had essentially burnt out, after which a constant decreasing rate comparable to that of the as-received MWNTs in the same temperature range was observed. The weight fraction of grafted PS on the Crosslinked-MWNTs was determined from the asymptotic cross-sections drawn from the thermogravimetric curve to be approximately 12%.The molecular weight of polystyrene between MWNTs was 15k determined by GPC. On the other hand, the Crosslinked-MWNTs were then blended with high molecular weight PS (Mw = 2M) in toluene for casting thin polymer films. The film thickness was around 0.5 μ m. The concentration of Crosslinked-MWNTs in the solution was adjusted so that the nanotube weight fraction, excluding the grafted polymer, was 10 wt.% in the solid films. As shown in Figure 29a, the solution of MWNT-PS was transparent, indicating that the global dispersion of the CNTs in the toluene was excellent. By contrast, the dispersion of Crosslinked-MWNTs was markedly inferior and Crosslinked-MWNTs were deposited on the bottom of the bottle. The result may be supposed that the polystyrene molecular weight between MWNTs was not enough. The mechanical properties of the nanocomposite thin films of Crosslinked-MWNT/PS were showed in Figure 29b. Some sporadic MWNTs aggregates were spotted under an optical microscope. After mechanical stretching, the film broke at 18% strain.

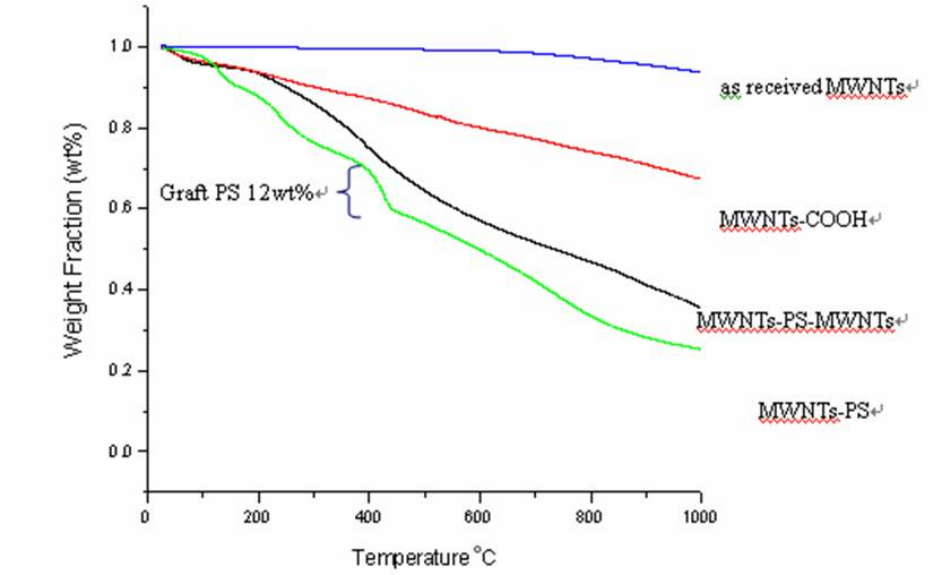

Figure 28. Thermogravimetric curves of the as-receivedMWNTs(purity >−96%), acid-treatedMWNTs , MWNTs-PS and MWNTs-PS-MWNTs(Crosslinked-MWNTs).

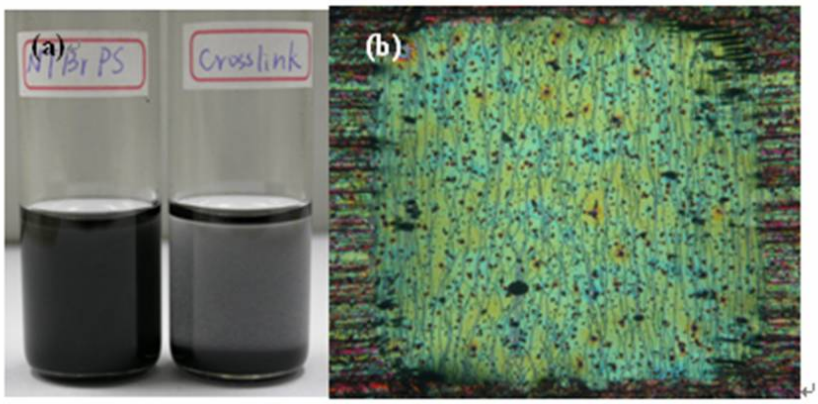

Figure 29. The toluene solutions of PS (*M*w = 2M) blended with 1%, respectively, of (a) MWNTs-PS (left) and Crosslinked-MWNTs (right). (b) Optical micrograph Crosslinked-MWNT/PS films coated on copper grids, with stretching at 18% strain and local deformation zones.

2.1 ATRP Methods for Covalently Bridged Nanotubes with Crosslinked Chains

The polystyrene is supposed to wrap on the surface of MWNTs because of π - π interaction. This makes the chain end of polystyrene still stay on the surface of MWNTs. In order to solve the problem, synthesis of prepolymer by employing ATRP was used and the polymer chain end reacts with functionalized MWNTs.

2.2.1 Experimental Section

A flask contained CuBr and PMDETA in DMAc solvent. Under N_2 environment styrene and Ethyl-2-bromoisobutyrate as an initiator were added into DMAc. The solvent was then placed under 110℃ in oil bathing. After 1 hour, divinyl benzene (abbreviated as DVB) was added into the flask. It was very important when DVB was added because the length between MWNTs was decided by the length of polystyrene after adding DVB. DVB was divided into two parts to add. The ratio of DVB compared with Initiator was 0.06. After the 24 hour reaction, MWNTs-CMS dispersed in styrene were added to form Crosslinked-Nanotubes. The products were then precipitated in methanol. The precipitation process was repeated at least three times. Excessive CuBr, PMDETA and unreactive monomers were then cleaned away. The flow chart is shown in Scheme 8.

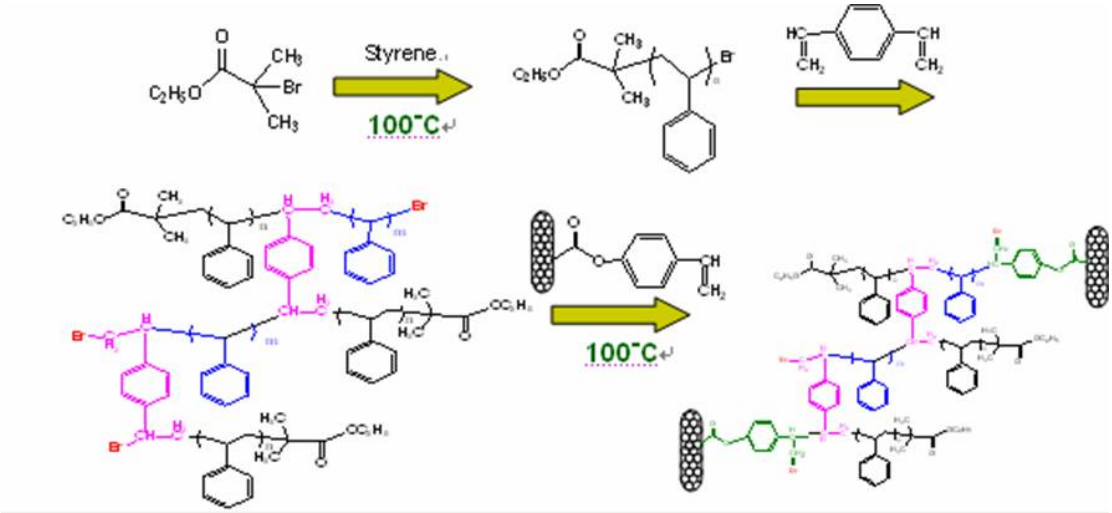

Scheme 8. The procedure of Crosslinked-MWNTs by synthesizing crosslinked polymer .

2.2.2 Results and Discussions

Mechanical properties on Microscopic Deformation Behavior

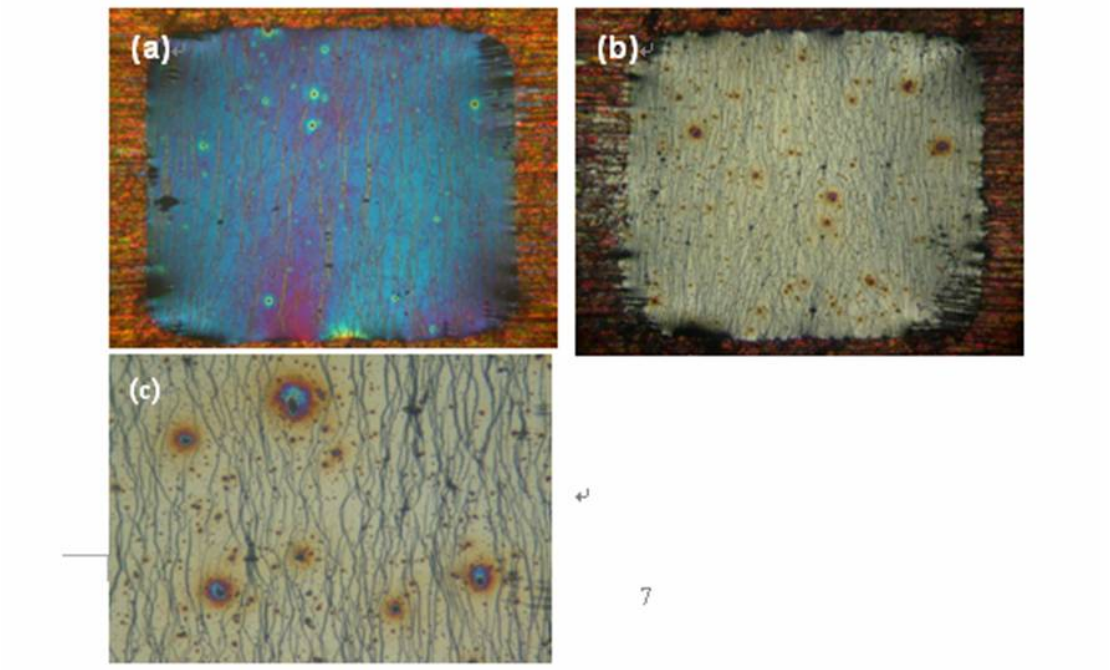

Figure 30.Optical micrograph of Crosslinked-MWNT/PS films coated on copper grids: (a) the film at 18.6% strain with 4.1% CNT and (b) the film at 19.7% strain with 11% CNT. (c)Different magnification of the film at 19.7% strain with 11% CNT.

The different percentages of Crosslink-MWNTs were added respectively. The Crosslinked-MWNTs were then blended with high molecular weight PS (Mw = 2M) in toluene for casting thin polymer films. The film thickness was around 0.35 μm. The different concentrations of Crosslinked-MWNs in the solution was adjusted so

that the nanotube weight fraction, excluding the grafted polymer, was 4.1% and 11% respectively in the solid films drawn from the thermogravimetric curve shown in Figure 31a and 31b.

Then the experiment of mechanical strengthening test was conducted. The result of the experiment was that the films with 4.1% CNT broke at 18.6% while the other broke at 9.7% strain. AFM analysis was used to identify the morphology of those films and the maximum attainablewidth of crazes was approximately 2 *u*m as determined from AFM surveys shown in Figure 32 and Figure 33.

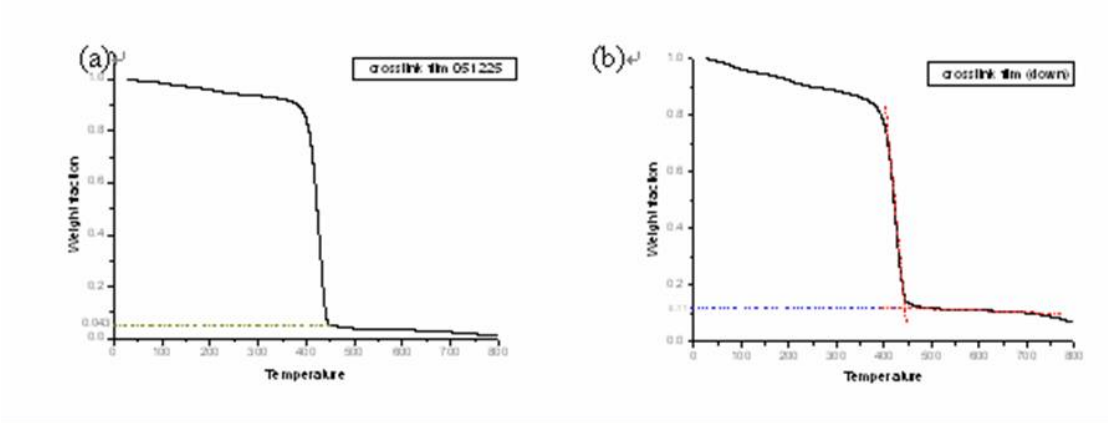

Figure 31.Thermogravimetric curves of the film mixed with Crosslinked-MWNTs and PS(Mw=2M).

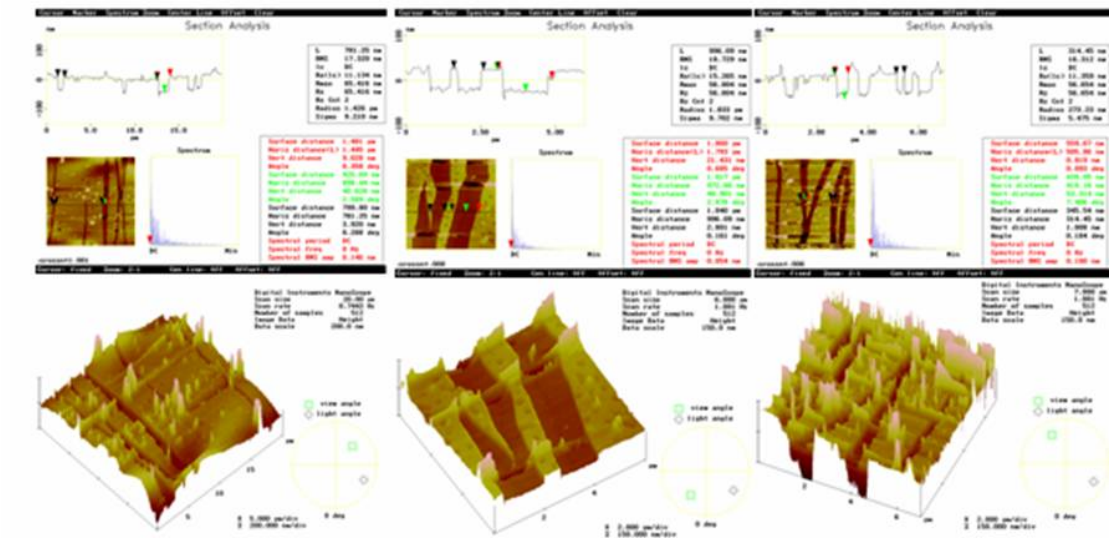

Figure 32. AFM micrograph of crazes in Crosslinked-MWNTs/PS films with 4.1% MWNT at 18.6% strain.

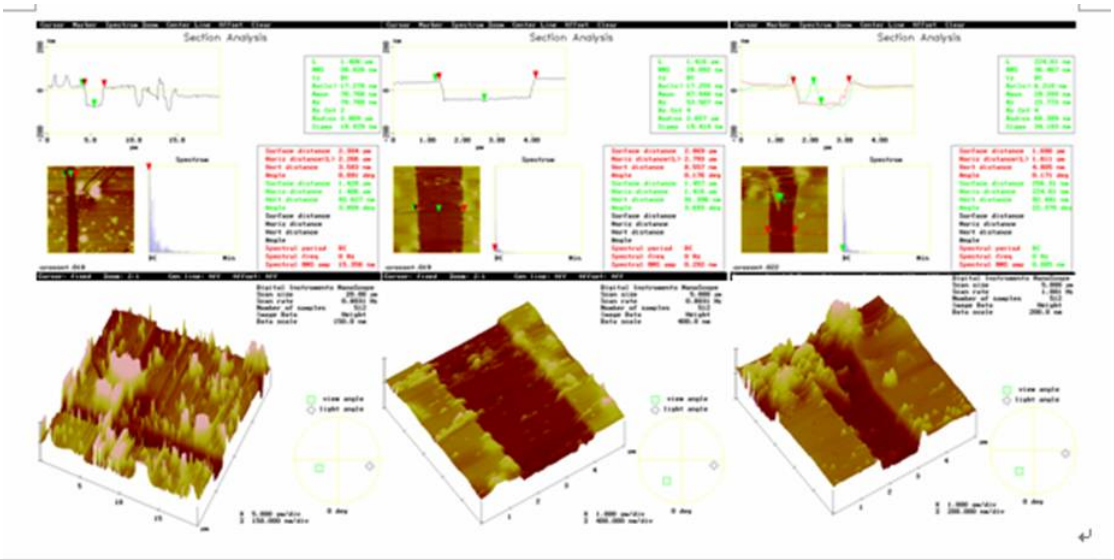

Figure 33. AFM micrograph of crazes in Crosslinked-MWNTs/PS films with11% MWNT at 19.7% strain.

Since MWNT-CMS does not disperse easily in Toluene or in DMAc, during crosslink MWNT procedure it produced a lot of aggregates. In order to improve the dispersion of MWNTs-CMS, grafting polymer to MWNTs-CMS was necessary. To solve this problem, we used ATRP method to graft polystyrene with a molecular weight of 6000 on MWNT-CMS to improve MWNT-CMS dispersedly. A flow chart was shown in scheme 9. The processes were divided into three parts. One was Prepolymer preparation. Next, Functionalization of MWNTs-CMS was described. Finally, the synthesis of Crosslinked-MWNTs was the focus.

2.3 Prepolymer Methods

Part 1：Prepolymer preparation

A. By using the method of ATRP to synthesize polystyrene. Since, the two ends of polystyrene is Br, therefore abbreviated as dibromopolystyrene. CuBr and PMDETA were added into DMAc solvent. Under nitrogen gas environment styrene monomer and initiatorα-dihalogeno-p-xylene (α) were added as an initiator into DMAc. The solvent was than placed under 110℃ in oil bathing for 24 hours. After the 24 hour reaction, the polystyrene was precipitated in methanol. The precipitation process was repeated at least three times. Excessive CuBr, PMDETA and unreactive monomers was then cleaned away. Poltstyrene that had already been cleaned was placed into vacuum oven at 60 ℃ for 24 hours to remove excessive methanol.

B. Br, the polymer chain end functionalized to vinyl group. This is because the chain end of polystyrene is vinyl group, thus it can be abbreviated as

divinylpolystyrene. Sodium was dissolved in dried ethanol, and this formed into EtoNa. EtoNa then went under depressurized distillation until ethanol was completely removed. Polystyrene dispersed in Toluene was then placed into EtoNa that had already undergone depressurized distillation. The mixed solution was then stirred under room temperature for 48 hours. The solution was precipitated in methanol several times to clear excessive EtoNa. The functionalized chain end of polytstyrene was set into a vacuumed oven at 60℃ for 24 hours to remove excessive solvent.

Part 2：Functionalization of MWNTs-CMS

A. Prepare 4-Vinylbenzyl chloride (abbreviated as CMS) to be grafted to MWNT (abbreviated as MWNT-CMS). EtoNa then went under depressurized distillation until all the ethanol was removed. Acid treatment MWNT was added into EtoNA and dispersed within Toluene. The solution was then placed in 40°C water and underwent ultrasonic vibration for 60 minutes. During this procedure MWNT-COOH transformed into MWNT-COONa. We then add CMS and continue ultrasonic vibration for two hours. After this procedure the MWNT-COONa will be replaced by MWNTs-COOR (R = $CH_2C_6H_4CHCH_2$). After removing excessive EtoNa and CMS and placing it in a vacuum oven at 40°C for 6 hours. The product is a black solid which is MWNT-CMS.

B. Using ATRP method on MWNT-CMS to graft polystyrene (abbreviated as MWNT-PS). CuBr and PMDETA were added into DMAc solvent. Under nitrogen gas environment added MWNT-CMS, styrene monomer was added. Subsequently, Ethyl 2-bromoisobutyrate was added as an initiator into DMAc. The solvent was than placed in oil bathing for 24 hours at under 110℃. After the 24 hour reaction, the product was precipitated in methanol. The precipitation process was repeated at least three times. Excessive CuBr, PMDETA and unreactive monomers were then cleaned away. The cleaned MWNT-PS was then placed in 80 ℃ vacuum oven for 24 hours to remove excessive methanol.

Part 3：Synthesis of Crosslinked-Nanotube

Divinylpolystyrene was disolved into the DMAc solvent. Under nitrogen gas environment MWNT-CMS, CuBr, and PMDETA were added to DMAc solvent because the MWNT-PS chain end is Bromide, an alkaline group that functions as an initiator. The chain end of divinylpolystyrene contains unsaturated double bond that acts as monomers.

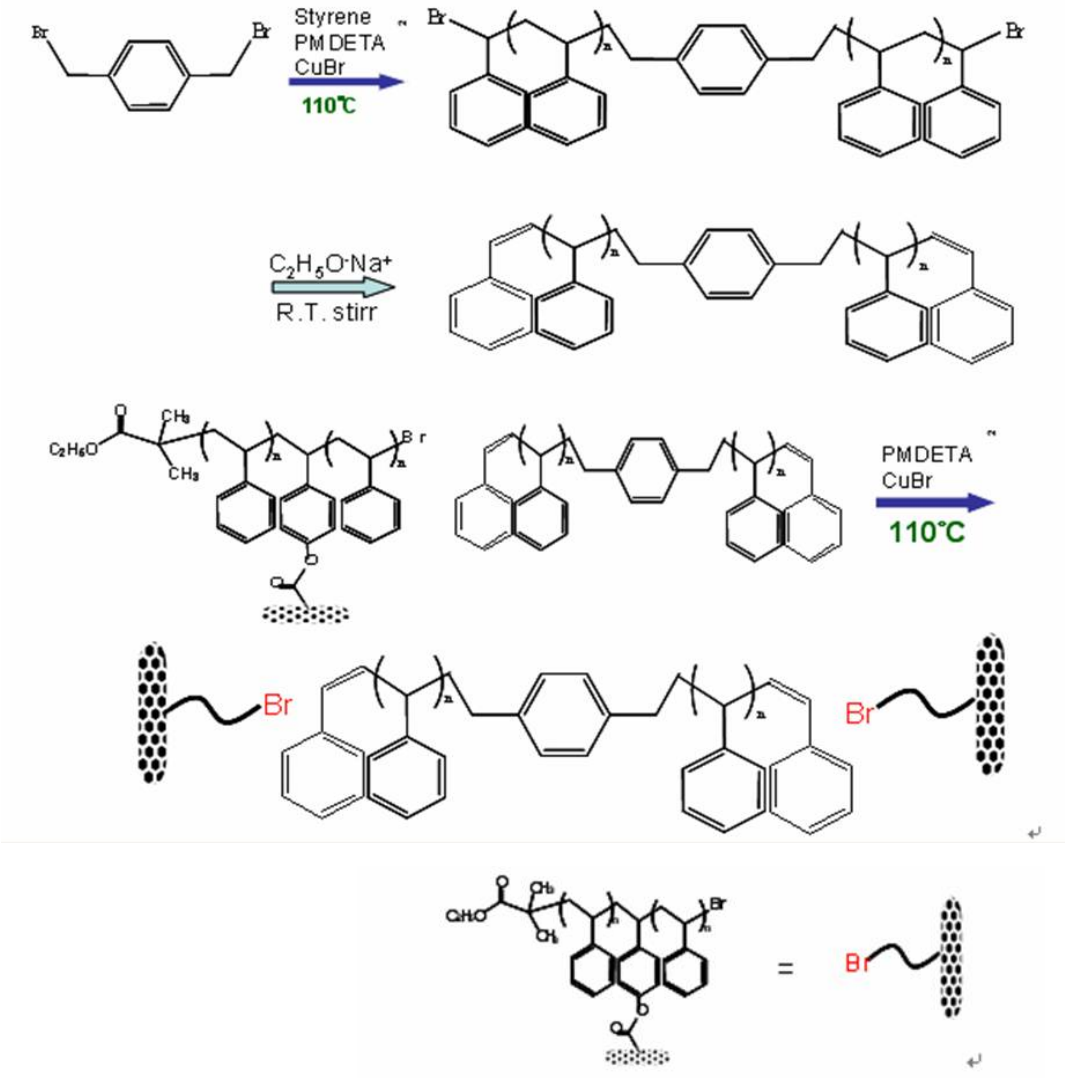

Scheme 9. Flow chart of the procedure for Crosslinked-MWNTs from functionalized MWNTs.

2.3.2 Results and Discussions

Structural identification of Polymer functionalization

ATRP procedure was used to graft polystyrene to MWNT, to improve MWNT dispersedly within solution. However, the grafted MWNT produced polystyrene with chain end Br. To enable the chain-link between MWNT and Nanotubes, we needed to functionalize the polymer chain end synthesized by ATRP. In other words, using the polymer chain end Br required us to transform it into vinyl. After the polymer chain end synthesized by ATRP, the polymer chain end has C-Br. Using FTIR, at around 475 ~ 500 cm^{-1} there is a strong peak of absorption, which is known as the C-Br peak. Afterwards, we used EtoNa substitute HBr to form vinyl polymer. From FTIR shown in Figure34, we observe that around 880~950 cm^{-1} there is a peak of absorption. This represents the absorption made by the chain end vinyl. Thus by using FTIR analysis

we can successfully synthesize polymers with vinyl chain ends. This can also aid us in performing cross-link nanotube grafting. The molecular weight was 300k, as determined by GPC, and could be regarded as the distance between MWNTs after crosslinking. One additional point needs to be made. In contrast to the method 2 of Crosslinked-MWNTs -the distance between MWNTs was calculated after adding DVB. By contrast, the distances between MWNTs in this method was calculated directly at the beginning of the polymerization.

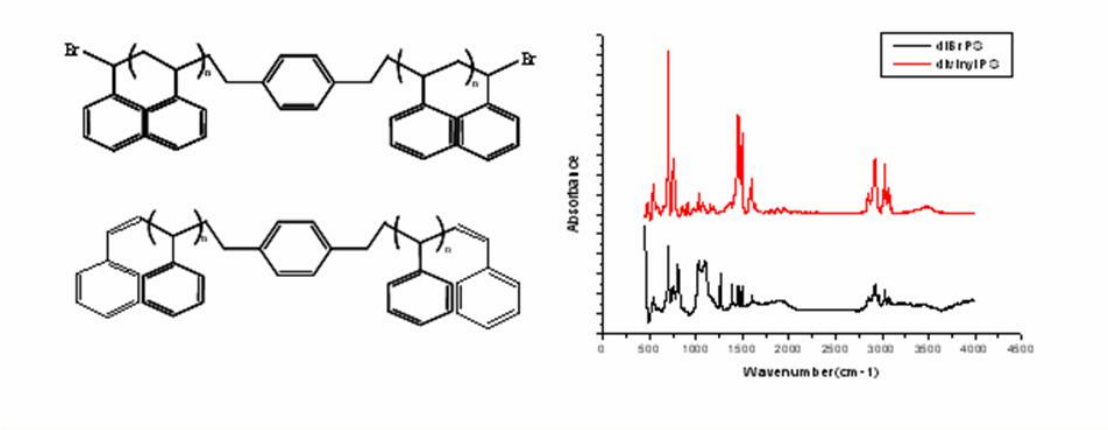

Figure 34.The FTIR spectra of the diBromid-polystyrene and divinyl-polystyrene.

The respective dispersion in Toluene of Crosslinked-MWNTs and MWNT-CMS grafting polystyrene (abbreviated as MWNT-PS) by the method of ATRP was observed. The solution of MWNT-PS was transparent, indicating that the global dispersion of the CNTs in the toluene was excellent. On the other hand, the dispersion of Crosslinked-MWNTs was markedly inferior and Crosslinked-MWNTs were deposited on the bottom of the bottle. Viewed in this light, MWNTs can be regarded as crosslinked by polystyrene. This result may be explained by the fact that the polystyrene molecular weight between MWNTs was inadequate (300k).

The Crosslinked-MWNTs were then blended with high molecular weight PS (Mw = 2M) in toluene for casting thin polymer films. The film thickness was around 0.5 μm. The concentration of Crosslinked-MWNTs in the solution was adjusted so that the nanotube weight fraction, excluding the grafted polymer, was 10 wt. % in the solid films drawn from the thermogravimetric curve shown in Figure 35(b).

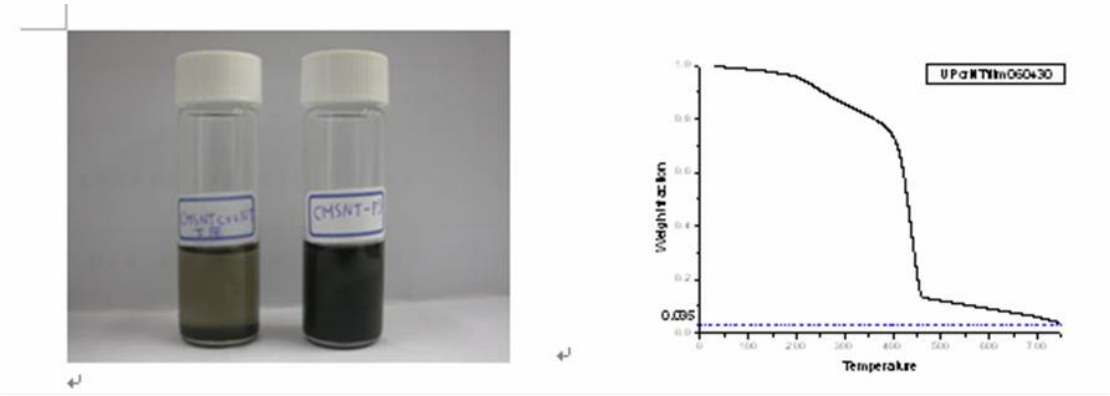

Figure 35. (a)The toluene solutions of Crosslinked-MWNTs(left)respectively and MWNTs-CMS grafting polystyrene by the method of ATRP.(b) Thermogravimetric curves of the film mixed with Crosslinked-MWNTs and PS(Mw=2M).

Mechanical properties on Microscopic Deformation Behavior

In the control experiment of pristine PS films, crazes were usually initiated near the edges of the film squares or local defects such as dust particles or aggregates shown in Figure 35a. After the initiation of crazes at approximately 1% strain (the crazing strain ε_c), most further deformation was concentrated toward the preexisting crazed areas, and the regions outside the crazes were subjected to virtually no strain beyond ε_c. The crazes were generally straight, widening steadily as the strain increased, and effectively absorbing the externally applied deformation into the tiny zones shown in Figure 36c and 36d. In the Crosslinked-MWNT/PS films, as the strain increased, the development of the tiny local deformation zones was effectively suppressed with the zone width increased only slightly shown in Figure 37b. At the same time however, a large number of new local deformation zones were initiated as the strain increased. Up to the point of maximum strain where the supporting copper grids broke at 21.5% strain shown in Figure 37c and 37d, virtually all the local deformation zones in the film remained short and narrow (less than 1 micron wide). Very few local breakdowns were observed. These results strongly indicated that the Crosslinked-MWNT networks embedded in the PS film effectively retarded the growth and broadening of the local deformation zones and thus dramatically increased the toughness of the glassy polymer.

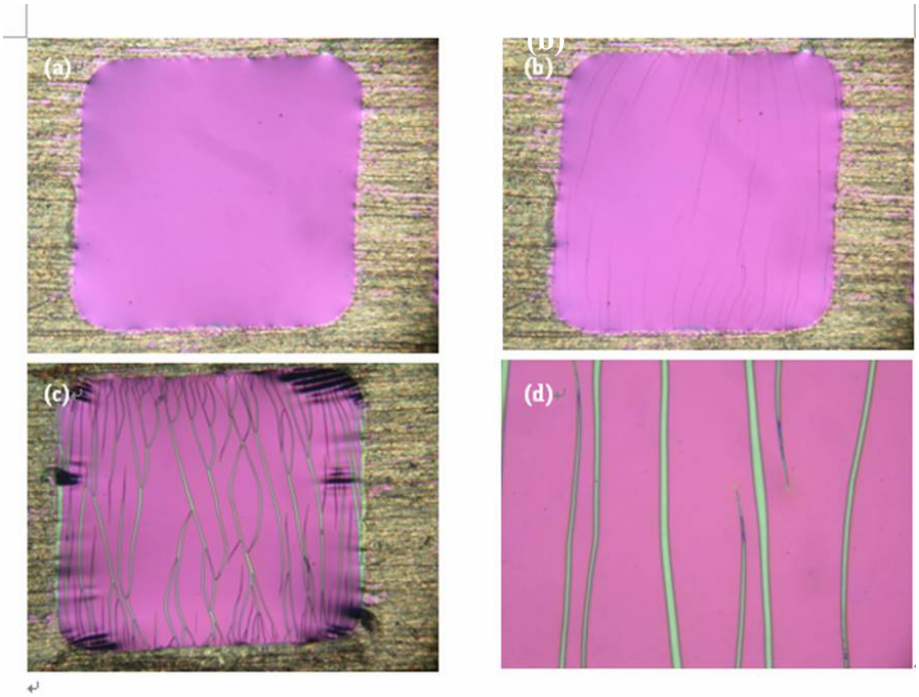

Figure 36. Optical micrograph of pristine PS films coated on copper grids: (a) without stretching, (b) with crazes (some marked with arrows) just initiated, (c) local craze breakdown, and (d) crazes at a higher magnification.

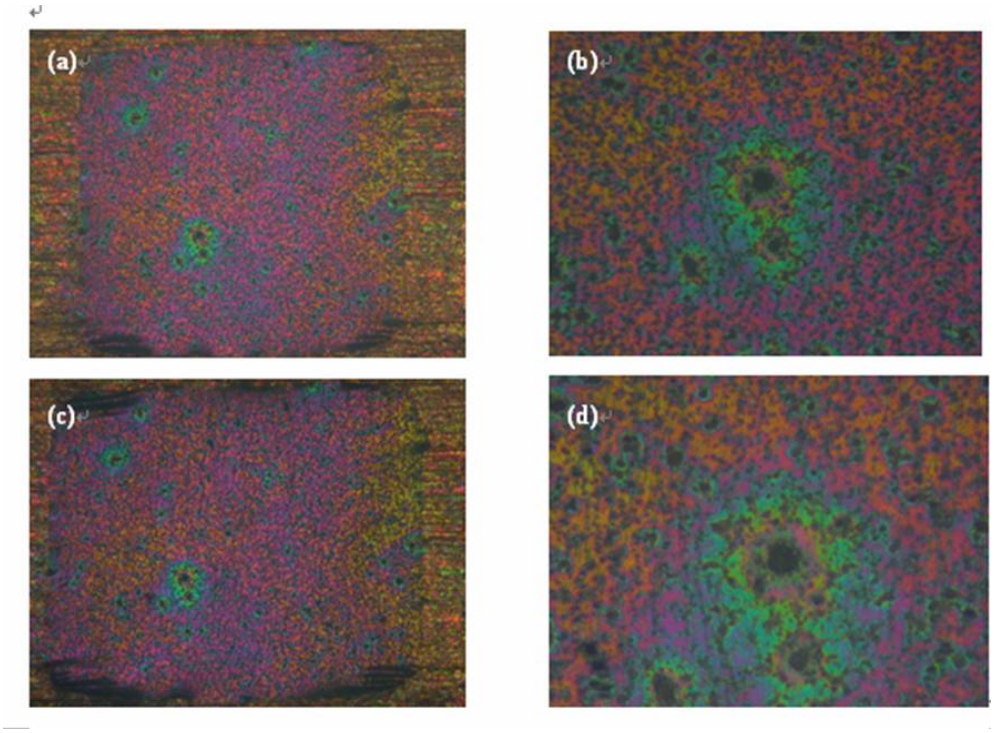

Figure 37. Optical micrograph of Crosslinked-MWNT/PS films coated on copper grids: (a) the film without mechanical strengthening and (c) many tiny local deformation zones at 21.5% strain. (b) and (d) are different magnification at 21.5% strain.

The microstructure of the local deformation zones were examined under AFM. In pristine PS films at 14.5% strain, the width of the craze at 14.5% strain was nearly 3 microns wide, which is shown in Figure 38a. After Crosslinked-MWNTs were added, the film at 21.5% strain obviously decreased to less than 1 micron in width, clearly shown in the SEM micrograph of the unplasma-etched Crosslinked-MWNT/PS film of Figure 38c.. Some crazes and aggregates are evident (Figure 37a and 37b). In order to show the structure of MWNTs, the oxygen plasma etching was used to remove polystyrene covering on the surface of the films. After etching, MWNTs-network of crosslinked-MWNT/PS film was clearly observed under a SEM, as shown in Figures 39c and 39d.

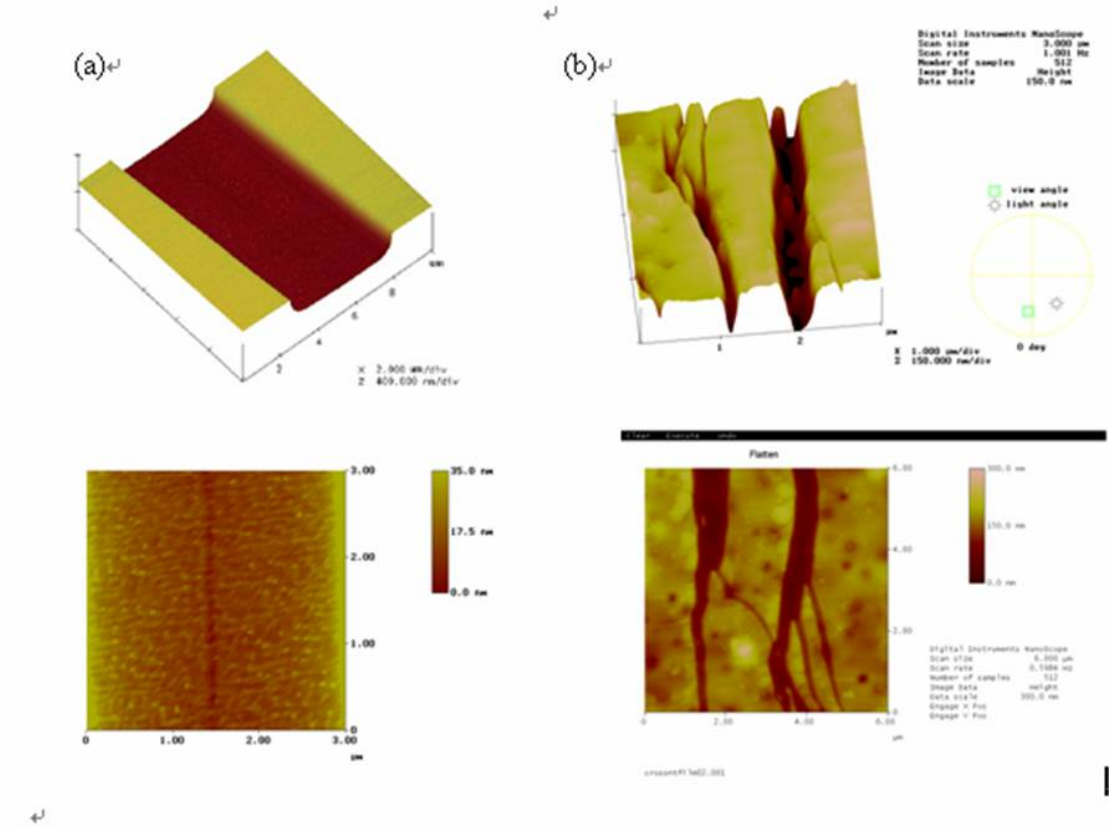

Figure 38. (a) AFM micrograph of crazes in pristine PS films at 14.5% strain; and (b) AFM micrograph of crazes in Crosslinked-MWNT/PS films at 21.5% strain.

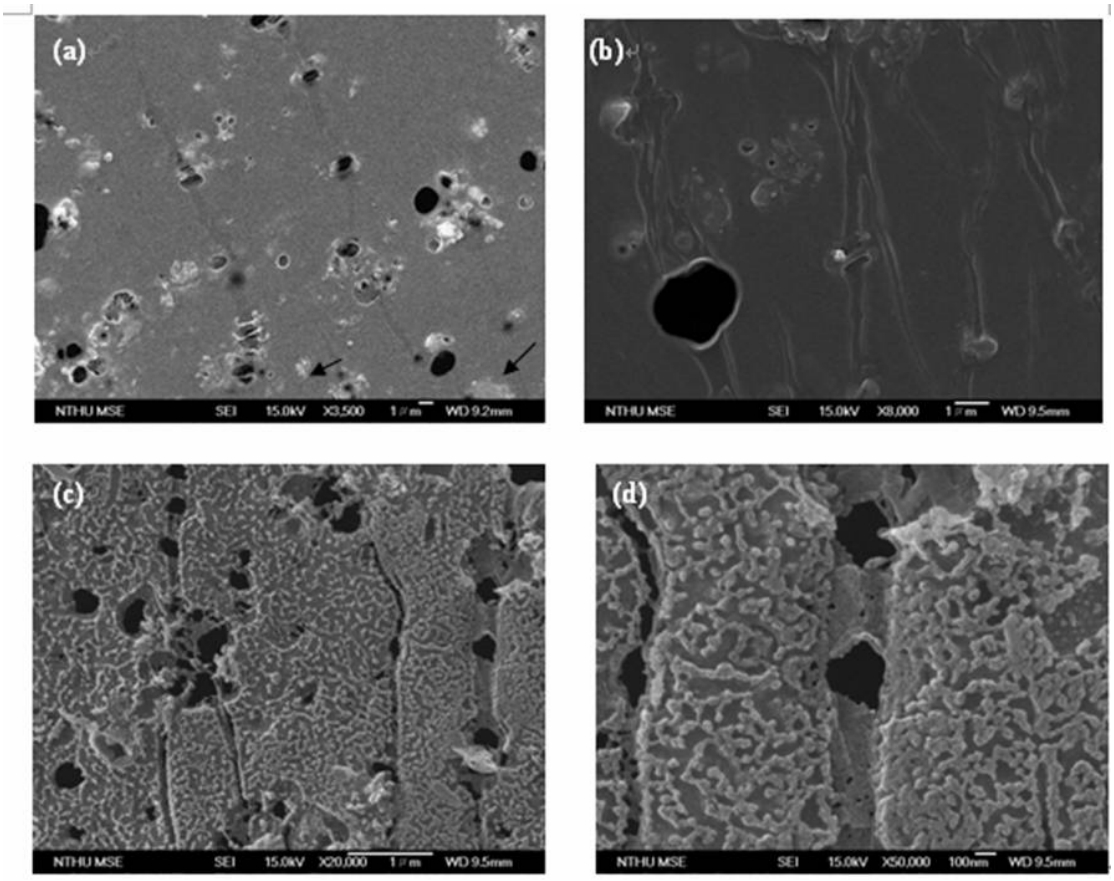

Figure 39. SEM micrograph of a, b) the unplasma-etched MWNT/PS film, and c,d) plasma-etched MWNT/PS film. Both clearly show surface network of nanotubes.

Future Work

We divide this section into two parts. One is the method of chemical synthesis by adding a crosslinker named ethylenediamine to form crosslinked film. The other involves using electron irradiation to crosslinked MWNTs-PS/PS films.

Part 1. Crosslinking of Poly-CMS

Firstly, the synthesis of Poly-CMS and MWNTs-CMS will used. The aggregates of MWNTs-CMS will assuredly be cleaned away by centrifugation. Then, the MWNTs-CMS were mixed with the PS-CMS in toluene solution and then added ethylenediamine as a cross-linker. Subsequently, the MWNTs-CMS/Poly-CMS films were spun cast from the solution and heated at 70℃ on the hot plate to undergo the crosslink reaction. Next, the MWNTs-CMS/Poly-CMS films were floated off the substrate on distilled water and bonded onto supporting copper grids. After following the proper bonding procedure, the specimen will be mounted in a strain jig and stretched under an optical microscope to observe the deformation structure. Below is a flow chart to present the procedure shown in Scheme 3.

(1)Preparation of MWNTs–COOH:

MWNTs synthesized via a chemical vapor deposition method (purchased from DESUN Nano Inc., Taiwan) had tube diameter of 10–30 nm and 5–15μm in length. The as-received MWNTs were first purified by reflux for 48 h in 2.6M nitric acid, followed by filtration with a PTFE membrane (0.2μm pore size) and finished by repeatedly washing with deionized water. The purified MWNTs were then immersed in H_2SO_4/HNO_3 (mixture of 3:1 in volume) at 90 ◦C for 2 h and then vacuum-filtered through a 0.2μm PTFE membrane. The solid was washed with deionized water again repeatedly until the pH of the filtrate reached 7. In this step, the nanotubes were oxidized by attachment of carboxylic acid groups on the MWNTs external walls. The tube lengths of the nanotubes were also reduced in this step; therefore, the length of the treatment time was carefully controlled to retain optimal tube lengths.

(2) *Esterification of MWNTs–COOH with 4-vinylbenzyl chloride (CMS)*:

The carboxylic acidified nanotubes (MWNTs–COOH) were then dispersed in toluene (10 mg of MWNTs–COOH in 10 ml toluene) with 68 mg of sodium ethoxylate at 40 ◦C by sonication continuously for 1 h to generate MWNT–COONa. Then, 1ml of CMS was added into the solution and the mixture was again sonicated for another 2 h to produce the esterification product (MWNTs–COOR, $R=CH_2C_6H_4CHCH_2$).

(3) *Synthesis of poly-CMS grafted-MWNT (MWNTs-CMS)*:

To grow Poly-CMS chains from the grafted functional groups on the CNTs, the esterification solution from the above procedure was added with 0.1 mg of AIBN and 1ml of CMS monomer at 100 ◦C to initiate the polymerization reaction. The reaction batch was stirred continuously for 3 h. At the end, the majority of toluene in the solution was removed by low pressure distillation. Then, the MWNTs-CMS were precipitated by adding methanol into the solution, and collected after filtration. The non-reacted or non-polymerized monomers (or oligomers) were herein washed and filtered out from the batch. The solid was then washed again in toluene by sonication and then vacuum-filtered through a 0.2μm PTFE membrane. The chain lengths of the grafted Poly-CMS on nanotubes were estimated from the SEC data of a batch without nanotubes but under the same polymerization conditions, to be around *M*w=100k.

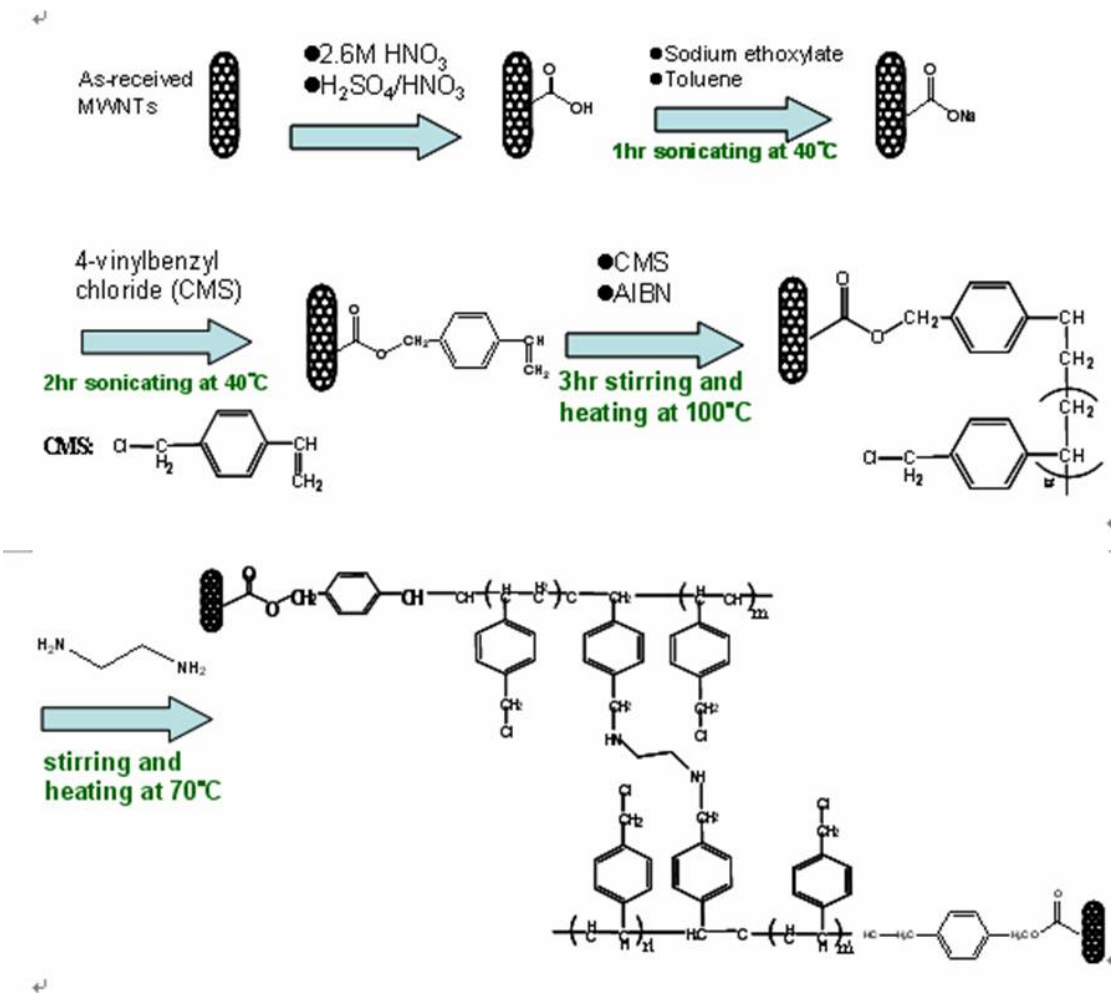

Scheme 10. The procedure of Crosslinking Poly-CMS.

Part 2. Electron irradiation to crosslinked MWNTs-PS/PS films [52]

(1)Synthesis of polystyrene grafted-MWNT (p-MWNTs):

To grow PS chains from the grafted functional groups on the CNTs, the esterification solution from the above procedure was added with 0.1 mg of AIBN and 1ml of styrene monomer at 95 ◦C to initiate the polymerization reaction. The reaction batch was stirred continuously for 3 h. At the end, the majority of toluene in the solution was removed by low pressure distillation. Then, the polystyrene–MWNTs (p-MWNTs) were precipitated by adding methanol into the solution, and collected after filtration. The non-reacted or non-polymerized monomers (or oligomers) were herein washed and filtered out from the batch. The solid was then washed again in toluene by sonication and then vacuum-filtered through a 0.2 μm PTFE membrane.

(2)Electron irradiation to form crosslinked polystyrene

The MWNT/PS films were floated off the substrate on distilled water and bonded onto supporting copper grids.Bonding of the film to the grid was achieved by

a short exposure to toluene vapor. After drying, the specimen was exposed to electron irradiation using electron microprobe.

Chapter 3

Electrical conductance in polymeric nanocomposites percolated with surface-grafted carbon nanotubes

PBO and PI have been widely used in many applications owing to their distinct mechanical and thermal characteristics in applications of, for example, aircraft structures, interlayer dielectrics and so on [54,55]. If these versatile polymers can be made electric conductive, their applications could be dramatically expanded into other important frontiers [54-56]. With great aspect ratios and excellent intrinsic conductive properties, nanotubes have been attempted to reduce surface resistivity of PI from the range of 10^6–$10^{10}\Omega$[56] by several orders of magnitude. However, owing to the strong van der Waals interaction, MWNTs tend to form into aggregates which invite poor dispersion in the polymer matrix and negative effects on the properties of the resulting composites [57-68]. It is the main purpose here to utilize the dispersion method based on surface-grafting to impart the important electric and thermal conductance to polymers. In this work, we use surface-grafted MWNTs as the fillers for PS and PI. The obtained data indicates that the electrical resistivity of these films can be reduce by more than 7 orders of magnitude.

3.1.1: The electrical resistivity of MWNTs grafted various carboxylic acid groups.

Figure 40 shows the electrical resistivity against various carboxylic acid group (COOH) concentrations for acid-treated MWNTs. The resistivity increases quadratically with the number of surface carboxylic acid groups suggest that carboxylic acid groups attack nanotubes from their intrinsic [defects such as tips, pentagons and heptagons. Futhermore, it implies that the carboxylic acid groups concentrate in specific areas. Once the nanotubes grafted acid groups turned to shorter than pure nanotubes, in the mean while the pentagons or heptagons of nanotubes decrease and the carboxylic acid groups randomly distribute on nanotube surfaces.

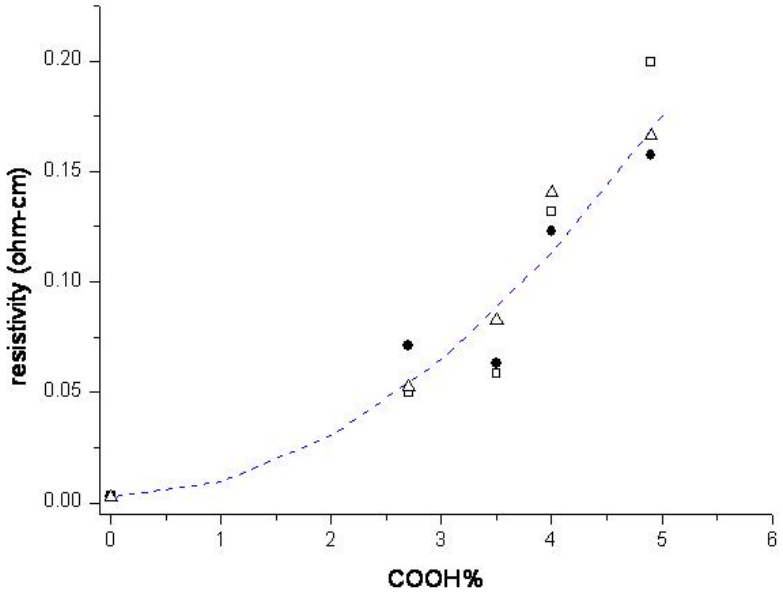

Figure 40. The electrical resistivity curve for acid-treated MWNT.

3.1.2: To calculate the number of carboxylic acid groups grafted on a single MWNT

Because of the electrical property of MWNT strongly depending on its aspect ratio and its diameter, and the acid-treated MWNTs (MWNT-COOH) might cause damages on their surface and lead to chop the nanotubes, the number of carboxylic acid groups is necessary to be calculated to control the carboxylic acid groups on nanotubes.

In brief, assume that the MWNT circumferences is $2\pi r$ ($r = 35 \sim 15$ nm) and inter-layer spacing is 0.34 nm, and the number of layers is 20. If pristine MWNTs average length is 20 μm, MWNT-COOH average length is 5 - 10 μm (the MWNT-COOH has been chopped into lengths of 13~14μm apiece, then we know there would be 894 pentagons on a single cycle of zigzag nanotube, as Figure 41 shown, simultaneously there would be 894 COOHs, so briefly a single MWNT is cut off by 20×894×13 COOHs. (i.e., 232440 COOHs)

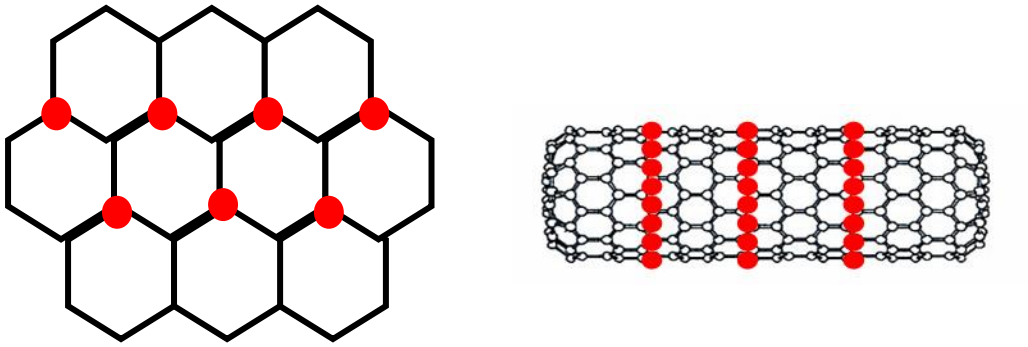

Figure 41. The zigzag structure of the nanotubes surface; red points represent the carboxylic acid groups

3.2.1 The electrical property of polystyrene (PS)/MWNT composites system.

The results of surface resistivity from $10^{15}\,\Omega$ to $10^{7}\,\Omega$ obtained in Figure 42 indicate that the surface resistivity decrease sharply as the nanotube volume fraction becomes greater than 5%, indicating a percolation threshold at a volume fraction less than 3%. Experimental results for composites are often analyzed in terms of statistical percolation theory [55,57].

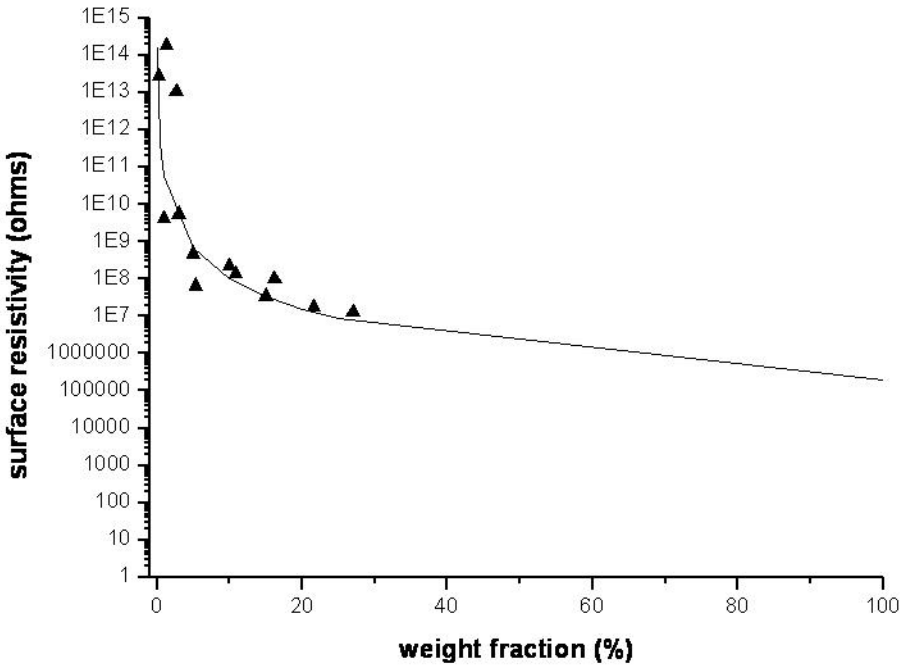

Figure 42. The surface resistivity curve of PS/MWNT composites

The percolation equation is as follows:

$$\rho_{composites}=\rho_c(f-f_c)^{-t}$$

the best fitting data are 0.05 wt% for f_c (the percolation threshold loading of filler), 200000 Ω-cm for ρ_c (the filler resistivity), and t is found around 2.7 (the critical exponent).

Although the surface resistivity has been improved greatly, the resistivity ρ_c of the grafted nanotubes is about several orders greater than that without grafting. This may have originated from the poor conductance of the grafted polymers. ($\rho_{PS} \sim 10^{20\text{-}22}$ Ω-cm, compared to $\rho_{NT} \sim 10^{-3}$ - 10^{-6} Ω-cm). The grafting polymer is then switched from PS to PBO. ($\rho_{PBO} = 10^{-3}$ Ω-cm; $\rho_{PS} = 10^{20\text{-}22}$ Ω-cm).

3.2.2 The polybenzoxazole (PBO) /MWNT composites system

The SEM of PI/PBO-MWNT(PBO-MWNT) composites (after oxygen plasma etching)

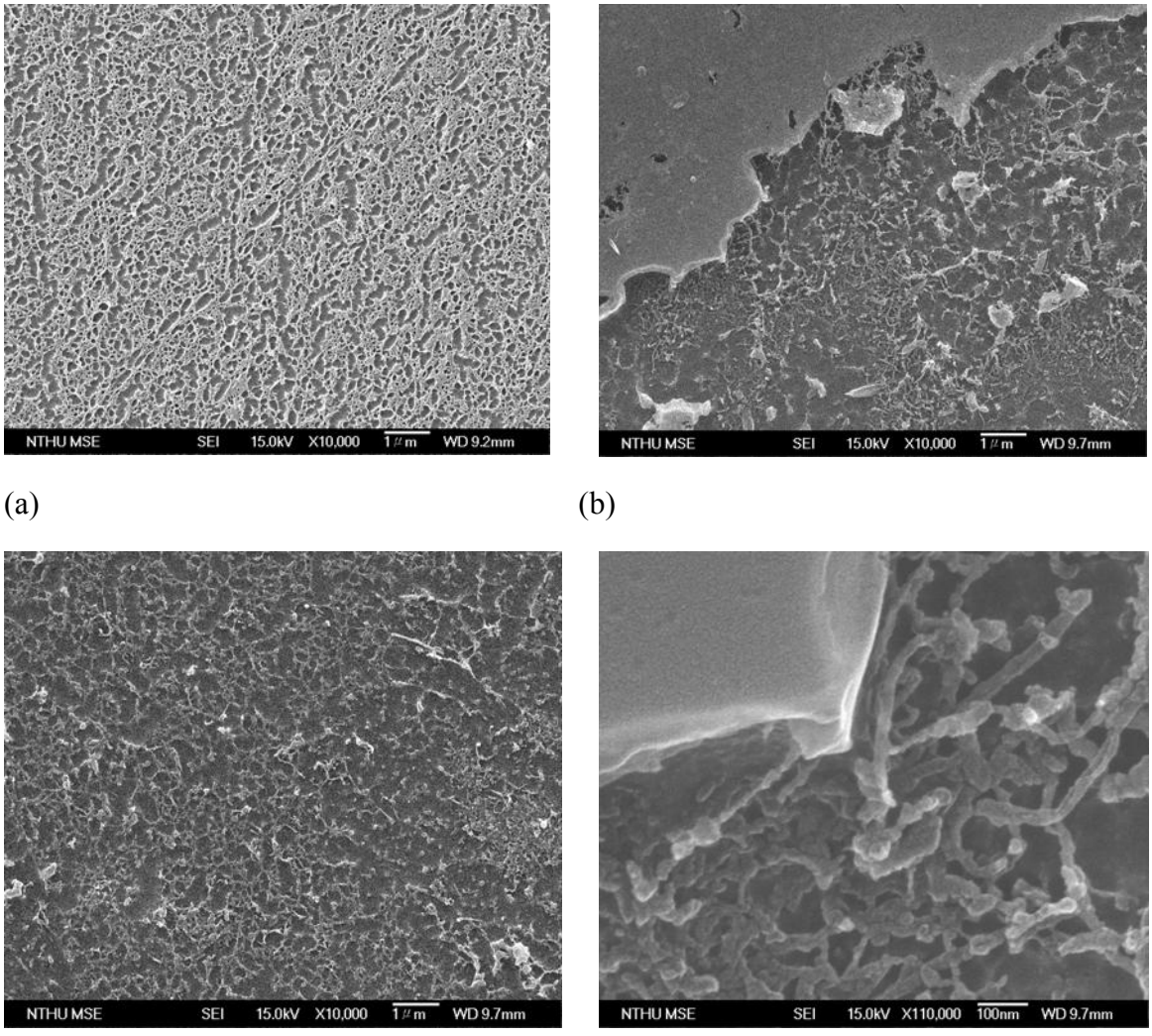

(a) (b)

(c) (d)

Figure 43. SEM images of films after oxygen plasma etching (a) polyimide film

surface, (b), (c), (d) show the 2.6 wt% PI/ PBO-MWNT composite nanotube network.

Figure 43 displays that the morphology of PI film dramatically differs from PI/PBO-MWNT composites (b) and (c). In addition, at the loading of 2.6 wt%, composite has been well dispersed and formed the nanotube network as the evidence for the percolation threshold. Also, Figure 43 (d) obviously shows that MWNTs incorporate each other and have the three dimension structure.

The TEM Micrographs of PBO-MWNTs

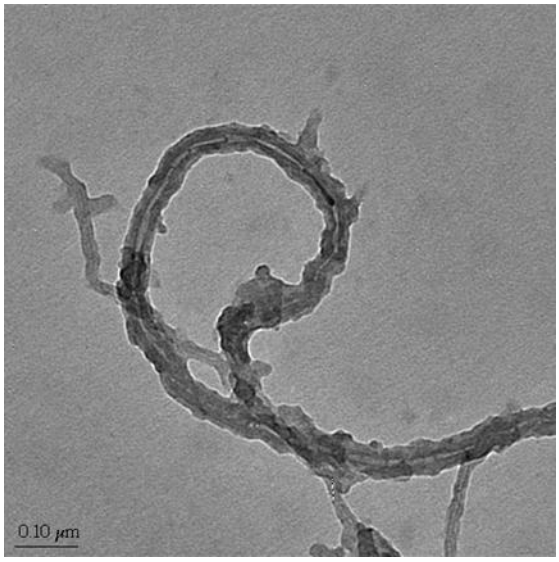

(a)

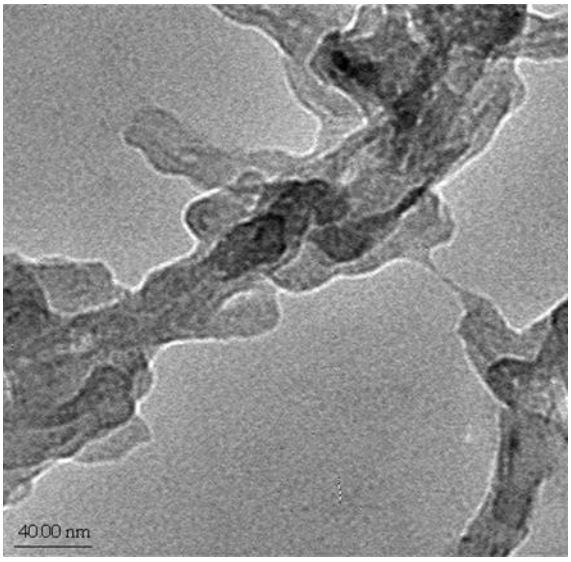

(b)

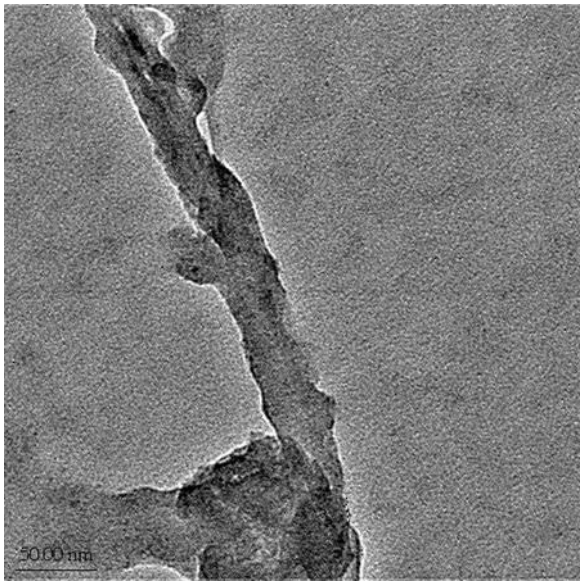

(c)

Figure 44. TEM images of nanotube coated by PBO.

Subsequently, polymer observed from Figure 44 has been grafted on the nanotube sidewall, where nanotube diameter is around 15-35 nm.

The x-ray diffraction (XRD) of MWNT grafted PBO

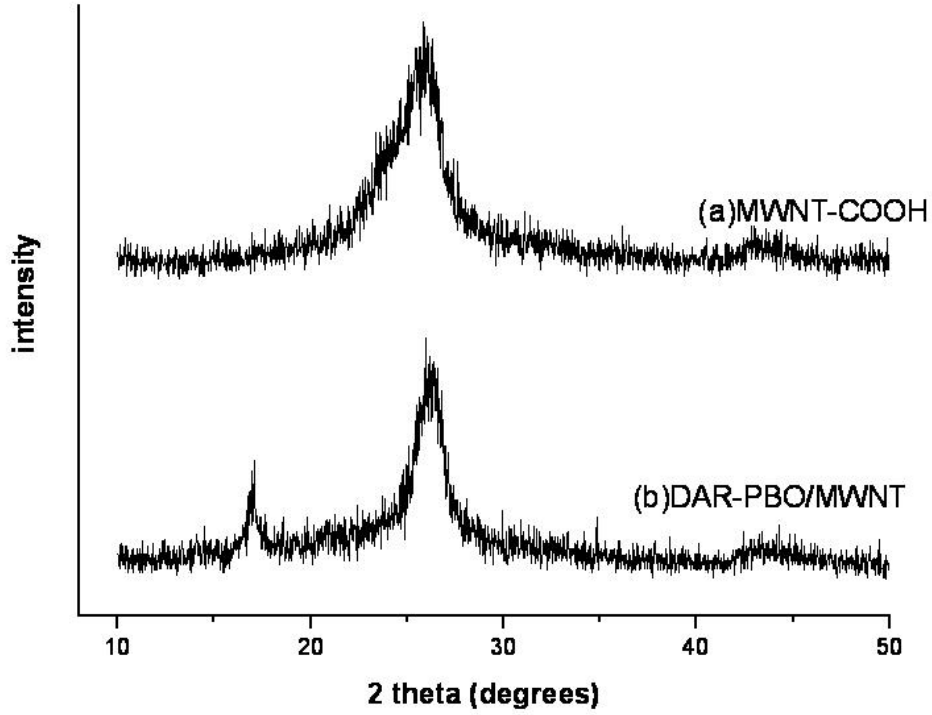

Figure 45. The XRD patterns of (a) MWNT-COOH and (b) MWNT grafted DAR-PBO.

In addition, the XRD characterizations of MWNT-COOH and MWNT grafted DAR-PBO which are showed in Figure 45 are also investigated. For MWNT-COOH, two peaks appeared at 26 and 43 corresponded to the interlayer spacing of the nanotube 002 and 100.[66] The XRD patterns of the DAR-PBO/MWNTs appear the both the characteristic peaks of the pure DAR-PBO and MWNTs.

The effect of various grafted molecular weight for the resistivity of PBO-MWNT

To further understand the effect of surface grafting, the viscosity average molecular weight of PBO is used in order to study the effect of the dispersion of MWNTs in polymer matrix and the functional group sites on MWNTs. The resistivity of MWNTs grafted with various PBO molecular weights is shown in Figure 46. The measurement described below is employed to obtain the molecular weight [69]. Initially, 3mg of PHA was dissolved in 10ml of NMP, for example, and then the flow time was

measured at 30℃, using the equation given by [69], we could obtain [η] = 0.1267, and calculate by the Mark-Houwink equation:

$$[\eta]=2.77\times10^{-7}\times (Mv)^{1.8}$$

The viscosity average molecular weight could be obtained from η (relative viscosity). Eight kinds of PBO-MWNT films are fabricated and the electrical resistivity is measured by a four-probe measurement.

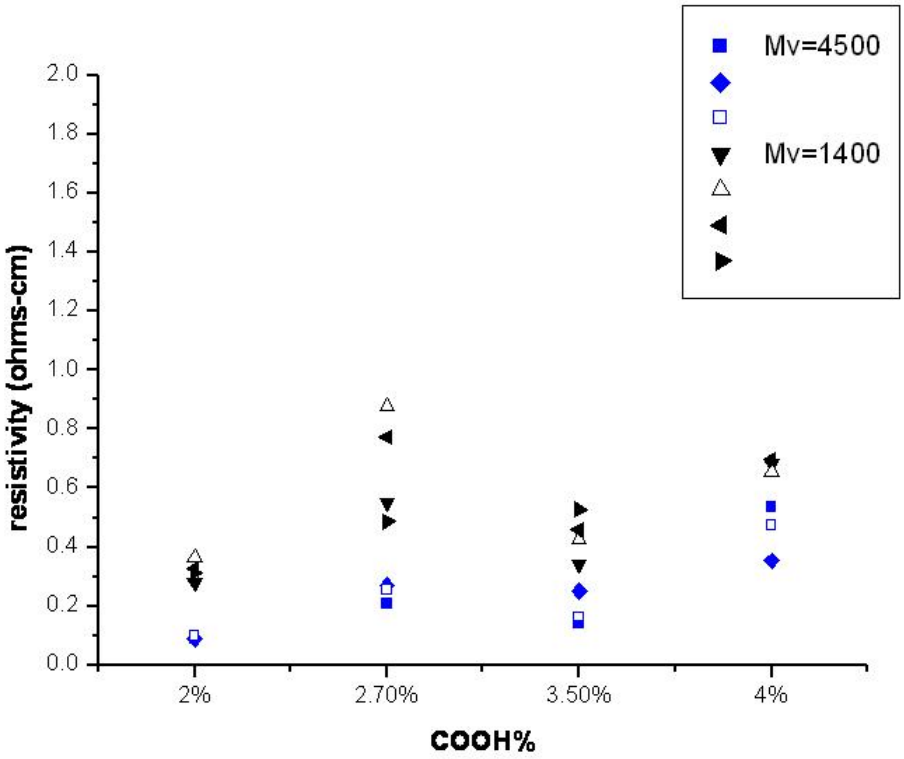

Figure 46. The electrical resistivity against various carboxylic acid group treated MWNTs grafted different viscosity molecular weight.

As shown in Figure 46, the resistivity of PBO-MWNT film embedded with grafted by chains of molecular weight 1400 (noted as L-PBO-MWNT) is significantly higher than those with a grafted molecular weight of 4500, (noted as H-PBO-MWNT). It is an unanticipated result for our understanding that the PBO-MWNT with more polymer coated on the nanotube sidewall will be obtained the poorer conductivity of carbon nanotube, and the cause may be originated from poor dispersion for the fabricating process. In addition, the resistivity slightly increases with the functional group sites (as same as COOH%), the result observed is consistent with the electrical resistivity of MWNT against different carboxylic acid groups as mentioned before. To check the weight percentage of PBO grafted on nanotube, the thermal-gravimetric analyses (TGA) is conducted. The results are showed in Figure 47.

Table 1 lists the weight percentage of PBO grafted on nanotube sidewall and the weight fraction of nanotube which are calculated from the TGA curve.

(a)

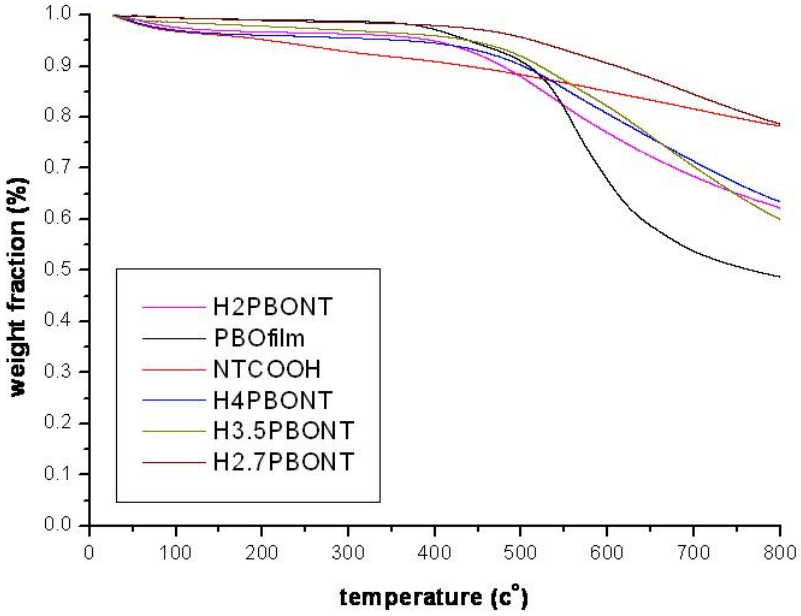

(b)

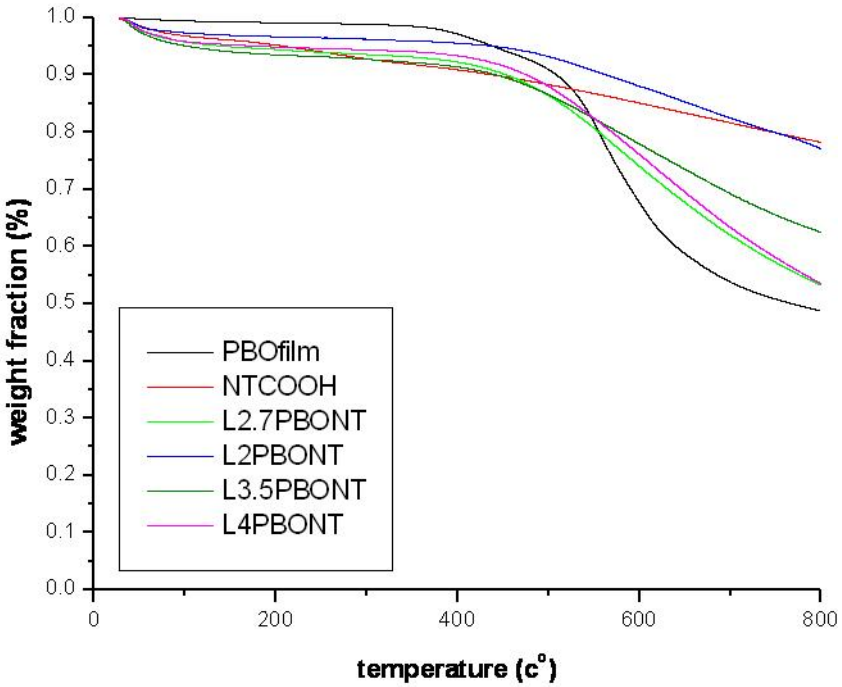

Figure 47. TGA curves for (a) various carboxylic acid concentration H-PBO-MWNTs and (b) various carboxylic acid concentration L-PBO-MWNTs.

Table 1

The weight percentages of PBO with different molecular weight grafted on nanotube and nanotube, respectively.

	PBO grafted on nanotube		nanotube	
	Mv = 4500	Mv = 1400	Mv = 4500	Mv = 1400
2% COOH	83.2 wt%	64 wt%	16.8 wt%	36 wt%
2.7% COOH	62 wt%	93.8 wt%	38 wt%	6.2 wt%
3.5% COOH	89 wt%	81.8 wt%	11 wt%	18.2 wt%
4% COOH	82 wt%	93.2 wt%	18 wt%	6.8 wt%

The electrical property of DARPBO/MWNT composites

Figure 48 shows that the surface resistivity of DARPBO/MWNT composites, as mentioned in the electrical property of PS/MWNT composites system, the measured resistivity also could be fitted by the percolation theory. The fitting data are obtained for ρ_c= 0.3 Ω-cm; f_c= 0.499%; t = 2.2. It suggests that the electrical resistivity of PBO-MWNTs is dramatically decreased by 6 orders of magnitude due to the natural property of grafting polymer. Furthermore, the surface resistivity has been greatly decreased at 2.6 wt% loading.

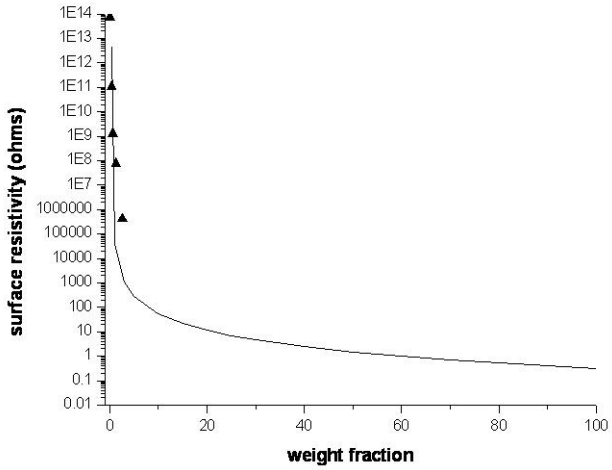

Figure 48. The surface resistivity for DARPBO-MWNT composites.

In order to investigate the effect of the polymer on nanotube sidewall [70,71], the

third system where what is called an ideal polymer/MWNT composites is established to compare with two kinds of polymer/MWNT systems. Using the percolation equation, the curve for an ideal polymer/MWNT composite which defined as well dispersion, high aspect ratio of MWNTs, and the fine conductivity property of polymer matrix is created. As figure 49 shown, the ideal curve is similar to the PBO/MWNT curve. It implies that the PBO/MWNT system may be close to an ideal model of the polymer/MWNT composite. However, the difference in an ideal polymer/MWNT system and PBO/MWNT system lies in the contact resistance which would be discussed later.

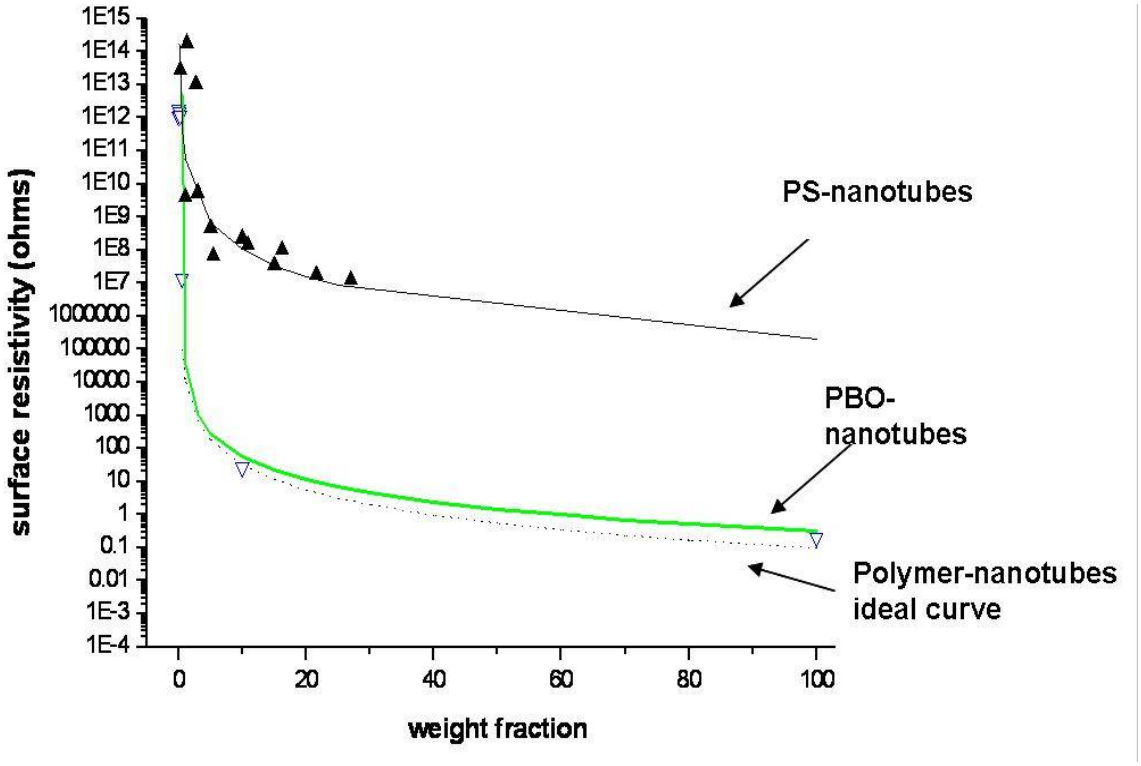

Figure 49. The surface resistivity of different polymer/MWNT composites.

Percolation theory and contact resistance

All results of the resistivity of various polymer/MWNT composites can be fitted by using the percolation theory**,** [72-75]

$$\rho_{composites} = \rho_c (f-f_c)^{-t}$$

where ρ_c is the resistivity of nanotubes, f_c is the percolation threshold fraction of filler, and t is the critical exponent .

The fitting results are shown in the following.

a) PS/MWNT composites: ρ_c = 200000 Ω-cm; f_c=0.05% (t = 2.7)
b) PBO/MWNT composites: ρ_c= 0.3 Ω-cm; f_c= 0.499% (t = 2.2)
c) Ideal polymer/MWNT composites: ρ_c= 0.097 Ω-cm; f_c= 0.11% (t = 2.2)

Although most papers about the electrical property ofcomposites have adopted the percolation theory to fit their results, yet the exponents in the percolation theory were not explained clearly enough [57]. Consequently, we make an effort to describe the behavior of MWNTs in nanocomposites using the gelation transition [69]. While the polymer chains crosslink with each other, the system goes through a transition of connection. If one structure forms the percolated network through the entire system, it is called the incipient gel for polymer physics [69]. In other words, it is beginning the percolation threshold. As the loading of fillers increases, the percolated structures also increase and incorporate with each other to form a complete conducting route [55,57]. For the more loading of fillers, the carriers could pass through more than one route, thus the conductive paths of carbon nanotubes which are similar to the parallel circuits structures have been constructed, as the measured resistivity are slightly decreased continually.

In addition, the contact resistance is also another significant issue for the electrical property of composites to overcome. The conception of contact resistance was carried out by P. J. Burke [76]. The equation is given by:

$$R = Rc + L \times 6\text{K}\Omega/\mu\text{m}$$

where L is nanotube length, can be calculated from ρ_c obtained from percolation modeling. Rc is contact resistance, can be used to investigate the electrical properties and the physical structure of the grafted polymer coils on carbon nanotubes. Contact resistances may be found in the difference between a percolation fitting and the composite, thus the polymer/MWNTs composite can be described in a model that considers the percolation theory and contact resistance. More in-depth exploration is underway.

Templating gold nanoparticles with MWNTs in noncovalent functionalization by aromatic organic molecules.

Very recently, the carbon nanotube coated by a layer of gold nanoparticles (Au NPs) has many promising applications for the electrical conductance of carbon nanotubes as gas sensor materials [77-79]. A non-covalent bonding method using π–π interactions is exploited for templating the gold nanoparticles on nanotube, which gives minimum damages to nanotubes from surface functionalization whilst

significantly enhances uniform dispersion of the nanotubes in the medium [80]. Furthermore, this preparation method could apply to other chemical synthesis of nanoparticles. The Au NPs were prepared and the sizes maintained by the thiols, according to the procedures of Brust *et al* [77,78,81,82]. The procedure is as following (Scheme 13): Pyreneburtic acid dissolved in toluene were reacted with sodium ethoxyliate an hour in ultra-sonication 40 ℃, after that, a mixture was obtained and (2-chloroethyl) trimethylammonium chloride was added in the mixture then stirred overnight at 60℃ [83]. The excess pyreneburtic acid and (2-chloroethyl) trimethylammonium chloride were precipitated in acetone and deioned water through centrifugation. The solvent was removed by a rotary evaporator. A controlled amount of 1-decanethiol, an excess of HAuCl4 in deioned water was added and stirred for a while, a controlled amount of NaBH4 was carefully dissolved later into the suspension and stirred continually at room temperature for 12 hours. More in-depth investigation is underway.

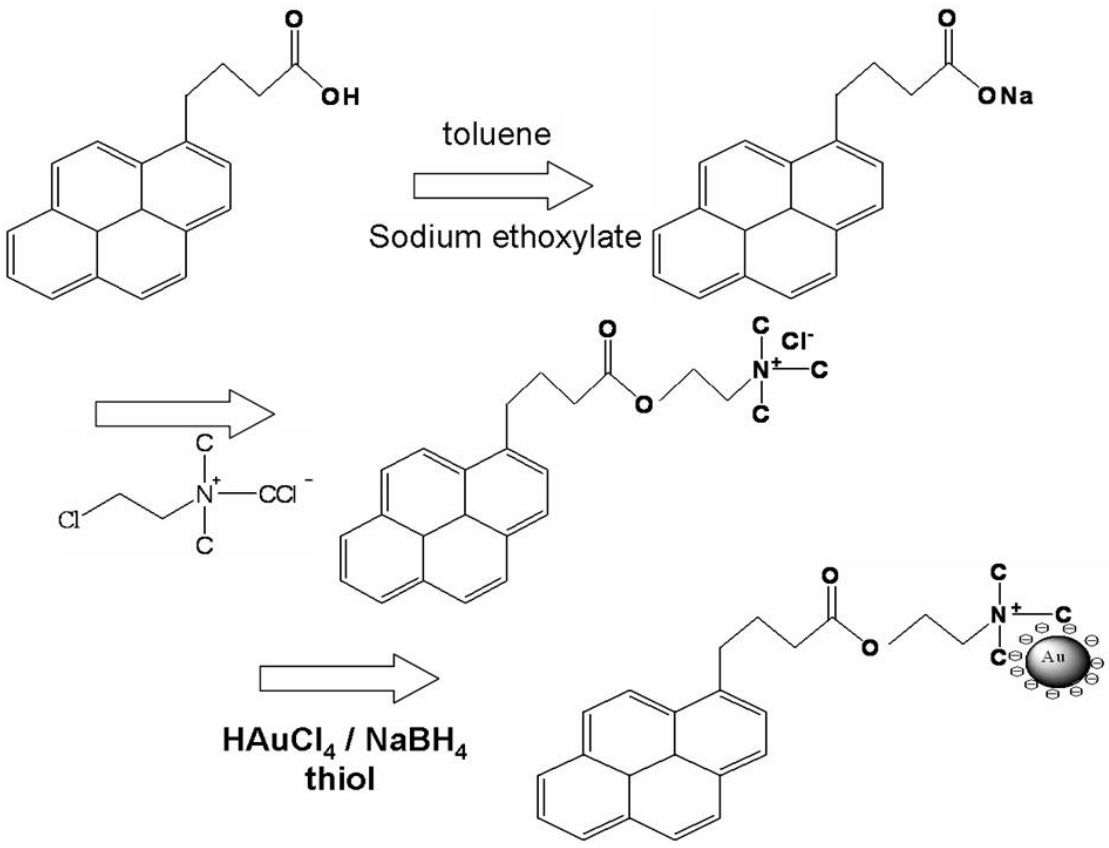

Scheme 13. The synthesis of gold nanoparticles with nanotube using the pyreneburtic acid molecule.

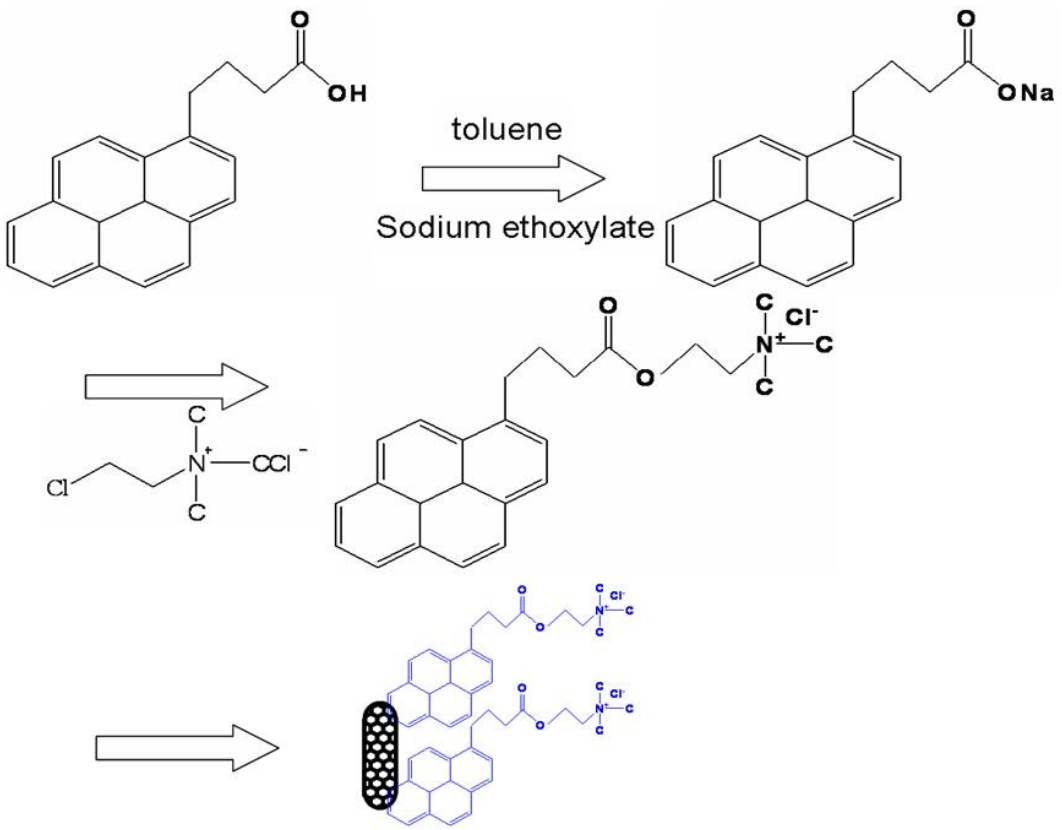

Scheme 14. the preparation of gold nanoparticles with nanotube

Conclusions

In summary, a percolated network of well-dispersed CNTs in a polymer matrix (PS, PBO and PI) can be obtained in thin films cast from solutions by prior CNT treatment with polymer grafting polymerization. In PS system, the grafted PS chains provide compatibility for intimate matrix mixing and the stereo hindrance contributes to the prevention of CNT re-aggregation. With only a small amount of CNTs in the thin film, a tremendous reinforcement effect was observed, indicative of the existence of a percolated CNT network in the polymer nanocomposite. The energy dissipation mechanism during tensile stressing was, thus, shifted from crazing and fracture to merely craze initiation which generated only short and narrow crazes that were quite stable against catastrophic fracture. For higher concentrations of nanotubes, solubility difference between the surface-grafted nanotubes and the host polymer gave rise to an intrinsic microstructure that shows roughened surface and non-uniform morphology which, however, seemed to have no negative effect on the toughness imparted by the nanotubes. The chain length of the grafted polymer on the nanotubes has important effect on the reinforcement and the onset of this micro-separation. Nanocomposites of high-temperature polymers of PBO and PI embedded with nanotubes surface-grafted with the respective polymer were prepared. Particularly, PBO was synthesized in either an one-step approach in poly(phosphoric acid) or a two-step approach where poly(hydroxyamide) (PHA) was first synthesized and then thermally cure to form PBO. The micro-deformation mechanism of the high concentration nanotubes in PS, PI, and PBO were being investigated.

Due to the strong $\pi-\pi$ interactions between growing chain ends and nanotubes surfaces during graft copolymerization, chain extension of the grafting macromolecules was restricted, causing severe nanotubes conglomerates when crosslinking reactions between nanotubes were completed. Approaches using prepolymer, prepared by using atomic transfer radical polymerization (ATRP), of controlled crosslinking density successfully made covalently linked nanotubes uniformly dispersed in a PS host that demonstrate excellent mechanical properties. Crosslinking methods either with delayed or inhibited cure agents or by controlled electron radiation were undergoing. This work will be extended to the high temperature polymer systems for testing the effects on conductivity and ultrahigh strength capability.

It was found that although surface-grafted nanotubes distributed uniformly in the host polymer, enabling full percolation with much less nanotubes, the intrinsic electric conductivity of the nanotubes decreased dramatically due to the insulation effect of

the grafted polymer over the nanotubes, rendering the composite inferior in conductance. The contact resistance between neighboring nanotubes holds key control over the conductance properties of the nanocomposite. This problem can be overcome by grafting the nanotubes with electric conducting polymer. PBO-grafted nanotubes have shown excellent conductance behavior, approaching the theoretical limit promised by the nanotubes. The surface-grafted approach, however, suffered negative impact due to damages to the native nanotubes from functionalization and improvements are being attempted by gold-particle templating and p-p interaction approach. Theoretical analysis is currently underway to examine the local resistance at nanotubes contacts.

References

[1] S. Iijima, *Nature* **1991**, 354, 56.

[2] A.B. Dalton, S. Collins, E. Mu˜noz, J.M. Razal, V.H. Ebron, J.P. Ferraris, J.N. Coleman, B.G. Kim, R.H. Baughman, *Nature* **2003,** 423, 703.

[3] B.E. Kilbride, J.N. Coleman, P. Fournet, M. Cadek, A. Drury, W.J. Blau, *J. Appl. Phys.* **2002**, 92, 4024.

[4] J.K.W. Sandler, J.E. Kirk, I.A. Kinloch, M.S.P. Shaffer, A.H. Windle, *Polymer* **2003,** 44, 5893.

[5] M.J. Biercuk, M.C. Llaguno, M. Radosavljevic, J.K. Hyun, J.E. Fischer, A.T. Johnson, *Appl. Phys. Lett.* **2002**, 80, 2767.

[6] C. Wei, K. Srivastava, K. Cho, *Nano Lett.* **2002,** 2, 647.

[7] C.H. Poa, S.R.P. Silva, P.C.P. Watts, W.K. Hsu, H.W. Kroto, D.R.M. Walton, *Appl. Phys. Lett.* 2002, 80, 3189.

[8] C.L. Cheung, J.H. Hafner, C.M. Lieber, *PNAS* **2000,** 97, 3809.

[9] H.-M. Cheng, Q.-H. Yang, C. Liu, *Carbon* **2001,** 39, 1447.

[10] E.T. Thostenson, T.-W. Chou, *J. Phys. D: Appl. Phys.* **2002,** 35, L77.

[11] (a) Treacy, M. M. J.; Ebbesen, T. W.; Gibson, J. M. *Nature* **1996**, *381*, 678. (b) Yakobson, B. I.; Brabec, C. J.; Bernholc, J. *Phys. Rev. Lett.* **1996**, *76*, 2511.

[12] Dalton, A. B.; Collins, S.; Mun˜ oz, E.; Razal, J. M.; Ebron, V. H.; Ferraris, J. P.; Coleman, J. N.; Kim, B. G.; Baughman, R. H. *Nature* **2003**, *423*, 703.

[13] Cadek, M.; Coleman, J. N.; Barron, V.; Hedicke, K.; Blau, W. J. *Appl. Phys. Lett.* **2002**, *81*, 5123.

[14] Kilbride, B. E.; Coleman, J. N.; Fournet, P.; Cadek, M.; Drury, A.; Blau, W. J. *J. Appl. Phys*. **2002**, *92*, 4024.

[15] Sandler, J. K. W.; Kirk, J. E.; Kinloch, I. A.; Shaffer, M. S. P.; Windle, A. H. *Polymer* **2003**, *44*, 5893.

[16] Biercuk, M. J.; Llaguno, M. C.; Radosavljevic, M.; Hyun, J. K.; Fischer, J. E.; Johnson, A. T. *Appl. Phys. Lett*. **2002**, *80*, 2767.

[17] Wei, C.; Srivastava, K.; Cho, K. *Nano Lett*. **2002**, *2*, 647.

[18] Qian, D.; Dickey, E. C. *Appl. Phys. Lett.* **2000**, *76*, 2868.

[19] Cadek, M.; Coleman, J. N.; Ryan, K. P.; Nicolosi, V.; Bister, G.; Fonseca, A.; Nagy, J. B.; Szostak, K.; Be´guin, F.; Blau, B. J. *Nano Lett.* **2004**, *4*, 353.

[20] Ward, I. M. *Mechanical Properties of Solid Polymers*, 2nd ed.; John Wiley & Sons Press: New York, 1983.

[21] Lin, J.-H.; Yang, A. C.-M. *Macromolecules* **2001**, *34*, 4865.

[22] Lin, J.-H.; Yang, A. C.-M. *Macromolecules* **2001**, *34*, 3698.

[23] Kramer, E. J. *Adv. Polym. Sci.* **1983**, *52*/*53*, 1.

[24] Yang, A. C.-M.; Wang, R. C.; Kunz, M. S.; Yang, I, C. *J. Polym. Sci., Polym. Phys. Ed*. **1996**, *34*, 1141.
[25] Kaush, H. H. *Polymer Fracture*; Springer-Verlag: Heidelberg, Germany, 1978.
[26] Donald, A. M.; Kramer, E. J. *Polymer* **1982**, *23*, 457.
[27] Donald, A. M.; Chan, T.; Kramer, E. J. *J. Mater. Sci*. **1981**, *16*, 669.
[28] Yang, A. C.-M.; Kramer, E. J. *J. Polym. Sci., Polym. Phys. Ed.* **1985**, *23*, 1353.
[29] Yang, A. C.-M.; Kramer, E. J.; Kuo, C. C.; Phoenix, S. L. *Macromolecules* **1986**, *19*, 2010.
[30] Yang, A. C.-M.; Kramer, E. J.; Kuo, C. C.; Phoenix, S. L. *Macromolecules* **1986**, *19*, 2020.
[31] Yang, A. C.-M.; Kunz, M. S.; Logan, J. A. *Macromolecules* **1993**, *26*, 1767.
[32] J. Liu, A.G. Rinzler, H. Dai, J.H. Hafner, R.K. Bradley, P.J. Boul, A. Lu, T. Iverson, K. Shelimov, C.B. Huffman, F. Macias-Rodriguez, Y.-S. Shon, T.R. Lee, D.T. Colbert, R.E. Smalley, *Science* **1998,** 280, 1253.
[33] D.E. Hill, Y. Lin, A.M. Rao, L.F. Allard, Y.-P. Sun, *Macromolecules* **2002,** 35 9466.
[34] I.-C. Liu, H.-M. Huang, C.-Y. Chang, H.-C. Tsai, C.-H. Hsu, R.C.-C. Tsiang, *Macromolecules* **2004,** 37, 283.
[35] S.J. Park, M.S. Cho, S.T. Lim, H.J. Choi, M.S. Jhon, *Marcomol. Rapid Commun.* **2003,** 24, 1070.
[36] S. Qin, D. Qin, W.T. Ford, D.E. Resasco, J.E. Herrera, *Macromolecules* **2004,** 37 752.
[37] A. Koshio, M. Yudasaka, M. Zhang, S. Iijima, *Nano Lett.* **2001,** 1, 361.
[38] C. Park, Z. Ounaies, K.A. Watson, R.E. Crooks, J. Smith Jr., S.E. Lowther, J.W. Connell, E.J. Siochi, J.S. Harrison, T.L. St. Clair, *Chem. Phy. Lett.* **2002**, 364, 303.
[39] R. Bandyopadhyaya, E. Nativ-Roth, O. Regev, R. Yerushalmi-Rozen, *Nano Lett.* **2002,** 2, 25.
[40] T. Fukushima, A. Kosaka, Y. Ishimura, T. Yamamoto, T. Takigawa, N. Ishii, T. Aida, *Science* **2003,** 300, 5628.
[41] A. Star, J.F. Stoddart, *Macromolecules* **2002,** 35, 7516.
[42] D.E. Hill, Y. Lin, A.M. Rao, L.F. Allard, Y.-P. Sun, *Macromolecules* 2002, 35 9466.
[43] C.A. Mitchell, J.L. Bahr, S. Arepalli, J.M. Tour, R. Krishnamoorti, *Macromolecules* **2002**, 35, 8825.
[44] Lin, T. S.; Hsiao, C. C.; Cheng, L. Y.; Yang, A. C.-M., *Mate. Chem. Phys.* **2005,** *94*, 438.
[45] C.-C. Hsiao, T.S. Lin, L.Y. Cheng, C.-C. Mar, C.-C.M. Ma, A.C.-M. Yang,

Macromolecules **2005**, *38*, 4811.
[46] Lin, C. H.; Yang, A. C.-M., *J. Mater. Sci*. **2000**, *35*, 4231.
[47] Bower, C.; Rosen, R.; Jin, L.; Han, J.; Zhou, O. *Appl. Phys. Lett.* **1999**, 74, 3317.
[48] D. R. Ulrich, *Polymer* **1987,** 28**,** 533.
[49] S. Kumar, T. D. Dang, F. E. Arnold, A. R. Bhattacharyya, B. G. Min, X. Zhang, R. A. Vaia, C. Park, W. W. Adams, R. H. Hauge, R. E. Smalley, S. Ramesh, P. A. Willis, *Macromolecules* **2002**, 35, 9039.
[50] D. B. Cotts, G. C. Berry, Macromolecules **1981**, 14, 930.
[51] H. Kong, C. Gao,* and D. Yan, *Macromolecules* **2004,** *37,* 4022.
[52] C. S. Henkee, E. J. Kramer, *J. Polym Sci.: Polym Phys Ed*. **1984**, 22, 721.
[53] C. S. Henkee, E. J. Kramer, *J Polym Sc.:, Polym Phys Ed*. **1996,** 34, 2821.
[54] Smith Jr JG, Connell JW, Delozier DM, Lillehei PT, Watson KA, Lin Y, et al. *Polymer* **2004,** 45, 825.
[55] Ounaies Z, Park C, Wise KE, Siochi EJ, Harrison JS. *Compos Sci Technol*. **2003,** 63, 1637**.**
[56] X. Jiang et al. *Polymer* **2005,** 46, 7418**.**
[57] N. Grossiord, J. Loos, O. Regev, and C. E. Koning, *Chem. Mater.* **2006,** 18, 1089**.**
[58] E. Bekyarova et al. *J. Am. Chem. Soc.* **2005,** 127, 5990.
[59] Y.J. Kim et al. *Carbon* **2005,** 43**,** 23,
[60] T. Ogasawaraa, Y. Ishidaa, T. Ishikawaa, R. Yokota, *Composites: Part A* **2004,** 35, 67.
[61] Shouping Li et al.
[62] ZhiMin Dang et al., *Appl. Phys. Lett.* **2004,** 85, 1.
[63] B.K. Zhu et al. *Composites Science and Technology* **2006**, 66, 548**.**
[64] Hiroki Ago et al., *Phys. Rev. B* **2000,** 61, 3.
[65] Yonglai Yang et al. *Nanotechnology* **2004**, 15, 1545.
[66] Xiaofeng Lu, Jiani Zheng, Danming Chao, Jingyu Chen, Wanjin Zhang, Yen Wei *J. of Appl. Poly. Sci.*, **2006,** 100, 2356.
[67] Tony McNallya, Petra Po¨tschke et al. *Polymer* **2005,** 46, 8222.
[68] Sandler J, Shaffer MSP, Prasse T, Bauhofer W, Schulte K, *Polymer* **1999,** 40, 5967.
[69] L. H. Sperling, *Introduction to Physical Polymer Science,* 3rd ed.*,* **John Wiley & Sons, Inc., New York, 2001.**
[70] H. Park, J. Zhao, and J. P. Lu, *Nano Lett.* **2006***,* 65, 916**.**
[71] V. Ska´kalova´, A. B. Kaiser, U. Dettlaff-Weglikowska, K. Hrncˇarikova´, and S. Roth *J. Phys. Chem. B* **2005,** 109, 7174.
[72] E. J. Garboczi, K. A. Snyder, J. F. Douglas, and M. F. Thorpe, *Phys. Rev. E* 52, 1,

1995.

[73] Kirkpatrick S. *Rev. Mod. Phys.* **1973,** 45, 574.

[74] I. Balberg et al. *Phys. Rev. Lett*. **1984,** 52, 1465.

[75] I. Balberg, *Phys. Rev. Le*tt. **1987,** 59, 12.

[76] Shengdong Li, Zhen Yu, Christopher Rutherglen, and Peter J. Burke, *Nano Lett.* **2004**, 10, 2003.

[77] X. Ma et al. *Diamond & Related Materials* **2005,** 14, 68.

[78] A. Carrillo et al. *Nano Lett.* **2003***,* 3, 10.

[79] J. J. Zhao et al., *Appl. Phys. Lett.* **2003,** 82, 21.

[80]Robert J. Chen, Yuegang Zhang, Dunwei Wang, and Hongjie Dai *J. Am. Chem. Soc.* **2001,** *123,* 3838.

[81] N. Nakashima, Y. Tomonari, and H. Murakamiy, *Chem. Lett.* **2002,** 638.

[82] Hiromi Kitano et al., *Phys. Chem. Chem. Phys.* **2006**, 8, 1178.

[83] M. Canepa, M. A. Fox, and J. K. Whitesell, *Photochem. Photobiol. Sci.* **2003,** 2, 1177.